Springer Theses
Recognizing Outstanding Ph.D. Research

Ruijun Hou

Catalytic and Process Study of the Selective Hydrogenation of Acetylene and 1,3-Butadiene

Springer

Springer Theses

Recognizing Outstanding Ph.D. Research

Aims and Scope

The series "Springer Theses" brings together a selection of the very best Ph.D. theses from around the world and across the physical sciences. Nominated and endorsed by two recognized specialists, each published volume has been selected for its scientific excellence and the high impact of its contents for the pertinent field of research. For greater accessibility to non-specialists, the published versions include an extended introduction, as well as a foreword by the student's supervisor explaining the special relevance of the work for the field. As a whole, the series will provide a valuable resource both for newcomers to the research fields described, and for other scientists seeking detailed background information on special questions. Finally, it provides an accredited documentation of the valuable contributions made by today's younger generation of scientists.

Theses are accepted into the series by invited nomination only and must fulfill all of the following criteria

- They must be written in good English.
- The topic should fall within the confines of Chemistry, Physics, Earth Sciences, Engineering and related interdisciplinary fields such as Materials, Nanoscience, Chemical Engineering, Complex Systems and Biophysics.
- The work reported in the thesis must represent a significant scientific advance.
- If the thesis includes previously published material, permission to reproduce this must be gained from the respective copyright holder.
- They must have been examined and passed during the 12 months prior to nomination.
- Each thesis should include a foreword by the supervisor outlining the significance of its content.
- The theses should have a clearly defined structure including an introduction accessible to scientists not expert in that particular field.

More information about this series at http://www.springer.com/series/8790

Ruijun Hou

Catalytic and Process Study of the Selective Hydrogenation of Acetylene and 1,3-Butadiene

Doctoral Thesis accepted by
Tsinghua University, Beijing, China

Springer

Author
Dr. Ruijun Hou
Department of Chemical Engineering
Tsinghua University
Beijing
China

Supervisor
Prof. Tiefeng Wang
Department of Chemical Engineering
Tsinghua University
Beijing
China

ISSN 2190-5053 ISSN 2190-5061 (electronic)
Springer Theses
ISBN 978-981-10-0772-9 ISBN 978-981-10-0773-6 (eBook)
DOI 10.1007/978-981-10-0773-6

Library of Congress Control Number: 2016961697

Printed on acid-free paper

This Springer imprint is published by Springer Nature
The registered company is Springer Nature Singapore Pte Ltd.
The registered company address is: 152 Beach Road, #22-06/08 Gateway East, Singapore 189721, Singapore

Supervisor's Foreword

This thesis describes the scientific achievements of Dr. Ruijun Hou, which were made during her doctoral program at the Department of Chemical Engineering, Tsinghua University. During the five years as a doctoral student, she demonstrated distinguished ability in scientific research and obtained a number of important results on the selective hydrogenation reactions of acetylene and 1,3-butadiene in both catalytic study and process study. As the supervisor of her undergraduate thesis and doctoral thesis, I can introduce the most important findings of her studies.

Dr. Hou's work focused on the selective hydrogenation of acetylene and 1,3-butadiene. After an extensive literature survey of several hundred publications, she chose to study this reaction system by both experiments and DFT calculations. She combined the experimental catalysis (catalyst synthesis, characterization, and reaction evaluation), computational catalysis (DFT calculation for metallic surfaces), and reaction engineering (process and reactor design).

The catalytic study started from model surfaces by UHV-TPD experiments and DFT calculations. The unique properties of the Pd-Ni bimetallic model surface inspired her to further study the supported catalysts. The good correlation between model surfaces and supported catalysts demonstrated the feasibility of designing effective bimetallic catalysts for selective hydrogenation reactions. Further, non-precious metal catalysts were designed by replacing the precious metal with non-precious metal carbide.

In the chemical process study, Dr. Hou modified the process of selective hydrogenation of acetylene by coupling the selective absorption with the selective hydrogenation in a liquid phase. As a result, the ethylene selectivity was greatly improved, and the heat transfer performance was also greatly enhanced. Lastly, she proposed a multi-stage slurry bed reactor for potential industrial applications.

Looking back on Dr. Hou's scientific achievements, I believe they are of great importance for both industrial and fundamental catalysis. I hope that the readers will be inspired by the novel catalysts and the new process in liquid-phase hydrogenation as a result of the author's efforts.

Beijing, China
September 2016

Prof. Tiefeng Wang

Parts of this thesis have been published in the following journal articles:

1. **Hou Ruijun**, Lan Xiaocheng, Wang Tiefeng(*), "Selective hydrogenation of acetylene on Pd/SiO_2 in bulk liquid phase: A comparison with solid catalyst with ionic liquid layer (SCILL)", Catalysis Today, 2015, 251: 47–52.
2. **Hou Ruijun**, Chang Kuan, Chen Jingguang G.(*), Wang Tiefeng(*), Replacing Precious Metals with Carbide Catalysts for Hydrogenation Reactions, Topics in Catalysis, 2015, 58(4-6): 240–246.
3. **Hou Ruijun**, Porosoff Marc D., Chen Jingguang G.(*), Wang Tiefeng(*), Effect of oxide supports on Pd–Ni bimetallic catalysts for 1,3-butadiene hydrogenation, Applied Catalysis A: General, 2015, 490: 17–23.
4. **Hou Ruijun**, Yu Weiting, Porosoff Marc D., Chen Jingguang G.(*), Wang Tiefeng(*), Selective hydrogenation of 1,3-butadiene on PdNi bimetallic catalyst: From model surfaces to supported catalysts, Journal of Catalysis, 2014, 316: 1–10.
5. **Hou Ruijun**, Wang Tiefeng(*), Lan Xiaocheng, Enhanced Selectivity in the Hydrogenation of Acetylene due to the Addition of a Liquid Phase as a Selective Solvent, Industrial & Engineering Chemistry Research, 2013, 52(37): 13305–13312.

Contents

Chapter 1
Introduction

1.1 Background

The selective hydrogenation of alkynes and dienes is an important reaction in chemical industry. They are widely applied in the purification of olefin streams to remove alkynes/dienes, the gasoline refinery process, and some of the fine chemical processes. The selective hydrogenation of acetylene also provides a new route for the production of ethylene from natural gas or coal. The selective hydrogenation is to hydrogenate the C–C triple bond to double bond or to hydrogenate two C–C double bonds to one double bond. Thus, the process requires the hydrogenation to stop at the first hydrogenation step, not to reach complete hydrogenation.

1.1.1 Purification of C2–C4 Olefins

Ethylene is one of the most important products in petrochemical industry. Its domestic capacity is usually an indicator to measure the development of a country's chemical industry. The light olefins from the steam cracker are the monomers or co-monomers for the production of polyolefin, synthetic materials, organic chemicals, and fine chemicals [1]. However, there are about 0.5–5% of alkynes/dienes in the cracking stream [2–5]. Even the minor amounts of alkynes/dienes will affect the polymerization process negatively. For example, the alkynes/dienes will poison the polymerization catalysts [6, 7]; the alkynes/dienes can easily react with the olefins and will disqualify the products [8]; the C–C triple bond in the alkynes will complex with the copper in the apparatus and form copper acetylide, which is explosive and dangerous [9]. As a result, the polymerization-grade olefins require the concentration of alkynes/dienes in the olefin stream at ppm level. Table 1.1 lists the requirements for C2–C4 olefin streams.

R. Hou, *Catalytic and Process Study of the Selective Hydrogenation of Acetylene and 1,3-Butadiene*, Springer Theses, DOI 10.1007/978-981-10-0773-6_1

Table 1.1 Concentration requirements for alkyne/diene in the polymerization-grade olefin stream

Olefin	Alkyne/diene initial concentration (%)	Requirement for alkyne (ppm)	Requirement for diene (ppm)
Ethylene [5]	0.5–2.3	5	–
Propene [3, 4]	3–5	5	10
1-Butene [2]	~1	10	12

The purification of olefin stream usually uses selective hydrogenation or solvent extraction processes. Solvent extraction process can recycle the alkynes/dienes as well as purify the olefin stream, but the process is complicated and the system is difficult to operate. On the contrary, selective hydrogenation is simple in process and is more effective in the alkynes/dienes removal. So far, it is the most economical and effective method [5, 6] in industry. In the C2–C4 streams, the molecules to be removed are acetylene, propyne, propadiene, and 1,3-butadiene; the desired products are ethylene, propene, and 1-butene [10]. In the C4 stream, 1-butene is the monomer for the production of polybutene and co-monomer for polyethylene, so 1-butene is the most desirable among the butene species [6].

1.1.2 Production of Ethylene from Acetylene

The current production of ethylene relies on oil refinery. As an important basic chemical in industry, the demand of ethylene in China exceeded 16 million tonnes in 2013 [11]. However, the oil resource in China is not abundant. The external dependence of oil was 56.4% in 2012 [12], and the number keeps increasing in recent years. It is important to seek for substitute route to produce ethylene from non-oil resources, in order to reduce the external dependence of oil.

Shale gas revolution in the USA has made a profound change in the worldwide energy structure since 2005. China has expanded the production of natural gas in recent years. The gas proportion of energy consumption is increasing and was about 5% in 2011. Moreover, the West-to-East Natural Gas Transmission Project in China has increased the utilization of natural gases in the west [13].

On the other hand, as the technology of acetylene production from gas and coal became mature [14], the supply of the downstream product polyvinyl chloride (PVC) exceeded the demand. The profit of PVC has become lower, and it is urgently needed to expand the downstream products of acetylene [15, 16]. Polyethylene (PE) is a possible product because the price of PE fluctuates with the price of oil, and its downstream products such as ethylene glycol, propylene glycol, acrylic acid, and polyvinyl alcohol (PVA) have good economic values [11, 17]. Therefore, the selective hydrogenation of acetylene could provide a new route for ethylene production and will decrease the dependence of ethylene on oil.

1.2 Properties of Selective Hydrogenation Reactions

Selective hydrogenation of C–C bond is a series reaction. It is desired that the hydrogenation stops at the first hydrogenation step but not further undergoes the second step. The selectivity is controlled by the hydrogenation of the C–C bonds. However, over one certain catalyst, the hydrogenation activities of the first step and the second step are positively correlated. The selectivity can only be controlled by controlling the adsorption properties of olefins. If the adsorption energy of olefin is low, the desired product could desorb quickly from the catalyst and avoid the complete hydrogenation. Moreover, the control of oligomerization of alkynes/dienes should not be neglected. To decrease the concentration of alkynes/dienes on the catalyst is the major way to control the oligomerization reactions.

Meanwhile, the hydrogenation reactions are exothermic. The reactors used in industry are fixed-bed reactor. The released heat in the reaction will lead to hot spot along the reactor and could possibly lead to runaway of temperature. The runaway of temperature is caused by the low efficiency of heat transfer in the fixed-bed reactor. It will affect the normal operation and will even destroy the loaded catalysts. The reaction heats of acetylene hydrogenation are listed as an example:

Main reaction:

$$HC{\equiv}CH + H_2 \rightarrow H_2C{=}CH_2 + 174.4\,kJ/mol \tag{1.1}$$

Side reactions:

$$H_2C{=}CH_2 + H_2 \rightarrow H_3C - CH_3 + 137.0\,kJ/mol \tag{1.2}$$

$$HC{\equiv}CH + 2H_2 \rightarrow H_3C - CH_3 + 311.4\,kJ/mol \tag{1.3}$$

$$nHC{\equiv}CH + mH_2C{=}CH_2 \rightarrow C4\ \text{and green oil} \tag{1.4}$$

As seen from the thermodynamic data, the heat released in the hydrogenation reactions is enormous. The industrial operation temperature is only slightly higher than the room temperature, and the temperature control is very difficult. The temperature rise along the reactor could be as high as 20–40 °C [18, 19].

1.3 Industrial Processes

The selective hydrogenation in industry usually utilizes fixed-bed reactor. When the inlet is gas phase, it is a conventional fixed-bed reactor of gas–solid phase; when the inlet is liquid phase, it is a trickle-bed reactor with gas, liquid, and solid phases [20–25].

The fixed-bed process has been improved by several ways to enhance the heat transfer. One way is to introduce a liquid phase in the fixed-bed process, in which some of the products are cooled to liquid and are cycled back to the reactor, in order to dilute the reactants in the inlet and absorb the reaction heat inside the reactor [26, 27]. Another way is to utilize multistage fixed-bed process, in which heat exchangers are installed between stages in order to control the temperature rise [28]. These methods have enhanced the heat transfer to some extent, but are complicated in process, with high energy consumption and high investment.

The catalysts in the fixed bed deactivate easily because of the oligomerization reactions of alkynes/dienes. The catalysts should be regenerated at regular intervals. A spare reactor is needed for most processes, adding to higher investment in equipment.

The selective hydrogenation of acetylene is a typical example, and the conventional processes of acetylene hydrogenation are discussed below.

The processes for the selective hydrogenation of acetylene are typically front-end and tail-end processes. As shown in Fig. 1.1, the hydrogenation reactor locates before the demethanizer in the front-end process, and locates after the demethanizer in the tail-end process.

In the front-end process, the gas stream from the cracker goes to the hydrogenation reactor right after caustic washing and drying. The inlet of the hydrogenation reactor contains not only C2 species, but also H_2, CH_4, CO, etc. After the hydrogenation reaction, the C1 and C3 species are separated from the C2 stream. In the tail-end process, the C2 species are firstly separated from the other gases; then, a certain amount of H_2 is mixed with the C2 stream, and the mixture is introduced into the hydrogenation reactor [30].

The gas-phase concentrations in the inlet and the typical operation conditions of the front-end and tail-end processes are shown in Table 1.2.

The advantages of the front-end process are as follows: (1) No extra H_2 is needed; (2) the separation process is simpler, leading to lower investment and lower energy consumption; and (3) the high concentration of hydrogen results in lower green oil formation and higher stability of catalysts. The disadvantages are as follows: (1) The H_2/C_2H_2 ratio could not be adjusted, so the selectivity to ethylene is low; (2) the complete hydrogen increases the risk of temperature runaway in the reactor; (3) the concentration of CO fluctuated in the inlet; because the CO concentration deceases the acetylene conversion, the outlet stream might not reach the requirement for the polymerization-grade ethylene; and (4) there is no spare reactor and only by stopping the whole process can replace the deactivated catalysts [31].

Compared with the front-end process, the advantages of the front-end process are as follows: (1) The H_2/C_2H_2 ratio could be adjusted, and the selectivity to ethylene is higher; (2) the temperature is more easily controlled; and (3) the operation is steadier. The disadvantages are as follows: (1) The formation of green oil is higher, and the catalysts are less stable; (2) due to the fast deactivation of catalyst, a spare reactor is needed for the frequent catalyst regeneration; and (3) the

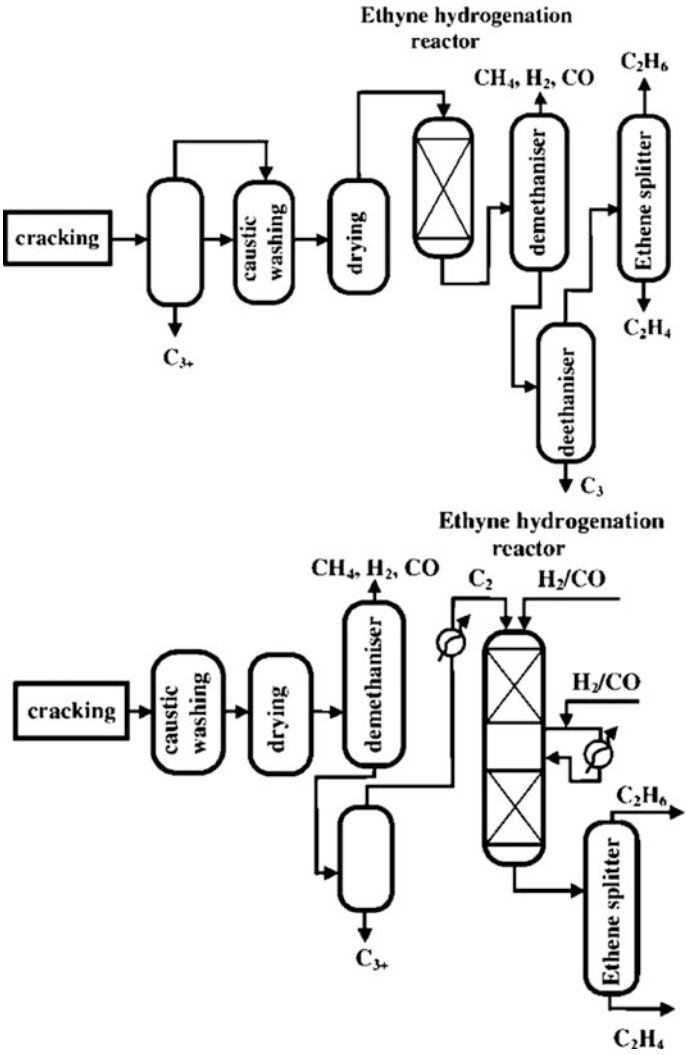

Fig. 1.1 Process chart of front-end (*up*) and tail-end (*down*) processes. Reprinted from Ref. [29] with permission from Taylor & Francis Ltd.

separation process is more complicated, with higher investment and higher energy consumption [29].

Because of the many differences between the front-end and tail-end processes, the requirements for catalysts are different. The catalyst for the front-end process requires the catalyst with high selectivity, while the catalyst for the tail-end process requires the catalyst with good stability.

Table 1.2 The gas-phase concentrations of inlet and typical operation conditions of front-end and tail-end processes

Parameter	Front-end	Tail-end
H_2 (molar %)	22	2.4
C_2H_2 (molar %)	0.2	2
C_2H_4 (molar %)	37	71
CH_4 (molar %)	12	–
C_2H_6 (molar %)	28.4	25
C_3H_6 (molar %)	0.12	–
CO (ppm)	2800	40
H_2/C_2H_2	110	1.5
Pressure (bar)	35	20
Temperature (K)	343	333
GHSV (h^{-1})	2000	3000

Reprinted from Ref. [29] with permission of Taylor & Francis Ltd.

1.4 Progress in Catalyst Development

The catalysts for selective hydrogenation date back to the 1940s. In the selective hydrogenation of gasoline to remove dienes, nickel sulfide or copper was applied. However, the catalysts were of low activity and required high operation temperature, which would lead to more polymerization reactions [1]. In the 1960s, with the fast development of the ethylene industry, the catalysts for selective hydrogenation were greatly studied. The active metals were focused on the VIII group metals, such as Pd [32–36], Pt [36–38], Ni [36], etc. Among them, Pd was widely applied in industry because of the high hydrogenation activity and the relatively high selectivity to ethylene. However, the selectivity to ethylene on Pd catalyst was far from satisfaction, and the catalyst stability is relatively low. In the 1970s, the Pd-based bimetallic catalysts emerged. In the late 1980s, Procatalyse, United Catalysts, Leunawerke, and AcreonCatalysts developed mature Pd-based bimetallic catalysts and applied them in production. Since the twenty-first century, the research on Pd-based bimetallic catalysts has been expanded from experimental to fundamental by quantum calculation, thus saving considerable amount of manpower, time, and resources. Other than Pd-based catalysts, the non-Pd catalysts and non-precious catalysts have also been investigated widely.

1.4.1 Reaction Mechanism on Pd Catalyst

The Pd monometallic catalyst has been extensively studied because of its wide application in industry. The mechanism, the phase change over the catalyst, and the deactivation progress in the selective hydrogenation of acetylene are summarized and discussed below.

1.4.1.1 Reaction Mechanism

The reaction pathways of selective hydrogenation of alkynes/dienes are shown in Fig. 1.2. It was reported that alkyne/diene firstly adsorbed on the catalyst surface and then underwent the first step of hydrogenation; the olefin either desorbed from the catalyst or underwent the second step of hydrogenation. The selectivity was defined from two sides: (1) kinetic selectivity, if $k_2 \gg k_4$, i.e., the hydrogenation activity of the first step is much faster than the second step, the catalyst would give a high selectivity in terms of kinetics; and (2) thermodynamics selectivity: if $k_1/k_{-1} \gg k_3/k_{-3}$, i.e., the alkyne/diene adsorbed much faster than olefin, the olefin could desorb easily from the catalyst, and the catalyst would give a high selectivity to olefin in terms of thermodynamics. Other than the hydrogenation reactions, there are oligomerization reactions on the Pd surface. The complete hydrogenation and the oligomerization reactions are the two main side reactions in the selective hydrogenation of acetylene [39].

The reaction pathway and the adsorbed intermediates were studied and detected by FT-IR and EELS under ultra-high vacuum conditions. As shown in Fig. 1.3, the acetylene firstly adsorbed on the catalyst by π-bond (1); after absorbing one hydrogen atom, the $C_2H_3^*$ adsorbed by π–σ-bond; the parallel adsorbed $C_2H_3^*$ could be rearranged to vertically adsorbed (4) or (5); (4) and (5) would undergo complete hydrogenation and form ethane; if the π-bonded $C_2H_2^*$ rearranged to σ-bonded (2), or hydrogenated into π-bonded $C_2H_4^*$, the selective hydrogenation reaction happened [40].

Borodzinski et al. [41, 42] proposed a reaction mechanism by the analysis of reaction kinetics on Pd/Al_2O_3. They believed there were three kinds of active sites as shown in Fig. 1.4: A_1, A_2, and E.

A_1 site was small Pd assembles separated by the surface hydrocarbon. It could adsorb acetylene and hydrogen. However, because of the steric hindrance, it hardly adsorbs ethylene. Hence, only selective hydrogenation and minor oligomerization reactions happened on A_1 site, but little complete hydrogenation reaction.

A_2 site was the site covered by hydrocarbon and could only adsorb acetylene. The adsorbed acetylene reacted with the hydrogen transferred from the hydrocarbon layer. The ethylene formed on this site could desorb quickly and not undergo complete hydrogenation.

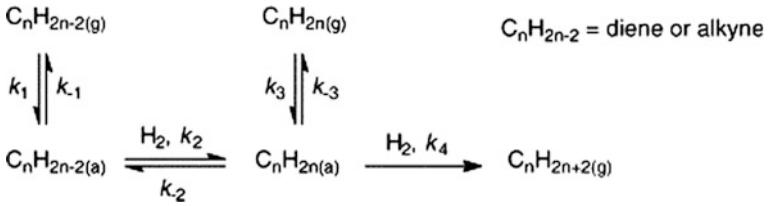

Fig. 1.2 Reaction pathway of selective hydrogenation of alkynes/dienes. Reprinted from Ref. [39], Copyright 2001, with permission from Elsevier

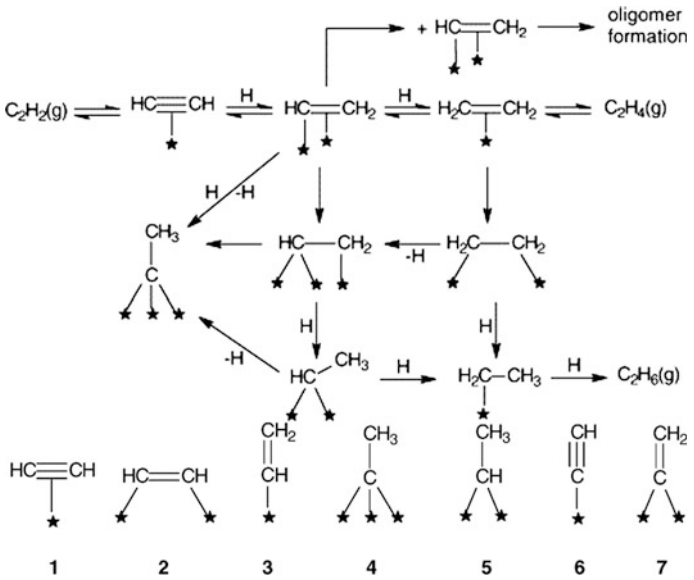

Fig. 1.3 Reaction network (*up*) and the adsorbed intermediates (*down*) of acetylene hydrogenation. Reprinted from Ref. [39], Copyright 2001, with permission from Elsevier

E site was large area of Pd assembles. It could adsorb all the reactants and products and could catalyze selective hydrogenation, complete reaction, and oligomerization reactions.

The ratio of A sites to E sites directly affected the selectivity to ethylene. Under low partial pressure of acetylene and high partial pressure of ethylene, large amount of ethylene adsorbed at E sites, and ethane formed at E sites; as a result, acetylene only adsorbed and was hydrogenated on A_1 sites. Under high partial pressure of acetylene, the hydrogenation of acetylene mainly happed on A_2 sites.

Borodzinski's model has been replenished and revised since 2000. Vincent et al. [43] proposed two models: One was the competitive adsorption model at low temperature, in which the hydrogen was provided by adsorbed hydrogen; the other was the non-competitive adsorption model, and the hydrogen was provided by the transfer via the surface hydrocarbons. The rate-limiting steps in the two models were both the hydrogenation of vinyl group. Mei et al. [44] calculated the elementary reaction kinetics and found that acetylene could easily adsorb on Pd; the rate-limiting step was the hydrogen adsorption, the hydrogenation of vinyl group, and the desorption of ethylene; further, they pointed out that the selectivity to ethylene not only related to the adsorption properties of ethylene and acetylene, but also related to the interaction between the adsorbed species and the adsorption kinetics. Hevia et al. [45] investigated the hydrogenation of acetylene under low pressure in a TAP reactor and found that the adsorption of hydrogen was reversible and there formed a layer of carbide on the Pd surface at the initial stage of the reaction.

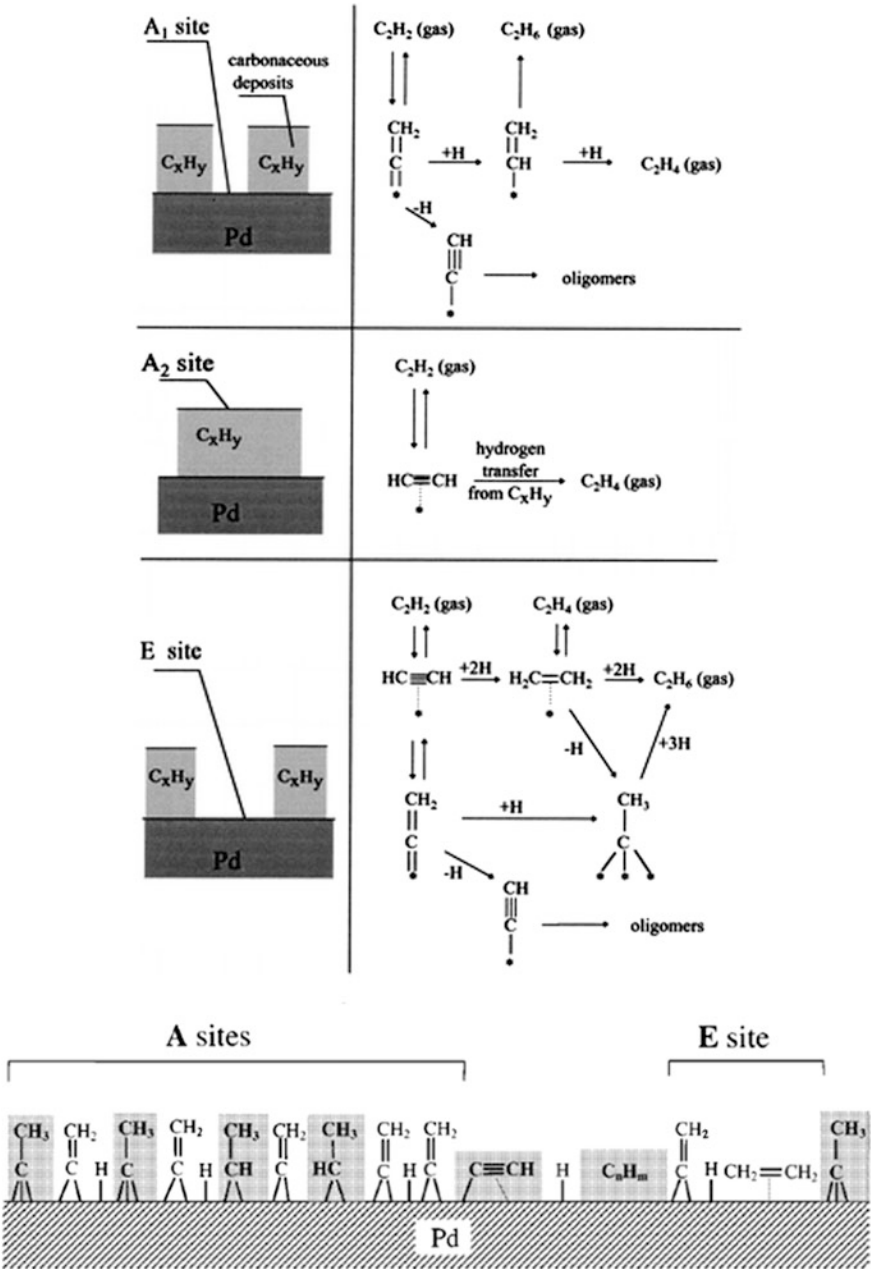

Fig. 1.4 Reaction mechanism of acetylene hydrogenation [41, 42]. Reprinted from Ref. [41], with kind permission from Springer Science+Business Media. Reprinted with permission from Ref. [42]. Copyright 1997 American Chemical Society

With the development of density functional theory (DFT) calculation, the fundamental study supported and further explained some of the experimental results. Sheth et al. [46] and Xie et al. [47] calculated the adsorption energy, the adsorption geometries, and the activation barriers in acetylene hydrogenation. They found that the formation of PdH_x phase affected the hydrogenation kinetics. Duca et al. [48, 49] studied the effect of carbon deposit and metal dispersion on the surface reaction kinetics by Monte Carlo method, and they found that the steric hindrance did not always decrease the surface activity. Li et al. [50, 51] studied the reaction pathway of acetylene hydrogenation on Pd_{2-8} clusters.

1.4.1.2 PdH_x and PdC_x

Pd can absorb a large amount of hydrogen, and the bulk Pd would become bigger in volume. The Pd metal particles on supported catalysts exist in nanoscale, and their properties are different from the bulk Pd. Nevertheless, the Pd particles could still absorb hydrogen. Two phases of Pd hydride have been reported: α-PdH_x at low hydrogen partial pressure and β-PdH_x at high hydrogen partial pressure. The phase diagram is shown in Fig. 1.5.

As shown in Fig. 1.5, the temperature and the partial pressure both affected the formation of PdH_x. In the hydrogenation reactions, the β-PdH_x phase showed higher activity than the α-PdH_x phase, but gave lower selectivity to olefins. By controlling the particle size, little β-PdH_x phase formed on small Pd particles less than 2.6 nm and gave higher selectivity to olefin.

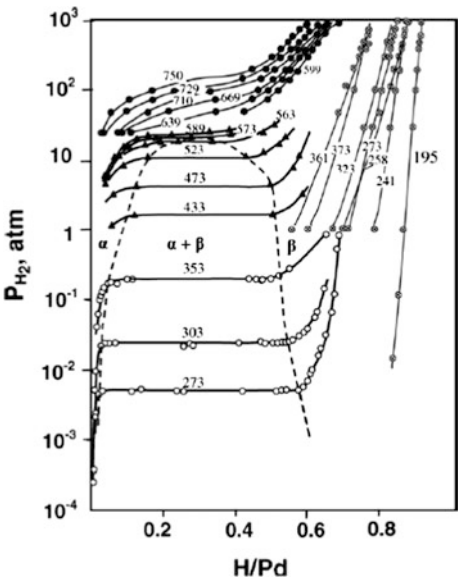

Fig. 1.5 Phase diagram of α-PdH_x and β-PdH_x (numbers on the graph are temperature in K) [52]. Reprinted from Ref. [52], Copyright 2001, with permission from Elsevier

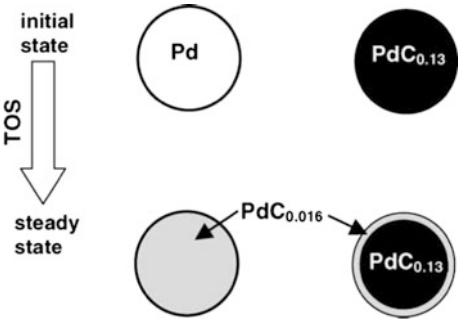

Fig. 1.6 Pd and $PdC_{0.13}$ phase change during reaction [29]

Other than the PdH_x phase, there was formation of $PdC_x(0 < x \leq 0.13)$ phase during the hydrogenation reaction. The PdC_x phase usually formed in the hydrocarbon environment under high temperature and decomposed in hydrogen or oxygen above 403 K. Hydrogen and carbon atoms competed to occupy the vacancies on the Pd catalyst and formed a Pd–C–H ternary structure. The presence of carbon atoms decreased the possibility of the β-PdH_x phase formation. When the saturated $PdC_{0.13}$ formed, the β-PdH_x phase did not exist. The carbon atoms in the PdC_x phase could involve in reactions, and the presence of PdC_x phase was not in favor to reduce the carbon deposit or to suppress the oligomerization reactions.

The phase change on Pd and $PdC_{0.13}$ is depicted in Fig. 1.6 [29]. On Pd, a phase of $PdC_{0.016}$ gradually formed as a bulk phase, while on $PdC_{0.13}$, because the carbon atoms were already saturated in the bulk phase, only the surface PdC_x turned to $PdC_{0.016}$. The activities at steady state were the same for the two phases, as verified by experiment.

1.4.1.3 Deactivation

Larsson et al. [53] proposed that the coke formation was influenced by the coverage of surface hydrogen. The higher the surface coverage of hydrogen, the more actively that coke formed. The mechanism of coke formation is shown in Fig. 1.7. At different coverage of surface hydrogen, two types of green oil formed; at low hydrogen coverage, the harmful green oil formed and was advantageous for hydrogen transfer; at high hydrogen coverage, the harmless green oil formed which covered the active sites. The existence of the two types of green oil was verified by

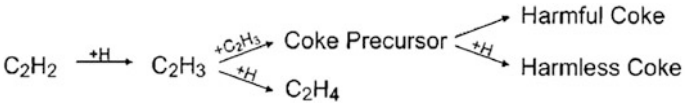

Fig. 1.7 Deactivation pathway in the hydrogenation of acetylene [53]. Reprinted from Ref. [53], Copyright 2001, with permission from Elsevier

Ahn et al. [54]. Xu et al. [55] found by TEM that the green oil aggregated around the Pd particles. The Pd particles were taken away from the support and were surrounded by green oil. The active sites for the formation of green oil were on the metal site, and ethylene did not involve in the oligomerization reaction independently; as the amount of green oil increased, it migrated onto the support surface [56]. Moon et al. [54, 57] found that 1,3-butadiene was the precursor for the coke formation and proposed a three-stage deactivation mechanism: The first step was the formation of light green oil, during which the deactivation was not significant; the second step was the formation of heavy green oil, and the green oil covered the active sites and migrated to the support; and the third step was the formation of heavy green oil in large amount, and the green oil blocked the support pores and deactivated the catalyst significantly. Sarkany [58] proposed a mechanism for the formation of C4 species: During the reaction, the carbon atoms dissolved into the Pd phase and formed a Pd–H–C ternary phase; the increase of carbon atoms in Pd decreased the number of available hydrogen atoms, thus decreasing the ethane formation and increasing the C4 species formation. Esmaeili et al. [59] proposed a deactivation mechanism based on pore structure. It was found that the branched green oil easily formed on the supports with small pores. The branched green oil would block the pores and deactivate the catalyst.

During the regeneration of catalyst, the metal particles aggregated more easily on used catalyst than on fresh catalyst under low temperatures [56]. The dispersion of regenerated catalyst decreased by 50%, but the activity was similar as fresh catalyst, which might be attributed to the fast deactivation of fresh catalyst at the initial stage. The selectivity of regenerated catalyst was lower than fresh catalyst, because the harmful coke (Fig. 1.7) formed on the catalyst surface enhanced hydrogen transfer and decreased the olefin selectivity [60].

1.4.2 Influencing Factors on Pd-Based Catalysts

There are many factors that influence the catalytic properties of Pd, such as metal dispersion, support, pretreatment, and additives. The detailed effects are discussed below.

1.4.2.1 Metal Dispersion

Metal dispersion represents the degree of metal utilization on a supported catalyst. The higher the metal dispersion, the higher degree the metal utilization. The metal dispersion affects differently the turnover frequency (TOF) and selectivities in different reaction system.

The low-loading Pd catalyst is usually used in industry in order to control the complete hydrogenation. The lower metal loading would lead to higher dispersion and a higher apparent activity, as well as a higher selectivity to olefin [32, 61].

In the selective hydrogenation of alkynes, the high metal dispersion was reported to result in a higher apparent activity [62–65] but lower TOF [65, 66]. The lower TOF was attributed to the intrinsic defect of the small metal particles and the interaction between the defects and the supports. The dispersion effect on selectivity was reported differently in the literature. In the selective hydrogenation of acetylene, it was commonly agreed that the higher the metal dispersion, the higher the selectivity to ethylene [62, 67, 68]. However, Duca et al. [32] found that the selectivity was not affected by metal dispersion by plotting the selectivity against conversion. Borodzinski [65] also reported that the olefin selectivity was not affected by the metal particle size when the particles were larger than 4 nm. In the hydrogenation of phenyl acetylene, TOF was not much affected by metal dispersion, while the selectivity to styrene increased with increasing metal dispersion [69].

Some literature reported that the metal dispersion did not affect the catalytic properties independently, but showed synergetic effect with other influencing factors. Feng et al. [70] found that the high surface area, low acidity, and high metal dispersion together affected the catalyst selectivity, activity, and stability positively. Komhom et al. [71] also showed that the high surface area and the high metal dispersion led to high selectivity and activity. Panpranot et al. [64] investigated the TiO_2-supported catalyst and believed that the ethylene selectivity was greatly affected by the support but not by the metal dispersion; however, McKenna et al. [72] believed that the TiO_2-supported catalytic property was indeed affected by the metal dispersion: The higher metal dispersion led to higher conversion but lower selectivity.

Similar to the hydrogenation of alkynes, in the selective hydrogenation of dienes, the higher metal dispersion usually resulted in higher apparent activity [73, 74] and lower TOF [74, 75]. The metal dispersion affected the catalytic properties together with other factors [76]. Boitiaux et al. [77] investigated into the catalytic properties at different metal dispersions for the selective hydrogenation of 1,3-butadiene. When the dispersion was lower than 20%, the TOF was not affected by the metal dispersion; when the dispersion was higher than 20%, the TOF decreased with increasing dispersion. The effects of dispersion on selectivity were reported differently. For example, Pattamakomsan et al. [73] found that the selectivity to olefins increased with increasing dispersion. Gotez et al. [74] reported that the selectivity to olefin was not affected by dispersion. In the hydrogenation of 1,3-cyclooctadiene, Liotta et al. [75] reported that the selectivity to olefin showed a volcano relationship with the metal dispersion, i.e., when the dispersion was lower than 32%, the selectivity increased with increasing dispersion; when the dispersion was higher than 32%, the selectivity decreased with increasing dispersion.

Borodzinski et al. [29] summarized the dispersion effect in the selective hydrogenation of acetylene. They believed that on a catalyst with high dispersion, the metal particles had more defects and would interact with the support more easily. The defects on the small metal particles contributed more electronic and geometric effects in the catalytic process. On a small Pd particle, the β-PdH_x phase was less easy to form than the PdC_x phase. As a result, the TOF of a small Pd

particle was lower, and the ethylene selectivity was higher for a highly dispersed catalyst. In the front-end process, the higher partial pressure of hydrogen would form more β-PdH_x phase on the Pd catalyst, and the metal dispersion would affect more significantly in the front-end process.

1.4.2.2 Support

The active metals are supported on supports in order to increase the metal dispersion and the catalytic efficiency [78]. The support surface area, pore structure, acidity, and the interaction with metal are important factors that affect the catalyst properties.

The supports with high surface area are commonly chosen for the industrial catalysts, on which the metal is highly dispersed and is more efficiently used. SiO_2 and Al_2O_3 are two typical industrial supports because they are widely available and cheap. Primet et al. [79] studied the support effect in the hydrogenation of 1,3-butadiene for the Pt catalyst and found that the support with lower acidity showed better performance in controlling complete hydrogenation and exhibited similar hydrogenation activity for the first hydrogenation step. Zhu et al. [80] investigated into a series of Pd/SiO_2 with different SiO_2 surface area for the hydrogenation of acetylene and found that lower surface area was advantageous for the enhancement of ethylene selectivity. To compare the effect of acidity and the effect of surface area, Feng et al. [70] synthesized a kind of Mg–Al support with high surface area. Compared with the conventional Al_2O_3, the Mg–Al-supported catalyst had a much higher dispersion and lower acidity. The apparent activity and selectivity were both enhanced on the Mg–Al-supported catalysts. The acidity on the catalyst enhanced the oligomerization and the bond transfer reactions and increased the formation of green oil [81]; the green oil formation on the catalyst on one side acted as media for hydrogen transfer, which promoted the complete hydrogenation [82], and on the other side, the green oil aggregated on the catalyst surface and changed the geometric effect of the active site [83]. Based on the above reports, the acidity should be lowered in the selective hydrogenation in order to obtain a high selectivity to olefin.

The metal–support strong interaction (SMSI) is another important factor that affects the catalytic properties. In 1978, Tauster et al. [84] reported the existence of SMSI on the TiO_2-supported VIII group (Pt, Pd, Ir, Ru, Rh, etc.) metal catalysts. On a catalyst with SMSI, the support would migrate or even cover on top of the metal particles. For the selective hydrogenation reactions, the SMSI was found to affect the catalytic properties. Kang et al. [85] found the SMSI existed on the TiO_2-modified Pd catalyst, and the interaction decreased the hydrogen adsorption on the catalyst and decreased the activity of acetylene hydrogenation; the modification by TiO_2 changed the Pd exposure rate and the electronic property and decreased the adsorption energy of ethylene, and the ethylene selectivity was improved. Lee et al. [86] reported that by the modification of TiO_2, the 1,3-butadiene activity was decreased; the interaction between Pd and TiO_2 reduced the isomerization degree of

1-butene. As seen from the above literature, the modification by TiO_2 mainly causes the coverage of Pd active site and the change in electronic properties, thus decreasing the hydrogenation activity and increasing the selectivity to olefin. However, not all TiO_2 could interact strongly with Pd. Weerachawanasak et al. [87] reported that on the micron-level TiO_2, no SMSI was found on the catalyst. Besides, the SMSI was also found to be effective on CeO_2 [88–90], ZrO_2 [91, 92], La_2O_3 [93], and Nb_2O_5 [93].

The crystal phase and size of TiO_2 and Al_2O_3 also affect the catalytic properties. Komhom et al. [67] found that neither large nor small crystal size of α-Al_2O_3 was good for the selective hydrogenation. When supporting Pd on a mixed phase of Al_2O_3, the ethylene selectivity was higher than that on a pure phase [71, 94]. On the TiO_2-supported Pd catalyst, different TiO_2 phases provided different amount of Ti^{3+}. Ti^{3+} changed the electronic properties of the Pd particles and further affected the selectivity to olefin [64].

1.4.2.3 Promoters/Pretreatment

The addition of promoters or the pretreatment could modify the active sites on the Pd catalyst and thus modify the catalyst activity and selectivity. The gas-phase pretreatment and the solid-phase promoters for the Pd catalysts are discussed below.

In the front-end process, CO is co-fed into the reactor. As studied, CO addition in the C2 stream could enhance the selectivity to ethylene but decrease the hydrogenation activity [95]. In some cases, CO is also co-fed in the tail-end process in order to increase ethylene selectivity. It is commonly believed that CO poisons the Pd surface and adsorbs competitively with C2 species on the active sites. As a result, the hydrogenation activities of the first step and the second step are both reduced, and the ethylene selectivity is thus enhanced. The poison of CO on Pd was reported to be reversible [95]. Perez-Ramirez et al. [96, 97] investigated into the interaction of CO with Pd by DFT calculation and found that CO not only occupied some of the active sites, but also changed the electronic properties and decreased the adsorption energy of ethylene. Zea et al. [98] reported that the addition of CO increased the activation barrier of ethylene hydrogenation and proposed a model that in the CO/C_2H_4 competitive adsorption, only when CO desorbed could the ethylene hydrogenation proceeded. However, the CO modifications on other metals are different. On the Au catalyst as reported, CO had little effect on selectivity and activity. The possible reason might be that the CO did not adsorb on Au, or the CO adsorption site was different from the active site [99]. On a Cu–Al catalyst, the CO interaction with the catalyst could improve the selectivity to ethylene at near 100% conversion. The presence of CO rearranged the atoms on the catalyst and made the Cu more dispersed [100].

Praserthdam et al. [101–103] investigated into the effect of NO_x pretreatment on the Pd–Ag catalyst. They found that the pretreatment by NO or N_2O enhanced the catalytic performance of the fresh catalyst [101, 102], but played little effect on the used or regenerated catalysts [103]. The enhancement by N_2O for the fresh catalyst

might be attributed to the interaction of N_2O with PdAg particles. As shown in Fig. 1.8, the pretreatment of N_2O promoted the oxygenation of Ag on the catalyst surface and reduced the Ag dilution effect on Pd. Thus, more Pd atoms exposed on the catalyst surface, and the activity was improved. On the other hand, the rearrangement of Pd–Ag modified the electronic effect and improved the ethylene selectivity. However, over the used or regenerated catalysts, the metal atoms already rearranged during reaction, and the N_2O could not change the structure.

The addition of alkali metals (such as Na, K, and Cs) may modify the acidity of the catalyst and has been widely investigated in the modification of selective hydrogenation catalysts [104–106]. Park et al. [107] found that by the modification of K, the adsorption/desorption properties of acetylene/ethylene were changed, and the selectivity to ethylene was improved as well as activity; however, the catalyst stability decreased. Kim et al. [108] reported the K effect on Pd/TiO_2 and found that a titanate salt of K formed during the preparation of catalyst which could promote the SMSI at a low temperature of 300 °C. Huang et al. [109] analyzed the alkali metal effect on the zeolite-supported catalyst and compared the modification of Na and K. The addition of alkali metal decreased the catalyst acidity, and the π-bond of acetylene with alkali metal ions enhanced the hydrogenation activity; the alkali metal modified the adsorption energy of ethylene and reduced the hydrogen spillover on the support, thus increasing the ethylene selectivity. Because K was less acidic than Na, the modification by K was more effective. Moreover, according to Panpranot et al. [82, 110], the addition of Zn or Ni to Pd/Al_2O_3 would lead to the formation of spinels. The spinels decreased the catalyst acidity and suppressed deactivation.

The modification by reducible oxide support or additives shows similar effect as the SMSI effect. The Ti-modified Pd/SiO_2 exhibited similar properties as Pd/TiO_2. The Ti modification diluted the active sites and changed the electronic and geometric properties of the Pd sites, thus improving the selectivity and stability. Differently, compared with the TiO_2-supported catalyst, the minor addition of Ti resulted in less decrease of hydrogenation activity [85, 111]. Moon et al. [112, 113] investigated into the modification by metals with different reducibilities (La, Ti, Nb, Ce). It was shown that the modification by La and Ti was similar; however, the

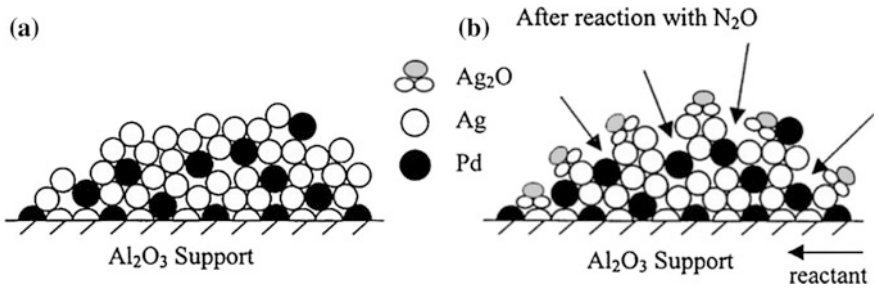

Fig. 1.8 Effect of N_2O pretreatment on PdAg catalyst. Reprinted from Ref. [101], with kind permission from Springer Science+Business Media

catalyst modified by La showed higher selectivity and lower activity, indicating a stronger modification by La. The effect of Nb was similar as Ti and La in selectivity, while showed increased hydrogenation activity due to the enhancement of hydrogen adsorption and dissociation by Nb. The enhancement of ethylene selectivity followed the order of La > Ti > Nb > Ce. On the La- or Nb-modified Pd/SiO_2, the addition of a third metal (Ti [93], Si [114]) further changed the surface electronic properties, stabilized the modification by La, and increased the selectivity to ethylene. Moreover, the deposition of Ag and Cu [115] on Pd changed the electronic properties and increased the ethylene selectivity to different extents. Because the Cu atom was small in diameter, it binded more easily with the defect sites on Pd and showed more significant modification effect than Ag. Other than that, the addition of La and Ce played a positive effect in the selective hydrogenation of light hydrocarbons [93, 116], gasoline [117], and benzene [118–120].

The modifications by organic groups have also been investigated. The effects were classified into four types: (1) to stabilize the metal particles and increase the dispersion [121, 122], to reduce the metal leaching [123]; (2) to modify electronic properties or to change metal structure [121, 124–126]; (3) to deactivate the catalyst and dilute the active sites [122, 123, 127, 128]; and (4) to affect the mass transfer and to decrease the formation of PdH_x phase [72]. The organic species contained N, P, B, Si, O, S, Cl, etc. Because the organic molecules are different in molecular sizes, structures, and elements, the modification mechanism was not fully defined. Boitiaux et al. [129] investigated into the modification of a series organic species and believed that the modification mainly acted as electronic effect. The effects were closely related to the chemical groups in the organic species.

1.4.3 Pd-Based Bimetallic Catalysts

By adding a second metal to the Pd catalyst and forming alloy, the selectivity could be greatly enhanced. Among the many bimetallic systems, Pd–Ag catalyst significantly improves the selectivity to ethylene and has been widely used in industry. The addition of Ag effectively increases the dispersion of Pd, decreases the hydrogenation activity, increases the ethylene selectivity, and increases the catalyst stability.

The synergetic effect of Pd–Ag could be explained by electronic effect and geometric effect. The geometric effect was the most important one in the Pd–Ag system [130–134]. Zhang et al. [130] and Khan et al. [132] investigated structural change by ambient pressure and ultra-high vacuum TPD experiments, respectively. After the addition of Ag, the Ag atoms segregated on the surface and diluted the Pd active sites. When the coverage of hydrogen was high, Pd tended to migrate onto the surface layer [132, 135]. The segregation of Ag in the sublayer decreased the amount of adsorbed hydrogen and decreased the formation of β-PdH_x phase, thus increasing the selectivity to ethylene. The adsorption properties of CO could reflect the catalytic properties. Khan et al. [131, 132], Smith et al. [98, 136], and Ma et al.

[134] found that the addition of Ag changed the CO adsorption geometry and CO adsorption energy. Sheth et al. [134] found by DFT calculation that the addition of Ag decreased the density of states, and the d-band center moved further from Fermi level. The electronic effect decreased the adsorption energies of the C1 and C2 species; therefore, the adsorption energy of ethylene was decreased; the bond formation reaction was more favored rather than bond breaking; as a result, the amount of dissociated hydrogen was decreased. The decreased adsorption energy of ethylene and the decreased dissociation degree of hydrogen together led to the increase in ethylene selectivity. Mei et al. [137] investigated the enhancement of Ag in the selective hydrogenation of acetylene by theoretical and experimental study. The decrease in the number of Pd active sites and the decrease in hydrogen adsorption energy both led to the decrease in the active hydrogen atoms. Combining the decrease in ethylene adsorption energy, the ethylene selectivity was enhanced. Pachulski et al. [138] proposed the idea that because of the decrease in formed hydrocarbon (which were useful for hydrogen transfer) on PdAg, the hydrogen availability was reduced, and the ethylene selectivity increased.

The addition of Ag not only improves the ethylene selectivity, but also improves the catalyst stability. Ahn et al. [57] found that due to the geometric effect, the green oil tended not to segregate on the catalyst surface because of the diluted Pd active sites; due to the electronic effect, the adsorption energy of 1,3-butadiene decreased and the possibility of oligomerization decreased. Combining the two reasons, Pd–Ag catalyst exhibited better stability. Pachulski et al. [138] investigated the Ag/Pd ratio effect and found that the lower Ag/Pd ratio was beneficial for the catalyst stability. The low Ag/Pd ratio could enhance the dispersion of Pd, while the high Ag/Pd ratio might lead to the Ag segregation and was not good for the dilution of Pd sites. According to the theoretical results [134], the addition of Ag suppressed the bond-breaking reactions and decreased the possibility of acetylene dissociation. Thus, the coke formation was suppressed. Lamberov et al. [139] investigated into the used industrial Pd–Ag catalysts and found that the metal loadings did not change much after reaction; however, after regeneration, due to the phase change, the amount of Ag that interacted with Pd decreased and the selectivity was lower than that of the fresh catalyst.

The preparation method also affects the properties of Pd–Ag catalyst. The reduction–deposition method was beneficial for Ag to bind with the defect Pd site, introducing more significant electronic effect [140]. On the core–shell Pd–Ag catalyst, the surface ratio of Ag was higher than the impregnated Pd–Ag catalyst. Ag covered more Pd active sites and form more profound geometric effect, resulting in a higher selectivity to ethylene [141]. The oxygenation and reduction processes were important for the Pd–Ag structure. The reduction at high temperature was beneficial for the improvement of ethylene selectivity and the control of green oil [98, 136]. The crystal phase of supports was considered as another factor that affected the Pd–Ag catalytic properties. The rutile–TiO_2-supported Pd–Ag showed enhanced ethylene selectivity; however, the anatase–TiO_2 showed little enhancement in selectivity. The possible reason was that the addition of Ag suppressed the Ti^{3+} formation [142, 143].

Table 1.3 The application of Pd-based bimetallic catalysts in selective hydrogenation reactions

Active metal	Reaction	Literature
Pd–Ag	Acetylene, 1,3-butadiene, phenyl acetylene	[57, 130–135, 137, 138, 157–161]
Pd–Au	Acetylene, 1,3-butadiene, 1-heptyne, isoprene	[159, 162–172]
Pd–Cu	Acetylene, phenyl acetylene, 1,3-butadiene, hexyne	[115, 127, 173–177]
Pd–Ga	Acetylene	[144–150]
Pd–Zn	Acetylene	[178, 179]
Pd–Sn	1,3-butadiene	[94, 180–184]
Pd–W	1-heptyne	[176, 185]
Pd–Co	Acetylene, 1,3-butadiene	[186, 187]
Pd–Mo	1,3-butadiene	[188]
Pd–Ni	1,3-butadiene	[189, 190]

Since 2006, Schlögl's group has investigated systematically into the Pd–Ga bimetallic catalyst. It was found that the Pd–Ga bimetallic catalyst showed similar selectivity to ethylene and similar stability as the Pd–Ag catalyst, as well as remained the similar activity as Pd [144–147]. The addition of Ga effectively diluted the Pd active sites, changed the band structure near Fermi level, and changed the adsorption properties. On Pd–Ga catalyst, the β-PdH_x phase was suppressed, and the amount of active hydrogen was decreased; thus, the selectivity to ethylene was enhanced [144, 145, 148]. Schlögl et al. [149] and He et al. [150] further verified the excellent performance of Pd–Ga bimetallic system by experimental study over supported catalysts. Other than that, the Pd–Ga system has also been studied via DFT calculations [151–156].

Other bimetallic systems have also been studied, such as Pd–Au, Pd–Cu, Pd–Zn, and Pd–Sn. The bimetallic formation mostly leads to geometric effect on the Pd catalyst and results in the improvement of ethylene selectivity. However, the bimetallic effects on the hydrogenation activity are different in different systems. In most bimetallic systems, the addition of the second metal always decreases the hydrogenation activity; examples are Pd–Ag, Pd–Au, Pd–Cu, Pd–Zn, etc. Only very few exhibit similar activity as Pd, such as Pd–Ga. The Pd-based bimetallic catalysts used for selective hydrogenation are summarized in Table 1.3.

1.4.4 Non-Pd Catalysts

Pd-based catalysts have been widely applied in industry and were extensively studied in research. Among the non-Pd catalysts, Au-based catalysts attracted a lot of attention because of its unique catalytic properties at nanoscale. In 2000, Jia et al.

[191] reported that the selectivity to olefin over Au monometallic catalyst could reach 100% at a temperature range of 313–523 K, but the activity strongly depended on the metal particle sizes. Choudhary et al. [192] compared the Au catalyst with the Pd catalyst and further verified Jia et al.'s [191] results. They also found that the activity of Au was much lower than that of Pd, and moreover, Au was less stable. By investigating the Au bimetallic catalysts [193–195], some metals could enhance the Au activity by alloyment, such as Au–Cu [193], Au–Fe [194], and Au–Ag [195].

On the other hand, considering the limited resource and the high cost of Pd, the non-precious metal catalysts have also been investigated. The Ni-based catalyst showed high hydrogenation activity among the non-precious monometallic catalysts. By alloying Ni with Cu [196], Co [196], or Sn [197], the olefin selectivity could be adjusted. Studt et al. [198] predicted that Ni-Zn had good selectivity to ethylene in the selective hydrogenation of acetylene and the prediction was verified by experiments [199, 200]. Besides, the transition metal carbides (e.g., Mo_2C [201]) and nitrides (e.g., Mo_2N [202, 203]) were reported to show good performance in the selective hydrogenation reactions.

1.5 Thesis Outline

Based on the three difficulties in the selective hydrogenation reactions: (1) the control of complete hydrogenation, (2) the control of the oligomerization reactions (coke formation), and (3) the control of temperature inside the fixed-bed reactor, the current thesis will focus on the catalytic and process study of selective hydrogenation.

The conventional catalysts for selective hydrogenation are Pd-based catalysts. The modification of the Pd monometallic catalyst always results in the dilution/poison of active sites and improves the selectivity to ethylene at the sacrifice of the catalyst activity. The thesis will investigate into the development of an efficient catalyst by adding a non-precious metal Ni into Pd, to improve the catalyst selectivity, and to improve the efficiency. Because Ni has high hydrogenation activity among non-precious metals, the addition of Ni might contribute to the activity. Moreover, a kind of non-precious metal catalyst will be designed by replacing Pd with a transition metal carbide (Mo_2C). The catalytic research will be divided into the following sections:

1. Investigation into the PdNiPd(111) model surface by UHV experimental method and DFT calculations; design and prediction of the bimetallic catalyst.
2. Synthesis, characterization, and evaluation of the supported Pd–Ni catalysts.
3. Support effect on Pd–Ni bimetallic catalysts.
4. Non-precious metal catalyst (Ni/Mo_2C).

The improvement of olefin selectivity is limited by the development of catalyst, and the fixed-bed reactor used in industry is not good in temperature control. Hence, a novel process will be proposed and discussed in the thesis, in order to further improve the olefin selectivity and enhance the heat transfer. In the process, a liquid phase that has a selective solubility to acetylene over ethylene will be introduced into the system, and the ethylene selectivity will be greatly enhanced by coupling the selective absorption to the selective hydrogenation. The process research will be divided into the following parts:

1. The comparison of the liquid-phase with the conventional gas-phase hydrogenation.
2. Optimization of operation parameters (temperature, GHSV, H_2/C_2H_2).
3. Selection criteria for solvents.
4. Comparison with the SCILL (ionic liquid modification)-type catalyst.
5. Process optimization; proposal of pressurized multistage slurry reactor.

References

1. Yan K (1999) Progress in catalyst development for the selective hydrogenation of C2–C4. Mod Chem Ind 03:13–15
2. Gao H (1990) Removal of alkynes and dienes from 1-butene stream by selective hydrogenation. Qilu Petrochem Tech 02:40–45
3. Gao H, Gao B, Zhang J et al (1999) Selective hydrogenation of C3 cracking stream by catalytic distillation. Qilu Petrochem Tech 04:241–244
4. Liao L, Cheng J, Wang Z et al (2003) Catalytic distillation application in the selective hydrogenation of C3 stream. Chem Ind Eng 02:18–20
5. Dai W, Zhu J, Wan W (2000) Progress in the selective hydrogenation of C2 stream. Petrochem Tech 07:535–540
6. Gao B, Zhang J, Wang Y et al (2001) Application and development of selective hydrogenation. Qilu Petrochem Tech 04:269–272
7. Wang J, Liu Z, Zhao D (2008) Progress in hysomer technology for the utilization of C4 species. Petrochem Tech 01:100–105
8. Li Y, Fan Y (2003) Study on the selective hydrogenation of dienes and alkynes. J Sanxia Univ (Nat Sci) 04:381–384
9. Mao X, Zou X (1986) The formation of copper acetylide and its explosive properties. Fire Sci Tech 04:21–23
10. Zhang Q, Liu X, Zhu Q (1998) Current development in the selective hydrogenation of alkynes and dienes. Petrochem Tech 01:55–60
11. Hong D (2014) Review and outlook in petrochemical industry (China 2013). Chem Ind Eng Prog 07:1633–1658
12. Yang C (2013) The development of coal chemical industry is beneficial to reduce the external dependence of oil in China. Sino-Glob Energ 11:1–6
13. Li J, Zheng M, Zhang G et al (2012) Outlook on conventional and unconventional natural gas resources in China. Acta Petrol Sin S1:89–98
14. Chen J, Cheng Y, Xiong X et al (2009) Progress in thermal plasma pyrolysis of coal to acetylene. Chem Ind Eng Prog 03:361–367
15. Zhu X (2010) Imbalance in the PVC supply and demand. China Petro Chem Ind 02:26
16. Liu Z (2008) Challenges and development of PVC in China. China Chlor-Alkali 03:1–6

17. Jiao Y (2013) Analysis and forecast of PE market. Guangzhou Chem Eng 10:58–59
18. Dong X (2014) Analysis of factors on the operation of C2 hydrogenation reactors in PetroChina Daqing. Jiangxi Petrochem Ind 02:85–88
19. Yang F, Zhang L, Xie C (2011) Optimization of C2 hydrogenation reactor. Contem Chem Ind 10:1007–1012
20. Ren Z, Yang Z, Zhang Q (2009) Progress in the Ni catalyst for the selective hydrogenation of gasoline. Petrchem Tech 01:98–102
21. Huang Y, Liu H (2008) Process study in the selective hydrogenation of 1-methyldicyclopentadiene. Tech Econ Petrochem 05:36–40
22. Wei H, Huang X, Lv H et al (2010) Operation parameters' effect on the selective hydrogenation of isoprene in trickle bed reactor. Petrochem Tech 12:1349–1353
23. Tian B, Dai W, Yang Z et al (2009) Selective hydrogenation of C5 dienes. Chem Ind Eng Prog 11:1932–1935
24. Zhang G (2006) Selective hydrogenation of OCT-M gasoline: process application. Petrochem Ind Tech 02:17–20
25. Li Z (2001) Design of tricle bed reactor for the liquid phase hydrogenation of hydrocarbons. Chem Eng (China) (03):33–36+33
26. Zhao B, Liu X, Li H (1991) Catalyst and process for the liquid phase hydrogenation of C3 stream. Petrochem Tech 04:255–261
27. Zhang S, Dai W, Qi D et al (2008) Application of novel catalyst in the selective hydrogenation of C3 stream. Chem Ind Eng Prog 03:464–467
28. Zhao B, Liu X (1987) Catalyst study in the liquid phase hydrogenation of propyne and propadiene. Petrochem Tech 12:821–827
29. Borodzinski A, Bond GC (2006) Selective hydrogenation of ethyne in ethene-rich streams on palladium catalysts. Part 1. Effect of changes to the catalyst during reaction. Catal Rev 48 (02):91–144
30. Huang L, Dai W, Tian B et al (2011) Progress in the selective hydrogenation of cracking stream. Petrochem Tech 04:450–456
31. Dai W, Zhu J, Wan W (2000) Process and catalyst progress in the selective hydrogenation of C2 stream. Petrochem Tech 07:535–540
32. Duca D, Frusteri F, Parmaliana A et al (1996) Selective hydrogenation of acetylene in ethylene feedstocks on Pd catalysts. Appl Catal A-Gen 146(2):269–284
33. Shell Int Res MIJ NV (1974) NL Patent 142934-B
34. Chemetron Corp. (1962) NL Patent 132820-B
35. Ventron Corp. (1976) CA Patent 1000306-A
36. Ventron Corp. (1974). US Patent 3804916-A
37. Frevel LK, Kressley LJ (1978) US Patent 4101451-A
38. Vadekar M, Robson H E (1983) US Patent 4387258-A
39. Molnar A, Sarkany A, Varga M (2001) Hydrogenation of carbon-carbon multiple bonds: chemo-, regio- and stereo-selectivity. J Mol Catal A-Chem 173(1–2):185–221
40. Molero H, Bartlett BF, Tysoe WT (1999) The hydrogenation of acetylene catalyzed by palladium: hydrogen pressure dependence. J Catal 181(1):49–56
41. Borodzinski A (1999) Hydrogenation of acetylene-ethylene mixtures on a commercial palladium catalyst. Catal Lett 63(1–2):35–42
42. Borodzinski A, Golebiowski A (1997) Surface heterogeneity of supported palladium catalyst for the hydrogenation of acetylene-ethylene mixtures. Langmuir 13(5):883–887
43. Vincent MJ, Gonzalez RD (2001) A Langmuir-Hinshelwood model for a hydrogen transfer mechanism in the selective hydrogenation of acetylene over a Pd/γ-Al_2O_3 catalyst prepared by the sol-gel method. Appl Catal A-Gen 217(1–2):143–156
44. Mei D, Sheth PA, Neurock M et al (2006) First-principles-based kinetic Monte Carlo simulation of the selective hydrogenation of acetylene over Pd(111). J Catal 242(1):1–15
45. Hevia MAG, Bridier B, Perez-Ramirez J (2012) Mechanistic study of the palladium-catalyzed ethyne hydrogenation by the temporal analysis of products technique. App Catal A-Gen 439:163–170

46. Sheth PA, Neurock M, Smith CM (2003) A first-principles analysis of acetylene hydrogenation over Pd(111). J Phys Chem B 107(9):2009–2017
47. Xie X, Song X, Dong W et al (2014) Adsorption mechanism of acetylene hydrogenation on the Pd (111) surface. Chin J Chem 32(7):631–636
48. Duca D, Barone G, Varga Z (2001) Hydrogenation of acetylene-ethylene mixtures on Pd catalysts: computational study on the surface mechanism and on the influence of the carbonaceous deposits. Catal Lett 72(1–2):17–23
49. Duca D, Varga Z, La Manna G et al (2000) Hydrogenation of acetylene-ethylene mixtures on Pd catalysts: study of the surface mechanism by computational approaches: metal dispersion and catalytic activity. Theor Chem Acc 104(3–4):302–311
50. Li JN, Pu M, He SH et al (2011) Reaction mechanism of acetylene hydrogenation catalyzed by Pd-8 cluster. Acta Phys Chim Sin 27(4):793–800
51. Li JN, Pu M, Ma CC et al (2012) The effect of palladium clusters (Pd-n, n = 2–8) on mechanisms of acetylene hydrogenation: a DFT study. J Mol Catal A-Chem 359:14–20
52. Scholten JJF, Konvalinka JA (1966) Hydrogen-deuterium equilibration and parahydrogen and orthodeuterium conversion over palladium: kinetics and mechanism. J Catal 5(1):1–17
53. Larsson M, Jansson J, Asplund S (1998) The role of coke in acetylene hydrogenation on Pd/α-Al_2O_3. J Catal 178(1):49–57
54. Ahn IY, Lee JH, Kum SS et al (2007) Formation of C4 species in the deactivation of a Pd/SiO_2 catalyst during the selective hydrogenation of acetylene. Catal Today 123 (1–4):151–157
55. Xu Q, Smith CM, Blackson J et al (2005) TEM study on catalyst deactivation during selective acetylene hydrogenation. Microsc Microanal 11(S02):1576–1577
56. Liu RJ, Crozier PA, Smith CM et al (2005) Metal sintering mechanisms and regeneration of palladium/alumina hydrogenation catalysts. App Catal A-Gen 282(1–2):111–121
57. Ahn IY, Lee JH, Kim SK et al (2009) Three-stage deactivation of Pd/SiO_2 and Pd-Ag/SiO_2 catalysts during the selective hydrogenation of acetylene. App Catal A-Gen 360(1):38–42
58. Sarkany A (2001) Formation of C4 oligomers in hydrogenation of acetylene over Pd/Al_2O_3 and Pd/TiO_2 catalysts. React Kinet Catal Lett 74(2):299–307
59. Esmaeili E, Rashidi AM, Mortazavi Y et al (2013) SMFs-supported Pd nanocatalysts in selective acetylene hydrogenation: pore structure-dependent deactivation mechanism. J Energ Chem 22(5):717–725
60. Almanza LO, Martinez OI (2001) Regeneration of supported palladium catalyst for selective hydrogenation of acetylene. In: Studies in surface science and catalysis, vol 139. Elsevier, pp 311–318
61. Liu JY, Lu HM, Ling ZG et al (2008) Catalytic properties of supported Pd/SBA-15 catalyst for selective hydrogenation of alkadienes. Chin J Catal 29(3):206–208
62. Riyapan S, Boonyongmaneerat Y, Mekasuwandumrong O et al (2014) Improved catalytic performance of Pd/TiO_2 in the selective hydrogenation of acetylene by using H_2-treated sol-gel TiO_2. J Mol Catal A-Chem 383:182–187
63. Leon MA, Nijhuis TA, van der Schaaf J et al (2012) Mass transfer modeling of a consecutive reaction in rotating foam stirrer reactors: selective hydrogenation of a functionalized alkyne. Chem Eng Sci 73:412–420
64. Panpranot J, Kontapakdee K, Praserthdam P (2006) Effect of TiO_2 crystalline phase composition on the physicochemical and catalytic properties of Pd/TiO_2 in selective acetylene hydrogenation. J Phys Chem B 110(15):8019–8024
65. Borodzinski A (2001) The effect of palladium particle size on the kinetics of hydrogenation of acetylene-ethylene mixtures over Pd/SiO_2 catalysts. Catal Lett 71(3–4):169–175
66. Tessier D, Rakai A, BozonVerduraz F (1996) Palladium-alumina catalysts: precursor, support and dispersion effects in selective hydrogenation. Bull Soc Chim Fr 133(6):637–642
67. Komhom S, Mekasuwandumrong O, Panpranot J et al (2009) Influence of preparation method on the nanocrystalline porosity of α-Al_2O_3 and the catalytic properties of Pd/α-Al_2O_3 in selective acetylene hydrogenation. Ind Eng Chem Res 48(13):6273–6279

68. Zakumbayeva GD, Toktabayeva NF, Kubasheva AZ et al (1994) Influence of the degree of dispersion of palladium on the selective hydrogenation of acetylene in an ethane-ethylene fraction. Petro Chem 34(3):249–258
69. Duca D, Liotta LF, Deganello G (1995) Selective hydrogenation of phenylacetylene on pumice-supported palladium catalysts. J Catal 154(1):69–79
70. Feng JT, Ma XY, Evans DG et al (2011) Enhancement of metal dispersion and selective acetylene hydrogenation catalytic properties of a supported pd catalyst. Ind Eng Chem Res 50(4):1947–1954
71. Komhom S, Mekasuwandumrong O, Praserthdam P et al (2008) Improvement of Pd/Al_2O_3 catalyst performance in selective acetylene hydrogenation using mixed phases Al_2O_3 support. Catal Comm 10(1):86–91
72. McKenna FM, Mantarosie L, Wells RPK et al (2012) Selective hydrogenation of acetylene in ethylene rich feed streams at high pressure over ligand modified Pd/TiO_2. Catal Sci Tech 2 (3):632–638
73. Pattamakomsan K, Aires FJCS, Suriye K et al (2011) Effects of impregnation solvent and reduction temperature on the catalytic performance of Pd/Al_2O_3 in the selective hydrogenation of 1,3-butadiene. React Kinet Mech Catal 103(2):405–417
74. Goetz J, Volpe MA, Touroude R (1996) Low-loaded Pd/α-Al_2O_3 catalysts: influence of metal particle morphology on hydrogenation of buta-1,3-diene and hydrogenation and isomerization of but-1-ene. J Catal 164(2):369–377
75. Liotta LF, Venezia AM, Martorana A et al (1997) Model pumices supported metal catalysts. 2. Liquid phase selective hydrogenation of 1,3-cyclooctadiene. J Catal 171(1):177–183
76. Pattamakomsan K, Suriye K, Dokjampa S et al (2010) Effect of mixed Al_2O_3 structure between θ- and α-Al_2O_3 on the properties of Pd/Al_2O_3 in the selective hydrogenation of 1,3-butadiene. Catal Comm 11(5):311–316
77. Boitiaux JP, Cosyns J, Vasudevan S (1983) Hydrogenation of highly unsaturated hydrocarbons over highly dispersed palladium catalyst: part I: behaviour of small metal particles. Appl Catal 6(1):41–51
78. Wehrli JT, Thomas DJ, Wainwright MS et al (1991) Selective hydrogenation of propyne over supported copper-catalysts: influence of support. Appl Catal 70(2):253–262
79. Primet M, Elazhar M, Guenin M (1990) Influence of the support towards platinum catalyzed 1,3-butadiene hydrogenation. Appl Catal 58(2):241–253
80. Zhu S, Hou R, Wang T (2012) Effects of supports and promoter ag on pd catalysts for selective hydrogenation of acetylene. Chin J Process Eng 12(3):489–496
81. Asplund S (1996) Coke formation and its effect on internal mass transfer and selectivity in Pd-catalysed acetylene hydrogenation. J Catal 158(1):267–278
82. Chinayon S, Mekasuwandumrong O, Praserthdam P et al (2008) Selective hydrogenation of acetylene over Pd catalysts supported on nanocrystalline α-Al_2O_3 and Zn-modified α-Al_2O_3. Catal Comm 9(14):2297–2302
83. Houzvicka J, Pestman R, Ponec V (1995) The role of carbonaceous deposits and support impurities in the selective hydrogenation of ethyne. Catal Lett 30(1–4):289–296
84. Tauster S, Fung S, Garten R (1978) Strong metal-support interactions: group 8 noble metals supported on titanium dioxide. J Am Chem Soc 100(1):170–175
85. Kang JH, Shin EW, Kim WJ et al (2002) Selective hydrogenation of acetylene on TiO_2-added Pd catalysts. J Catal 208(2):310–320
86. Lee DC, Kim JH, Kim WJ et al (2003) Selective hydrogenation of 1,3-butadiene on TiO_2-modified Pd/SiO_2 catalysts. App Catal A-Gen 244(1):83–91
87. Weerachawanasak P, Praserthdam P, Arai M et al (2008) A comparative study of strong metal-support interaction and catalytic behavior of Pd catalysts supported on micron- and nano-sized TiO_2 in liquid-phase selective hydrogenation of phenylacetylene. J Mol Catal A-Chem 279(1):133–139
88. Monteiro RD, Noronha FB, Dieguez LC et al (1995) Characterization of Pd-CeO_2 interaction on alumina support and hydrogenation of 1,3-butadiene. App Catal A-Gen 131 (1):89–106

89. Binet C, Jadi A, Lavalley JC et al (1992) Metal support interaction in Pd/CeO_2 catalysts—Fourier-transform infrared studies of the effects of the reduction temperature and metal loading.1. Catalysts prepared by the microemulsion technique. J Chem Soc-Faraday Trans 88 (14):2079–2084
90. Kepinski L, Wolcyrz M (1997) Microstructure of Pd/CeO_2 catalyst: effect of high temperature reduction in hydrogen. App Catal A-Gen 150(2):197–220
91. Shao Y, Xu Z, Wan H et al (2010) Influence of ZrO_2 properties on catalytic hydrodechlorination of chlorobenzene over Pd/ZrO_2 catalysts. J Hazard Mater 179(1–3):135–140
92. Zhou J, Han Y, Wang W et al (2013) Reductive removal of chloroacetic acids by catalytic hydrodechlorination over Pd/ZrO_2 catalysts. Appl Catal B-Environ 134:222–230
93. Kim E, Shin EW, Bark CW et al (2014) Pd catalyst promoted by two metal oxides with different reducibilities: properties and performance in the selective hydrogenation of acetylene. App Catal A-Gen 471:80–83
94. Pattamakomsan K, Ehret E, Morfin F et al (2011) Selective hydrogenation of 1,3-butadiene over Pd and Pd-Sn catalysts supported on different phases of alumina. Catal Today 164 (1):28–33
95. Borodzinski A, Bond GC (2008) Selective hydrogenation of ethyne in ethene-rich streams on palladium catalysts, part 2: steady-state kinetics and effects of palladium particle size, carbon monoxide, and promoters. Catal Rev 50(3):379–469
96. Garcia-Mota M, Bridier B, Perez-Ramirez J et al (2010) Interplay between carbon monoxide, hydrides, and carbides in selective alkyne hydrogenation on palladium. J Catal 273(2): 92–102
97. Lopez N, Bridier B, Perez-Ramirez J (2008) Discriminating reasons for selectivity enhancement of CO in alkyne hydrogenation on palladium. J Phys Chem C 112(25): 9346–9350
98. Zea H, Lester K, Datye AK et al (2005) The influence of Pd-Ag catalyst for ethylene hydrogenation restructuring on the activation energy in ethylene-acetylene mixtures. App Catal A-Gen 282(1–2):237–245
99. Azizi Y, Petit C, Pitchon V (2008) Formation of polymer-grade ethylene by selective hydrogenation of acetylene over Au/CeO_2 catalyst. J Catal 256(2):338–344
100. Bridier B, Hevia MAG, Lopez N et al (2011) Permanent alkene selectivity enhancement in copper-catalyzed propyne hydrogenation by temporary CO supply. J Catal 278(1):167–172
101. Praserthdam P, Phatanasri S, Meksikarin J (2000) Activation of acetylene selective hydrogenation catalysts using oxygen containing compounds. Catal Today 63(2–4):209–213
102. Ngamsom B, Bogdanchikova N, Borja MA et al (2004) Characterisations of $Pd\text{-}Ag/Al_2O_3$ catalysts for selective acetylene hydrogenation: effect of pretreatment with NO and N_2O. Catal Comm 5(5):243–248
103. Panpranot J, Aungkapipattanachai S, Sangvanich T et al (2007) Effect of N_2O pretreatment on fresh and regenerated $Pd\text{-}Ag/\alpha\text{-}Al_2O_3$ catalysts during selective hydrogenation of acetylene. React Kinet Catal Lett 91(2):195–202
104. Tao J, Yu Z, Liu S (2001) CN Patent 1317367-A
105. Khrenov EG, Perminova EA, Falkov IG A (1997) RU Patent 2074027-C1
106. Chamberlain LR, Gibler CJ, Kemp RA et al (1993) US Patent 5177155-A
107. Park YH, Price GL (1992) Promotional effects of potassium on Pd/Al_2O_3 selective hydrogenation catalysts. Ind Eng Chem Res 31(2):469–474
108. Kim WJ, Kang JH, Ahn IY et al (2004) Effect of potassium addition on the properties of a TiO_2-modified Pd catalyst for the selective hydrogenation of acetylene. Appl Catal A-Gen 268(1–2):77–82
109. Huang W, Pyrz W, Lobo RF et al (2007) Selective hydrogenation of acetylene in the presence of ethylene on K^+-beta-zeolite supported Pd and PdAg catalysts. App Catal A-Gen 333(2):254–263

110. Wongwaranon N, Mekasuwandumrong O, Praserthdam P et al (2008) Performance of Pd catalysts supported on nanocrystalline α-Al_2O_3 and Ni-modified α-Al_2O_3 in selective hydrogenation of acetylene. Catal Today 131(1–4):553–558
111. Kim WJ, Kang JH, Ahn IY et al (2004) Deactivation behavior of a TiO_2-added Pd catalyst in acetylene hydrogenation. J Catal 226(1):226–229
112. Ahn IY, Kim WJ, Moon SH (2006) Performance of La_2O_3 or Nb_2O_5 added Pd/SiO_2 catalysts in acetylene hydrogenation. App Catal A-Gen 308:75–81
113. Kang JH, Shin EW, Kim WJ et al (2000) Selective hydrogenation of acetylene on Pd/SiO_2 catalysts promoted with Ti, Nb and Ce oxides. Catal Today 63(2–4):183–188
114. Kim WJ, Ahn IY, Lee JH et al (2012) Properties of Pd/SiO_2 catalyst doubly promoted with La oxide and Si for acetylene hydrogenation. Catal Comm 24:52–55
115. Kim SK, Lee JH, Ahn IY et al (2011) Performance of Cu-promoted Pd catalysts prepared by adding Cu using a surface redox method in acetylene hydrogenation. App Catal A-Gen 401 (1–2):12–19
116. Song S, Dai W, Zhu J et al (2004) Characterization of ethylene fraction selective hydrogenation catalyst using la promoted Al_2O_3 as support. Petrochem Tech 33(3):197–201
117. Liu T, Jin Y, Wei M et al (2003) Selective hydrogenation of FCC light gasoline on the Ni-La/Al_2O_3 catalyst. J Petrochem Univ 16 (4):24–26, 34
118. Wang H, Liu ZY, Shi RJ et al (2005) Deactivation and regeneration of amorphous Ru-La-B/ZrO_2 catalyst for selective hydrogenation of benzene to cyclohexene. Chin J Catal 26(5):407–411
119. Liu SC, Liu Z, Wang Z et al (2008) Characterization and study on performance of the Ru-La-B/ZrO_2 amorphous alloy catalysts for benzene selective hydrogenation to cyclohexene under pilot conditions. Chem Eng J 139(1):157–164
120. Sun HJ, Pan YJ, Li SH et al (2013) Selective hydrogenation of benzene to cyclohexene over Ce-promoted Ru catalysts. J Energ Chem 22(5):710–716
121. Chen PR, Chew LM, Kostka A et al (2013) The structural and electronic promoting effect of nitrogen-doped carbon nanotubes on supported Pd nanoparticles for selective olefin hydrogenation. Catal Sci Tech 3(8):1964–1971
122. Tailleur RG, Nascar JR (2012) Effect of H_2S on selective hydrogenation of diolefins using $NiPdCe_x$/Si-Al-coated structured packing catalyst. App Catal A-Gen 439:125–134
123. Crespo-Quesada M, Dykeman RR, Laurenczy G et al (2011) Supported nitrogen-modified Pd nanoparticles for the selective hydrogenation of 1-hexyne. J Catal 279(1):66–74
124. Wang KJ, Chen YY, Li XS et al (2009) Unusual catalytic performance for selective acetylene hydrogenation over Pd nanoparticles fabricated on N, O-containing organic groups modified silica. Catal Lett 127(3–4):392–399
125. Chan CWA, Mahadi AH, Li MMJ et al (2014) Interstitial modification of palladium nanoparticles with boron atoms as a green catalyst for selective hydrogenation. Nat Comm 5 (5):5787
126. Yang B, Burch R, Hardacre C et al (2014) Selective hydrogenation of acetylene over Pd-boron catalysts: a density functional theory study. J Phys Chem C 118(7):3664–3671
127. Cooper A, Bachiller-Baeza B, Anderson JA et al (2014) Design of surface sites for the selective hydrogenation of 1,3-butadiene on Pd nanoparticles: Cu bimetallic formation and sulfur poisoning. Catal Sci Tech 4(5):1446–1455
128. Shin EW, Choi CH, Chang KS et al (1998) Properties of Si-modified Pd catalyst for selective hydrogenation of acetylene. Catal Today 44(1–4):137–143
129. Boitiaux JP, Cosyns J, Robert E (1989) Additive effects in the selective hydrogenation of unsaturated-hydrocarbons on platinum and rhodium catalysts: 1. Influence of nitrogen-containing compounds. Appl Catal 49(2):219–234
130. Zhang QW, Li J, Liu XX et al (2000) Synergetic effect of Pd and Ag dispersed on Al_2O_3 in the selective hydrogenation of acetylene. Appl Catal A-Gen 197(2):221–228
131. Khan NA, Uhl A, Shaikhutdinov S et al (2006) Alumina supported model Pd-Ag catalysts: a combined STM, XPS, TPD and IRAS study. Surf Sci 600(9):1849–1853

132. Khan NA, Shaikhutdinov S, Freund HJ (2006) Acetylene and ethylene hydrogenation on alumina supported Pd-Ag model catalysts. Catal Lett 108(3–4):159–164
133. Sheth PA, Neurock M, Smith CM (2005) First-principles analysis of the effects of alloying Pd with Ag for the catalytic hydrogenation of acetylene-ethylene mixtures. J Phys Chem B 109(25):12449–12466
134. Ma Y, Diemant T, Bansmann J et al (2011) The interaction of CO with PdAg/Pd(111) surface alloys-A case study of ensemble effects on a bimetallic surface. Phys Chem Chem Phys 13(22):10741–10754
135. Gonzalez S, Neyman KM, Shaikhutdinov S et al (2007) On the promoting role of Ag in selective hydrogenation reactions over Pd-Ag bimetallic catalysts: a theoretical study. J Phys Chem C 111(18):6852–6856
136. Jin YM, Datye AK, Rightor E et al (2001) The influence of catalyst restructuring on the selective hydrogenation of acetylene to ethylene. J Catal 203(2):292–306
137. Mei D, Neurock M, Smith CM (2009) Hydrogenation of acetylene-ethylene mixtures over Pd and Pd-Ag alloys: first-principles-based kinetic Monte Carlo simulations. J Catal 268 (2):181–195
138. Pachulski A, Schodel R, Claus P (2011) Performance and regeneration studies of Pd-Ag/Al_2O_3 catalysts for the selective hydrogenation of acetylene. App Catal A-Gen 400 (1–2):14–24
139. Lamberov AA, Egorova SR, Il'yasov IR et al (2007) Changes in the course of reaction and regeneration of a Pd-Ag/Al_2O_3 catalyst for the selective hydrogenation of acetylene. Kinet Catal 48(1):136–142
140. Lee JH, Kim SK, Ahn IY et al (2011) Performance of Pd-Ag/Al_2O_3 catalysts prepared by the selective deposition of Ag onto Pd in acetylene hydrogenation. Catal Comm 12(13):1251–1254
141. Han YX, Peng D, Xu ZY et al (2013) TiO_2 supported Pd@Ag as highly selective catalysts for hydrogenation of acetylene in excess ethylene. Chem Comm 49(75):8350–8352
142. Kontapakdee K, Panpranot J, Praserthdam P (2007) Effect of Ag addition on the properties of Pd-Ag/TiO_2 catalysts containing different TiO_2 crystalline phases. Catal Comm 8 (12):2166–2170
143. Panpranot J, Nakkararuang L, Ngamsom B et al (2005) Synthesis, characterization, and catalytic properties of Pd and Pd-Ag catalysts supported on nanocrystalline TiO_2 prepared by the solvothermal method. Catal Lett 103(1–2):53–58
144. Osswald J, Giedigkeit R, Jentoft RE et al (2008) Palladium-gallium intermetallic compounds for the selective hydrogenation of acetylene—Part I: preparation and structural investigation under reaction conditions. J Catal 258(1):210–218
145. Osswald J, Kovnir K, Armbruester M et al (2008) Palladium-gallium intermetallic compounds for the selective hydrogenation of acetylene—Part II: surface characterization and catalytic performance. J Catal 258(1):219–227
146. Kovnir K, Osswald J, Armbruester M et al (2006) PdGa and Pd_3Ga_7: highly-selective catalysts for the acetylene partial hydrogenation. In: Studies in surface science and catalysis, vol 162. Elsevier, pp 481–488
147. Armbruester M, Wowsnick G, Friedrich M et al (2011) Synthesis and catalytic properties of nanoparticulate intermetallic Ga-Pd compounds. J Am Chem Soc 133(23):9112–9118
148. Kovnir K, Armbruester M, Teschner D et al (2009) In situ surface characterization of the intermetallic compound PdGa—A highly selective hydrogenation catalyst. Surf Sci 603(10–12):1784–1792
149. Ota A, Armbruester M, Behrens M et al (2011) Intermetallic compound Pd_2Ga as a selective catalyst for the semi-hydrogenation of acetylene: from model to high performance systems. J Phys Chem C 115(4):1368–1374
150. He Y, Liang L, Liu Y et al (2014) Partial hydrogenation of acetylene using highly stable dispersed bimetallic Pd-Ga/MgO-Al_2O_3 catalyst. J Catal 309:166–173
151. Bechthold P, Jasen P, Gonzalez E et al (2012) Hydrogen adsorption on PdGa(110): a DFT study. J Phys Chem C 116(33):17518–17524

152. Klanjsek M, Gradisek A, Kocjan A et al (2012) PdGa intermetallic hydrogenation catalyst: an NMR and physical property study. J Phys-Cond Matter 24(8):9
153. Rosenthal D, Widmer R, Wagner R et al (2012) Surface investigation of intermetallic PdGa (111). Langmuir 28(17):6848–6856
154. Bechthold P, Ardenghi JS, Nagel O et al (2014) Hydrogen adsorption on PdGa(100), (111) and (111) surfaces: a DFT study. Int J Hydrogen Energ 39(5):2093–2103
155. Prinz J, Gaspari R, Stockl QS et al (2014) Ensemble effect evidenced by CO adsorption on the 3-fold PdGa surfaces. J Phys Chem C 118(23):12260–12265
156. Prinz J, Pignedoli CA, Stockl QS et al (2014) Adsorption of small hydrocarbons on the three-fold PdGa surfaces: the road to selective hydrogenation. J Am Chem Soc 136 (33):11792–11798
157. Lu FF, Sun DH, Huang JL et al (2014) Plant-mediated synthesis of Ag-Pd alloy nanoparticles and their application as catalyst toward selective hydrogenation. ACS Sustain Chem Eng 2(5):1212–1218
158. Wei H-H, Yen CH, Lin H-W et al (2013) Synthesis of bimetallic Pd-Ag colloids in CO_2-expanded hexane and their application in partial hydrogenation of phenylacetylene. J Supercrit Fluids 81:1–6
159. Redjala T, Remita H, Apostolescu G et al (2006) Bimetallic Au-Pd and Ag-Pd clusters synthesised by gamma or electron beam radiolysis and study of the reactivity/structure relationships in the selective hydrogenation of buta-1,3-diene. Oil Gas Sci Technol 61 (6):789–797
160. Sarkany A (1997) Semi-hydrogenation of 1,3-butadiene over Pd-Ag/α-Al_2O_3 poisoned by hydrocarbonaceous deposits. Appl Catal A-Gen 165(1–2):87–101
161. Sarkany A (1997) Self-poisoning and aging of Pd-Ag/Al_2O_3 in semi-hydrogenation of 1,3-butadiene: Effects of surface inhomogeneity caused by hydrocarbonaceous deposits. In: Studies in surf sci and catalysis, vol 111. Elsevier, pp 111–118
162. Zhang YY, Diao WJ, Williams CT et al (2014) Selective hydrogenation of acetylene in excess ethylene using Ag- and Au-Pd/SiO_2 bimetallic catalysts prepared by electroless deposition. App Catal A-Gen 469:419–426
163. Pei GX, Liu XY, Wang AQ et al (2014) Promotional effect of Pd single atoms on Au nanoparticles supported on silica for the selective hydrogenation of acetylene in excess ethylene. New J Chem 38(5):2043–2051
164. Sarkany A, Horvath A, Beck A (2002) Hydrogenation of acetylene over low loaded Pd and Pd-Au/SiO_2 catalysts. Appl Catal A-Gen 229(1–2):117–125
165. Kittisakmontree P, Yoshida H, Fujita S et al (2015) The effect of TiO_2 particle size on the characteristics of Au-Pd/TiO_2 catalysts. Catal Comm 58:70–75
166. Wang Z, Zhang K, Yang K, Liu C (2014) Effect of alkali metal modification on selective hydrogenation of isoprene on Pd-Au/Al_2O_3 catalysts. China Pet Process Petrochem 45 (12):38–42
167. Zhang K, Wang Z, Ze B et al (2014) Selective hydrogenation of isoprene on Pd-Au/Al_2O_3 catalysts modified with Bi. Petrochem Tech 43(2):132–137
168. El Kolli N, Delannoy L, Louis C (2013) Bimetallic Au-Pd catalysts for selective hydrogenation of butadiene: influence of the preparation method on catalytic properties. J Catal 297:79–92
169. Kittisakmontree P, Pongthawornsakun B, Yoshida H et al (2013) The liquid-phase hydrogenation of 1-heptyne over Pd-Au/TiO_2 catalysts prepared by the combination of incipient wetness impregnation and deposition-precipitation. J Catal 297:155–164
170. Pongthawornsakun B, Fujita SI, Arai M et al (2013) Mono- and bi-metallic Au-Pd/TiO_2 catalysts synthesized by one-step flame spray pyrolysis for liquid-phase hydrogenation of 1-heptyne. App Catal A-Gen 467:132–141
171. Piccolo L, Piednoir A, Bertolini JC (2005) Pd-Au single-crystal surfaces: segregation properties and catalytic activity in the selective hydrogenation of 1,3-butadiene. Surf Sci 592 (1–3):169–181

172. Miura H, Terasaka M, Oki K et al (1993) Preparation of eggshell type Pd-Ag and Pd-Au catalysts by selective deposition and hydrogenation of 1,3-butadiene. In: Studies in surface science and catalysis, vol 75. Elsevier, pp 2379–2382
173. Wang ZQ, Zhou ZM, Zhang R et al (2014) Selective hydrogenation of phenylacetylene over Pd-Cu/γ-Al_2O_3 catalysts. Acta Phys-Chim Sin 30(12):2315–2322
174. McCue AJ, McRitchie CJ, Shepherd AM et al (2014) Cu/Al_2O_3 catalysts modified with Pd for selective acetylene hydrogenation. J Catal 319:127–135
175. Kang M, Song MW, Kim KL (2002) SMSI effect on ceria supported Cu-Pd catalysts in the hydrogenation of 1, 3-butadiene. React Kinet Catal Lett 75(1):177–183
176. Insorn P, Suriyaphaparkorn K, Kitiyanan B (2013) Selective hydrogenation of 1-hexyne using Pd-Cu and Pd-W supported on alumina catalysts. In: 11th international conference on chemical and process engineering, Pts 1–4 32:847–852
177. Guczi L, Schay Z, Stefler G et al (1999) Pumice-supported Cu-Pd catalysts: influence of copper on the activity and selectivity of palladium in the hydrogenation of phenylacetylene and but-1-ene. J Catal 182(2):456–462
178. Mashkovsky IS, Baeva GN, Stakheev AY et al (2014) Novel Pd-Zn/C catalyst for selective alkyne hydrogenation: evidence for the formation of Pd-Zn bimetallic alloy particles. Mendeleev Comm 24(6):355–357
179. Tew MW, Emerich H, van Bokhoven JA et al (2011) Formation and characterization of PdZn alloy: a very selective catalyst for alkyne semihydrogenation. J Phys Chem C 115 (17):8457–8465
180. Esmaeili E, Mortazavi Y, Khodadadi AA et al (2012) The role of tin-promoted Pd/MWNTs via the management of carbonaceous species in selective hydrogenation of high concentration acetylene. Appl Surf Sci 263:513–522
181. Choi SH, Lee JS (2000) XAFS study of tin modification of supported palladium catalyst for 1,3-butadiene hydrogenation in the presence of 1-butene. J Catal 193(2):176–185
182. Verdier S, Didillon B, Morin S et al (2003) Pd-Sn/Al_2O_3 catalysts from colloidal oxide synthesis—II. Surface characterization and catalytic properties for buta-1,3-diene selective hydrogenation. J Catal 218(2):288–295
183. Breinlich C, Haubrich J, Becker C et al (2007) Hydrogenation of 1,3-butadiene on Pd(111) and PdSn/Pd(111) surface alloys under UHV conditions. J Catal 251(1):123–130
184. Esmaeili E, Rashidi AM, Khodadadi AA et al (2014) Palladium-Tin nanocatalysts in high concentration acetylene hydrogenation: a novel deactivation mechanism. Fuel Process Technol 120:113–122
185. Lederhos CR, Juliana Maccarrone M, Badano JM et al (2011) Hept-1-yne partial hydrogenation reaction over supported Pd and W catalysts. App Catal A-Gen 396 (1–2):170–176
186. Menezes WG, Altmann L, Zielasek V et al (2013) Bimetallic Co-Pd catalysts: study of preparation methods and their influence on the selective hydrogenation of acetylene. J Catal 300:125–135
187. Sarkany A, Zsoldos Z, Stefler G et al (1995) Promoter effect of Pd in hydrogenation of 1,3-butadiene over Co-Pd catalysts. J Catal 157(1):179–189
188. Zina MS, Ghorbel A (2004) Pd-Mo bimetallic catalysts supported on Y-Zeolite: effect of molybdenum on structural and catalytic properties of palladium in partial hydrogenation of 1,3 butadiene. In: Recent advances in the science and technology of zeolites and related materials, Pts A–C, vol 154. Studies in surface science and catalysis, pp 2364–2370
189. Miegge P, Rousset JL, Tardy B et al (1994) Pd_1Ni_{99} and Pd_5Ni_{95}—Pd surface segregation and reactivity for the hydrogenation of 1,3-butadiene. J Catal 149(2):404–413
190. Gomez G, Belelli PG, Cabeza GF et al (2010) The adsorption of 1,3-butadiene on Pd/Ni multilayers: the interplay between spin polarization and chemisorption strength. J Solid State Chem 183(12):3086–3092
191. Jia JF, Haraki K, Kondo JN et al (2000) Selective hydrogenation of acetylene over Au/Al_2O_3 catalyst. J Phys Chem B 104(47):11153–11156

192. Choudhary TV, Sivadinarayana C, Datye AK et al (2003) Acetylene hydrogenation on Au-based catalysts. Catal Lett 86(1–3):1–8
193. Murugadoss A, Sorek E, Asscher M (2014) Structure and composition of Au-Cu and Pd-Cu bimetallic catalysts affecting acetylene reactivity. Top Catal 57(10–13):1007–1014
194. Sarkany A, Schay Z, Frey K et al (2010) Some features of acetylene hydrogenation on Au-iron oxide catalyst. App Catal A-Gen 380(1–2):133–141
195. Liu XY, Li YN, Lee JW et al (2012) Selective hydrogenation of acetylene in excess ethylene over SiO_2 supported Au-Ag bimetallic catalyst. App Catal A-Gen 439:8–14
196. Rodriguez JC, Marchi AJ, Borgna A et al (2001) Gas phase selective hydrogenation of acetylene: importance of the formation of Ni-Co and Ni-Cu bimetallic clusters on the selectivity and coke deposition. In: Studies in surface science and catalysis, vol 139. Elsevier, pp 37–44
197. Onda A, Komatsu T, Yashima T (2000) Characterization and catalytic properties of Ni-Sn intermetallic compounds in acetylene hydrogenation. Phys Chem Chem Phys 2(13):2999–3005
198. Studt F, Abild-Pedersen F, Bligaard T et al (2008) Identification of non-precious metal alloy catalysts for selective hydrogenation of acetylene. Science 320(5881):1320–1322
199. Xu JH, Huang YQ, Yang XF et al (2014) Enhancement of acetylene hydrogenation activity over Ni-Zn bimetallic catalyst by doping with Au. J Nanosci Nanotechno 14(9):6894–6899
200. Trimm DL, Cant NW, Liu IOY (2011) The selective hydrogenation of acetylene in the presence of carbon monoxide over Ni and Ni-Zn supported on $MgAl_2O_4$. Catal Today 178 (1):181–186
201. Yuanzhi L, Yining F, Jie H et al (2004) Selective liquid hydrogenation of long chain linear alkadienes on molybdenum nitride and carbide modified by oxygen. Chem Eng J 99(3): 213–218
202. Wu ZL, Hao ZX, Ying PL et al (2000) An IR study on selective hydrogenation of 1,3-butadiene on transition metal nitrides: 1,3-butadiene and 1-butene adsorption on Mo_2N/γ-Al_2O_3 catalyst. J Phys Chem B 104(51):12275–12281
203. Hao ZX, Wei ZB, Wang LJ et al (2000) Selective hydrogenation of ethyne on gamma-Mo_2N. App Catal A Gen 192(1):81–84

Chapter 2
Experimental and Theoretical Methods

2.1 Chemicals and Instruments

The chemicals used for catalyst preparation are shown in Table 2.1.

The gases used in the experiments are shown in Table 2.2.

The instruments used in the experiments are shown in Table 2.3.

2.2 Measurements of Model Surfaces

2.2.1 Ultra-High Vacuum (UHV) System

The UHV system is shown in Fig. 2.1, which is composed of two layers of stainless chamber.

Inside the chamber, the single crystal was placed at the center by directly spot-welding the crystal to two tantalum posts, for resistive heating and cooling with liquid nitrogen. A chromel-alumel K-type thermocouple was welded to the back of the crystal for temperature measurements. The UHV system is equipped with metal source, sputter gun, Auger electron spectroscopy (AES), low-energy electron diffraction (LEED), and mass spectrometer (MS) [1].

2.2.2 Preparation of Single-Crystal Surfaces

The Pd(111) (Princeton Scientific, 99.99%, 2 mm thick and 10 mm in diameter) surface was cleaned using sputtering-annealing cycles. The Ni-terminated, NiPdPd (111) and Pd-terminated, PdNiPd(111) bimetallic surfaces were prepared by controlling the current of the Ni source, the temperature of the Pd(111) surface and the

R. Hou, *Catalytic and Process Study of the Selective Hydrogenation of Acetylene and 1,3-Butadiene*, Springer Theses, DOI 10.1007/978-981-10-0773-6_2

Table 2.1 Chemicals used for catalyst preparation

Chemical	Standard	Purchase source
$Pd(NO_3)_2{\cdot}2H_2O$	99.9%	Alfa Aesar
$Ni(NO_3)_2{\cdot}6H_2O$	98%	Alfa Aesar
$PdCl_2$	99.9%	Alfa Aesar
HCl	AR	Beijing Chemical Works
γ-Al_2O_3	–	Alfa Aesar
SiO_2	–	Alfa Aesar
SiO_2	AR	Beijing Yili Fine Chemicals
CeO_2	99%	Alfa Aesar
ZrO_2	99%	Alfa Aesar
TiO_2	99.5%	Xiya Reagent
$(NH_4)_2MoO_4$	99.997%	Alfa Aesar
$C_6H_{12}N_2PO_3$	–	Linzhou Keneng Material Technology
(NMP)	CP	Sinoreagent
$C_{10}H_{22}$	CP	Sinoreagent

Table 2.2 Gases used in the experiments

Gas	Formula	Standard	Purchase source
Acetylene	C_2H_2	High purity	Dongfang Gases
Hydrogen	H_2	≥99.999%	Beiwen Gases
Nitrogen	N_2	≥99.999%	Beiwen Gases
Air	O_2/N_2	High purity	Beiwen Gases
5% 1,3-butadiene in nitrogen	5% C_4H_6/N_2	High purity	Beiwen Gases
4% hydrogen in nitrogen	4% H_2/N_2	High purity	Beiwen Gases
Methane	CH_4	High purity	Beiwen Gases
1% oxygen in nitrogen	1% O_2/N_2	High purity	Beiwen Gases

Table 2.3 Instruments used in the experiments

Instrument	Version/model	Purchase source
Electronic analytical balance	JA503B	Shanghai Yueping
Ultrasonic cleaner	KQ100DB	Kunshan Ultrasonic
Heating and drying oven	DHG-9035A	Shanghai Yiheng Technology
Muffle furnace	SX-G07103	Tianjin Zhonghuan Oven
Gas chromatography	GC7900	Shanghai Tianmei Tech.
GC-column	HP-Al/S PLOT	Angilent
Autoclave	GS-0.25/17.5	Weihai Chemical Machinery
Heating magnetic stirrer	DF-101S	Zhengzhou Changcheng
Precision pressure gauge	KY2010	Beijing Kaihangweiye Tech.
Point welding machine	250 dp/230	Miyachi Unitek
Thermocouple wire	spal-005-100	Omega
Tungsten mesh	40,924	Alfa Aesar

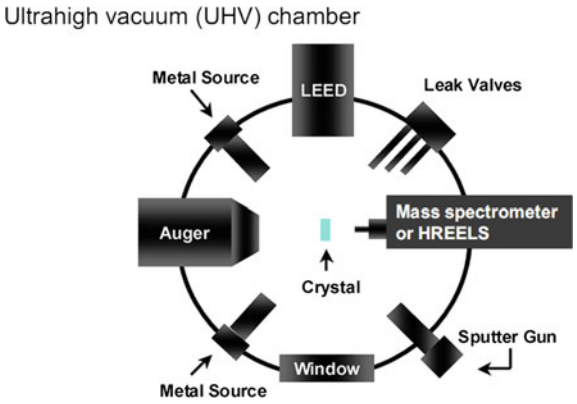

Fig. 2.1 UHV system

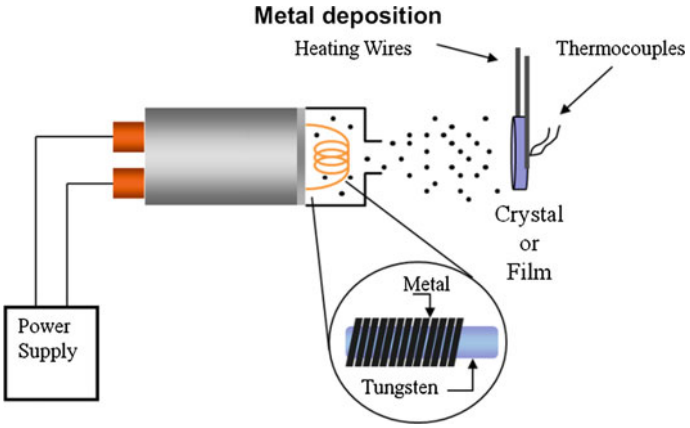

Fig. 2.2 Preparation of single-crystal surfaces

deposition time. The deposition process is shown in Fig. 2.2. The NiPdPd(111) surface was prepared by depositing Ni onto the Pd(111) surface while the surface was maintained at 300 K. The PdNiPd(111) surface was obtained by annealing the NiPdPd(111) surface at 600 K.

2.2.3 Temperature-Programmed Desorption (TPD)

In the TPD experiment, the single-crystal surface was firstly cooled to 120 K by liquid nitrogen; the gases were introduced into the UHV chamber and were allowed to adsorb on the crystal surface at the very low temperature; the single-crystal

surface was then heated at 3 K/s and the mass spectrometer (MS) was used to detect the desorbed gas-phase concentration. The mass balance was calculated by accounting the TPD desorption peaks, and the residues on the crystal surface was analyzed by AES.

2.3 Density Functional Theory (DFT) Calculations

All DFT calculations of binding energies were performed with the Vienna ab initio Simulation Package (VASP) [2–5]. The PW 91 functional [6] was used in the generalized gradient approximation (GGA) [7] calculation and a kinetic cutoff energy of 396 eV was chosen for the plane wave truncation. The surfaces were modeled using a periodic 4 × 4 unit cell, and the calculations used a 3 × 3 × 1 Monkhorst-Pack k-point grid. The clean Pd(111) surface was modeled by adding six equivalent layers of vacuum onto four Pd layers, in which the two bottom layers were frozen at metal distances of 2.80 Å in each layer and 2.3 Å between the layers, while the top two layers were allowed to relax to reach the lowest energy configuration. The Pd-terminated bimetallic surface, designated as PdNiPd(111), was derived by replacing the second layer of Pd atoms with Ni atoms. The binding energy of adsorbed molecules on the surface was calculated by subtracting the energies of the bare slab and of the free molecule from the total energy of the slab plus the adsorbed molecule. The configurations from VASP calculations were further optimized using the Cambridge Serial Total Energy Package (CASTEP) suite of programs to identify the transition state and calculate the activation energy for each reaction step.

2.4 Catalyst Preparation

2.4.1 Supported Catalyst

The supported catalysts were prepared by the incipient wetness impregnation method. An aqueous precursor solution was prepared by dissolving the desired amounts of metal salts in an amount of water just sufficient to fill the pores of 3 g of the support. The precursor solution was then added to the support by dropwise addition and was stirred thoroughly between droplets.

The Pd–Ni catalysts used in Chaps. 3 and 4 were dried at 100 °C for 10 h and calcined at 290 °C for 2 h. A ramp rate of 0.4 °C/min was used up to 100 and 0.8 °C/min up to 290 °C. A co-impregnation synthesis procedure was used for the bimetallic catalysts to produce the greatest extent of bimetallic bond formation, as verified previously for supported Pt–Ni catalysts [8]. The corresponding monometallic Ni and Pd catalysts were prepared to serve as control samples. The

Table 2.4 Temperature program and gas environment in the carburization

Step	Starting Temp./°C	Ending Temp./°C	Gas environment	Time/min
1	RT	600	20% CH_4/H_2	285
2	600	600	20% CH_4/H_2	120
3	600	600	H_2	60
4	600	30	H_2	Natural cooling
5	30	RT	1% O_2/N_2	360

compositions of the synthesized catalysts are as follows: 1.51 wt% Ni/γ-Al_2O_3, 0.91 wt% Pd/γ-Al_2O_3, and 1.51 wt% Ni-0.91 wt% Pd/γ-Al_2O_3, corresponding to a Ni:Pd atomic ratio of 3:1. The catalysts were reduced at 450 °C before use.

The 0.01% Pd/LSA-SiO_2 catalyst used in Chap. 6 was dried at 100 °C for 1 h and calcined at 400 °C for 4 h at the ramp rate of 5 °C/min. The precursor solution of H_2PdCl_4 was prepared by dissolving the desired amounts of equimolar $PdCl_2$ (99.9%, Alfa Aesar) and HCl (AR, Sinopharm) in deionized water. The reduction temperature was 200 °C.

The SCILL (supported catalyst with ionic liquid layer) was prepared by impregnating the ionic liquid onto the reduced catalyst and was dried at 80 °C overnight.

2.4.2 Mo_2C-Based Catalyst

The Mo_2C-based catalysts were prepared by the carburization of MoO_3 in CH_4/H_2. The MoO_3 was obtained by the calcination of ammonium molybdate at 350 °C for 6 h. When preparing Ni/Mo_2C, proper amount of $Ni(NO_3)_2$ was firstly impregnated with MoO_3, and the impregnated catalyst was dried and calcined as stated in Sect. 2.4.1 for Pd–Ni catalysts.

The carburization was carried out in a tubular furnace (internal diameter 60 mm). The calcined MoO_3 or Ni/MoO_3 was placed into a porcelain boat and the boat was placed in the center of the furnace. The temperature program and the gas environment for each step of the carburization are shown in Table 2.4

2.5 Catalyst Characterization

2.5.1 SEM

SEM (JSM 7401, JEOL) was used to measure the catalyst. The scan mode was LEI at an electron emission voltage of 3 kV and a current of 20 μA.

2.5.2 TEM

TEM measurements were performed using a JEOL2010F equipped with a Schottky field emission gun at 200 keV. All TEM images were taken in scanning (STEM) mode with a 12-nm camera length and a 1-nm-diameter nanoprobe. The TEM samples were prepared by first reducing the catalyst samples, then grinding the reduced sample into fine powders and suspending them in acetone. Droplets of the suspension were placed onto a carbon-coated copper grid. The grid was dried overnight before loading the sample into the TEM.

2.5.3 XRD

The crystalline phase of the catalysts was characterized from 20° to 80° 2θ by a Bruker Advance D8 X-ray diffractometer with Cu K_α ($\lambda = 1.5418$ Å) monochromatic radiation. The samples were dried and ground before being loaded onto the XRD instrument.

2.5.4 TG-DTA

The hydrocarbon species deposited on the catalysts were analyzed by TG-DTA (NETZSCH STA 409PC). In the measurement, 20 mg catalyst was used and was heated up from 30 to 800 °C at a ramp rate of 20 °C/min in an oxygen flow of 50 mL/min.

2.5.5 Physisorption

The surface area of the support was determined by Brunauer–Emmett–Teller (BET) method using N_2 adsorption-desorption on an Autosorb-1-C instrument (Autosorb iQ and AsiQwin, Quantachrome).

2.5.6 CO-Chemisorption

The number of active sites on each catalyst was measured through CO uptake with an AMI-200ip (Altamira). A quartz reactor was loaded with 100 mg of catalyst and reduced in 40 sccm of 50% H_2 in He at 450 °C for 1 h. After reduction, the catalyst was cooled to room temperature in He before pulsing CO. The amount of CO

flowing out of the reactor was measured with a thermal conductivity detector. Each adsorbed CO molecule was assumed to correspond to one active site, which provided a means to quantitatively compare the number of active sites between catalysts.

2.5.7 XAFS

EXAFS measurements were used to confirm the presence of Pd–Ni bimetallic bonds. Measurements of the Pd K-edge were performed on the X18B beamline at the National Synchrotron Light Source (NSLS), Brookhaven National Laboratory. The catalyst samples were pressed into a pellet with a thickness twice the absorption length to maximize the signal-to-noise ratio. The catalysts were placed in a chamber as shown in Fig. 2.3. The catalysts were reduced in situ in 40 sccm of 50% H_2 in He at 450 °C for 1.5 h, and the EXAFS spectra were collected at room temperature. The EXAFS spectra were calibrated to the Pd K-edge energy from a Pd reference foil.

The X-ray signal was analyzed using the IFEFFIT 1.2.11 data analysis package (Athena, Aretmis, Atoms, and FEFF6) [9, 10]. The structural information was obtained by Fourier-transforming the absorbance signal into R-space and then fitting each data set to the theoretical standards generated in FEFF6 [11]. The theoretical monometallic photoelectron amplitude and phase were calculated for the bulk Pd fcc structure. The passive electron reduction factor S_0^2 was found to be 0.878 from fitting the Pd-foil data. The seven parameters used in the fitting procedure were the correction to the edge energy, the coordination numbers of the Pd–Pd and Pd–Ni bonds, corrections to their model interatomic distances, and the mean square deviations in interatomic distances (EXAFS Debye-Waller factors).

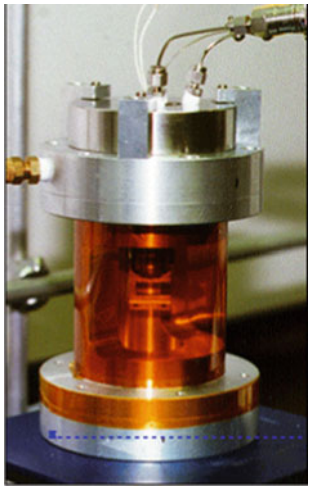

Fig. 2.3 Catalyst chamber for XAFS

2.6 Catalyst Evaluation

Three kinds of reactors were used in this thesis: the batch reactor equipped with a Fourier transform infrared (FT-IR) spectroscopy, the fixed-bed reactor equipped with gas chromatography (GC), and the slurry reactor with GC. The batch reactor was used to evaluate the catalyst activity and to obtain the kinetics; the fixed-bed reactor was used for steady-state operation, and for the evaluation of catalyst stability; the slurry reactor was used in the novel liquid-phase hydrogenation.

2.6.1 Batch Reactor

The batch reactor is composed of the in situ reaction chamber, the operation arm, and the gas pipelines, as shown in Fig. 2.4. FT-IR spectroscopy was used to monitor the gas-phase concentrations of reactants and products during the hydrogenation 1,3-butadiene. The reaction chamber is located in the IR detector cell and is connected with the operation arm, pumps, and the pipelines. The pipelines are in connection with gas cylinders and liquid sources. The FT-IR spectra were recorded with 4 cm^{-1} resolution using a Thermo Nicolet Nexus 470 spectrometer equipped with a mercury cadmium telluride (MCT-A) detector. Before each experiment, the catalyst was pressed onto a tungsten mesh and was connected to the heating and thermocouple systems.

For all FT-IR experiments, ~13.6 mg of supported catalyst was loaded into the IR cell, which was then evacuated for 12 h, until the system reached a pressure

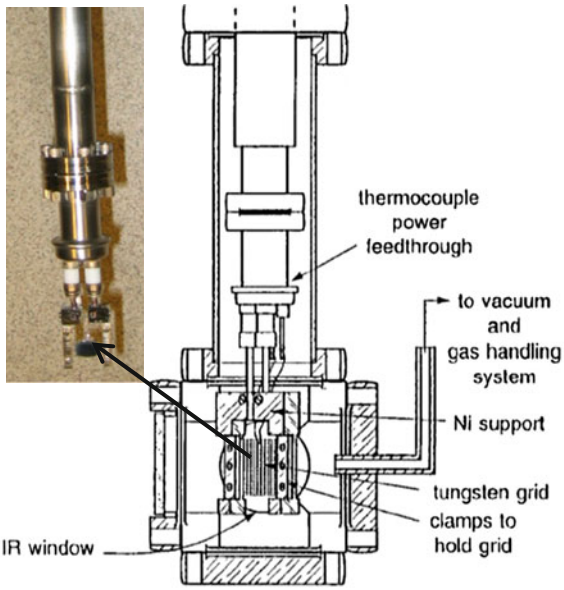

Fig. 2.4 Catalyst chamber for XAFS

below 10^{-6} Torr. The catalysts were reduced at 723 K in 30 Torr hydrogen for 30 min and the cell was then evacuated and a high-temperature flash (723 K) was performed to remove any surface species generated during the reduction period. The reduction cycle was repeated three times before performing the reaction experiments. After reducing the catalyst, a gas mixture was introduced into the reaction vessel simultaneously.

During the reaction, the gas-phase reactants and products were monitored by recording IR spectra (32 scans) every 30 s. The concentrations of the reactant and products were estimated using the absorbance intensities of their characteristic vibration modes as follows [8, 12, 13]: ν(C=C–C=C) at 1586 cm^{-1} for 1,3-butadiene,ν(C=C) at 1655 cm^{-1} for 1-butene, and$\nu(-CH_3)$ at 1466 cm^{-1} for *n*-butane. Because both 1-butene and butane contribute to the peak at 1466 cm^{-1}, in order to calculate the butane concentration, the intensity contributed by 1-butene should be substracted from the intensity at 1466 cm^{-1}:

$$\text{Intensity}_{\text{Butane (1466)}} = \text{Intensity}_{\text{Total (1466)}} - \alpha \cdot \text{Conc}_{\text{1-Butene (1655)}} \tag{2.1}$$

No 2-butene characteristic vibration modes (1697 and 1540 cm^{-1}) were found in the gas-phase products, as shown in Fig. 2.5. At present, we do not understand why 2-butene was not detected in the batch reactor. One potential explanation is that, in the batch environment, gas-phase products constantly undergo readsorption and reaction. More detailed study is needed to understand such phenomena; however, because our batch reactor results are primarily used for activity comparison, the absence of 2-butene does not affect the batch reactor conclusions of trends in hydrogenation activity (Fig. 2.5).

The concentrations of 1,3-butadiene, 1-butene, and butane were summed up for the estimation of carbon balance, as shown in Fig. 2.6. All carbon atoms were accounted for by performing a carbon balance, confirming the absence of 2-butenes and any other hydrocarbon fragments.

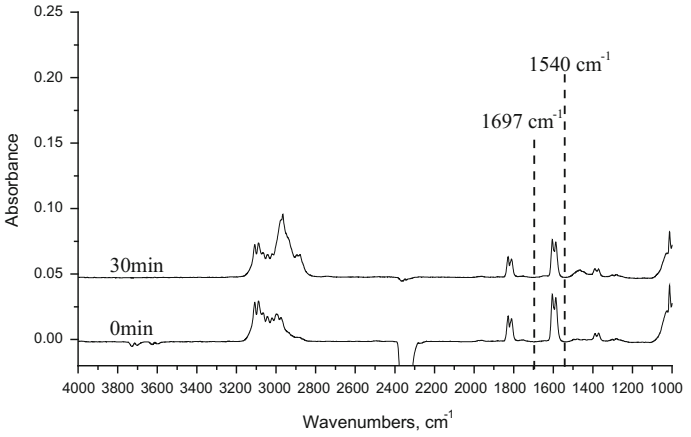

Fig. 2.5 IR spectra of the gas phase before and during the hydrogenation of 1,3-butadiene

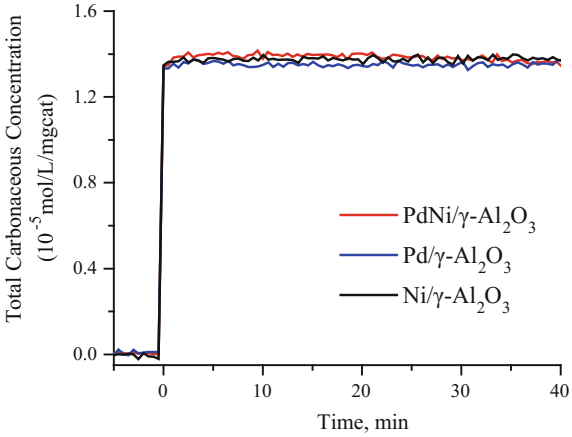

Fig. 2.6 Mass balance in the hydrogenation of 1,3-butadiene

2.6.2 Fixed-Bed Reactor

The fixed-bed reactor is shown in Fig. 2.7, composed of the inlet, reaction, control, and analysis sections. The reactant gases flow through filters, then to mass flow meters and finally to the fixed-bed reactor. The reactions studied in the thesis were performed at ambient pressure. The gas products were analyzed by a gas chromatograph by an auto six-way valve.

The fixed-bed reactor is 5 mm i.d. and 600 mm long. The catalyst was mixed with quartz particles in a ratio of 1:29 (100 mg catalyst and 2.9 g quartz particles). The temperature was monitored by a K-type thermocouple placed in the catalyst bed. Prior to reaction, the catalysts were reduced in hydrogen and then cooled to reaction temperature.

The outlet stream was analyzed online by a gas chromatograph equipped with a FID detector (GC 7900, Techcomp Ltd.) and an HP-Al/S PLOT column (Agilent, 30 m × 0.53 μm). The gas-phase carbon balance is above 95%. The selectivity of each product was calculated by dividing its concentration by the total products.

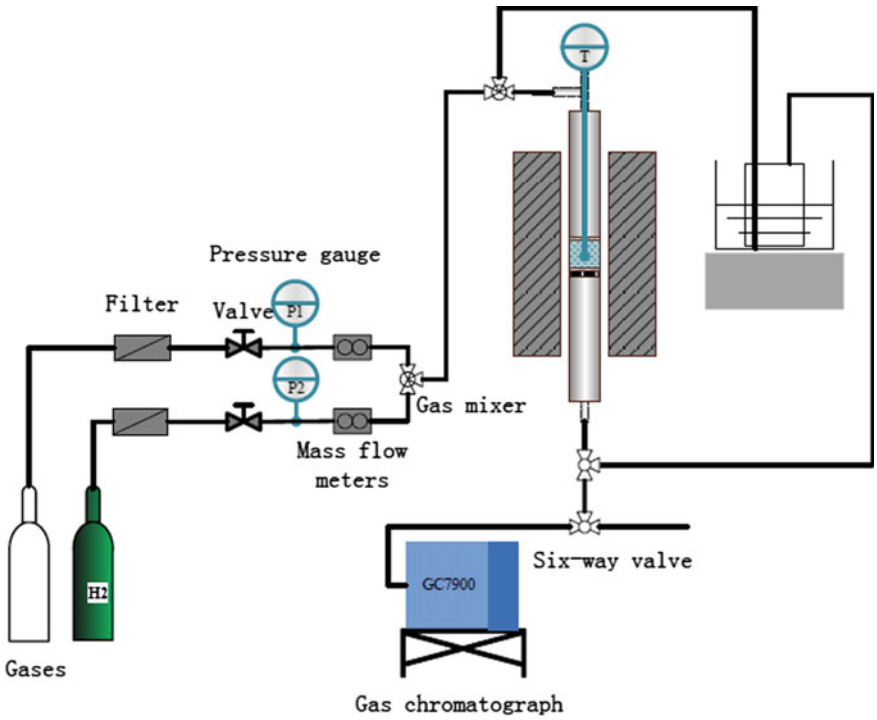

Fig. 2.7 Fixed-bed reactor system

2.6.3 Slurry Reactor

The liquid-phase hydrogenation of acetylene was carried out in a slurry reactor performed in a flat bottom flask with a magnetic stirrer and an oil bath to control the reaction temperature. The other parts were the same as in the gas-phase apparatus. The reduced catalyst and 80 mL NMP were placed in the flask. Experiments on the effect of stirring speed showed that under a low space velocity of 3600 ml/(gcat h), the acetylene conversion increased with increasing stirring speed until 600 rmp. In all the following experiments, a stirring speed of 700 rmp was used to eliminate the effect of gas–liquid mass transfer limitation.

2.7 Measurement of Solubility

The solubilities of acetylene and ethylene were measured isothermally from pressure decay observations using an apparatus similar to that used by Palgunadi et al. [14]. The apparatus is shown in Fig. 2.8. Two stainless steel vessels were used as

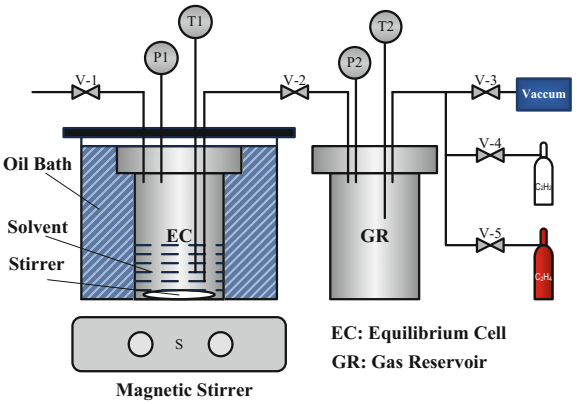

Fig. 2.8 Apparatus for the measurement of solubility

the equilibrium cell (EC) and gas reservoir (GR). The EC was placed in an oil bath with a magnetic stirrer and the GR was at room temperature. Both vessels were equipped with a thermocouple and a pressure gauge (0.4% in precision). The volumes of the two vessels with their tubes and fittings, V_{EC+TF1} and V_{GR+TF2}, were determined by the displacement of water with nitrogen gas (V_{EC+TF1} = 283 mL, V_{GR+TF2} = 291 mL).

The solubility was calculated with the following equation:

$$n_{sol} = n_{in} - n_{gas} = \frac{(P_2 - P_1)V_{GR}}{RT_2} - \left(\frac{(P_3 - P_1)(V_{EC} - V)}{RT_1} + \frac{(P_3 - P_1)V_{GR}}{RT_2}\right) \tag{2.2}$$

where the amount of gas was determined by the ideal gas law. An oil bath was used to control the temperature from 20 to 100 °C.

References

1. Yu WT, Barteau MA, Chen JG (2011) Glycolaldehyde as a probe molecule for biomass derivatives: reaction of C–OH and C=O functional groups on monolayer Ni surfaces. J Am Chem Soc 133(50):20528–20535
2. Ammann CM, Meehl GA, Washington WM et al (2003) A monthly and latitudinally varying volcanic forcing dataset in simulations of 20th century climate. Geophys Res Lett 30 (12):1657
3. Kresse G, Furthmuller J (1996) Efficient iterative schemes for ab initio total-energy calculations using a plane-wave basis set. Phys Rev B 54(16):11169–11186
4. Kresse G, Furthmuller J (1996) Efficiency of ab-initio total energy calculations for metals and semiconductors using a plane-wave basis set. Comput Mater Sci 6(1):15–50
5. Kresse G, Hafner J (1993) Abinitio molecular-dynamics for liquid-metals. Phys Rev B 47 (1):558–561

6. Perdew JP, Chevary JA, Vosko SH et al (1992) Atoms, molecules, solids, and surfaces—applications of the generalized gradient approximation for exchange and correlation. Phys Rev B 46(11):6671–6687
7. Teter MP, Payne MC, Allan DC (1989) Solution of Schrodinger-equation for large systems. Phys Rev B 40(18):12255–12263
8. Lonergan WW, Vlachos DG, Chen JG (2010) Correlating extent of Pt–Ni bond formation with low-temperature hydrogenation of benzene and 1,3-butadiene over supported Pt/Ni bimetallic catalysts. J Catal 271(2):239–250
9. Newville M (2001) IFEFFIT: interactive XAFS analysis and FEFF fitting. J Synchrot Radiat 8:322–324
10. Ravel B, Newville M (2005) ATHENA, ARTEMIS, HEPHAESTUS: data analysis for X-ray absorption spectroscopy using IFEFFIT. J Synchrot Radiat 12:537–541
11. Rehr JJ, Albers RC (2000) Theoretical approaches to x-ray absorption fine structure. Rev Mod Phys 72(3):621–654
12. Qi S, Yu W, Lonergan WW et al (2010) Low-temperature hydrogenation and dehydrogenation of 1, 3-cyclohexadiene on Pt/Ni bimetallic catalysts. Chin J Catal 31(8):955–960
13. Qi S, Yu W, Lonergan WW et al (2010) General trends in the partial and complete hydrogenation of 1,4-cyclohexadiene over Pt–Co, Pt–Ni and Pt–Cu bimetallic catalysts. ChemCatChem 2(6):625–628
14. Palgunadi J, Kim HS, Lee JM et al (2010) Ionic liquids for acetylene and ethylene separation: Material selection and solubility investigation. Chem Eng Process 49(2):192–198

Chapter 3
Selective Hydrogenation of 1,3-Butadiene on Pd–Ni Bimetallic Catalyst: From Model Surfaces to Supported Catalysts

3.1 Introduction

The industrial catalysts for selective hydrogenation are Pd-based precious metal catalysts. The addition of Ag in industrial catalyst could enhance the selectivity but significantly decreases the hydrogenation activity, which brings up the catalyst cost regarding the price per activity unit. Thus, it is important to find efficient and inexpensive catalyst for selective hydrogenation processes.

Bimetallic catalysts usually exhibit better performance than the corresponding monometallic catalysts. According to the state of the art, the bimetallic effect commonly leads to geometry effect, by which the active sites are diluted by the second metal and the activity per gram of catalyst is reduced. Some examples are Pd–Ag [1–14], Pd–Au [12, 15–25], Pd–Cu [26–32], and Pd–Zn [33, 34]. One exception is Pd–Ga—it exhibits higher selectivity and similar activity as the Pd monometallic catalyst [35–41]. However, the production of Ga strongly depends on the production of Zn and Al as a by-product [42], and as a result the industrial application of Ga is limited.

With regard to the selectivity enhancement and activity depreciation of bimetallic catalyst, the current chapter focuses to increase the catalyst efficiency in terms of activity per gram catalyst by adding a non-precious metal to Pd, as well as to enhance the selectivity and to maintain the catalyst cost.

Among the non-precious metals, Ni possesses excellent hydrogenation activity [43–47]. Chen et al. [48–55] have reported that the Pt–Ni bimetallic catalysts exited higher activity in various hydrogenation reactions. Based on the similarity of Pt and Pd, it is speculated that the synergic effect of Ni and Pd would probably enhance the catalytic activity. So far there have been some reports on Pd–Ni bimetallic system. Bertolini et al. [56–61] investigated on the minor Pd modification on Ni single-crystal surfaces such as Pd_5Ni_{95} and Pd_8Ni_{92}, and it was found the annealed Pd/Ni surface displayed higher hydrogenation activity (based on surface Pd atom) than the Pd surface in the hydrogenation of 1,3-butadiene. Goda et al. [62]

R. Hou, *Catalytic and Process Study of the Selective Hydrogenation of Acetylene and 1,3-Butadiene*, Springer Theses, DOI 10.1007/978-981-10-0773-6_3

calculated the adsorption energy by DFT and found that the ethylene adsorption energy on PdNiPd(111) was lower than on Pd(111). Wang [63] validated the low adsorption of ethylene on Pd–Ni bimetallic surface and further found that the activation barrier of acetylene hydrogenation was lower on Pd–Ni than on Pd. According to the above theoretical results [62, 63], the Pd–Ni bimetallic catalysts should exhibit higher activity and higher olefin selectivity for the selective hydrogenation reactions.

The current chapter will start from the fundamental study of PdNiPd(111) surface using ultra-high vacuum (UHV) experimental method and density functional theory (DFT) calculation. Then by using the surface science result, the properties of supported catalyst will be predicted. In parallel, supported Pd–Ni catalysts were characterized and evaluated in both batch and fixed-bed reactors to verify the predictions from the model surfaces. The schematic outline is shown in Fig. 3.1.

The prediction from surface science results are based on the following assumptions:

1. The adsorption properties are mainly affected by the surface layers of metal atoms on supported catalysts;
2. The most stable surface on the supported Pd catalyst is Pd(111) during hydrogenation reaction;
3. The Pd atoms tend to stay on the surface layer during hydrogenation reactions, which has been verified in UHV experiment [56–61].

Because of the difficulty in handling acetylene in the UHV system, the current work will use 1,3-butadiene as model molecule. The hydrogenation of 1,3-butadiene is used for the purification of butene streams. Among the products of 1,3-butadiene hydrogenation, 1-butene is the desired product for manufacturing polybutene and polyethylene.

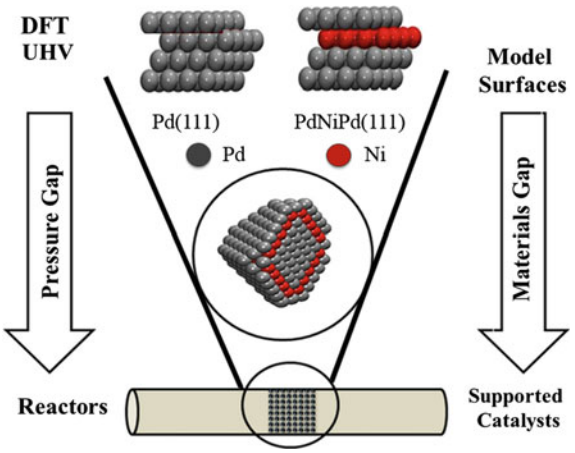

Fig. 3.1 Schematic outline of this chapter

3.2 DFT Calculation

The adsorption energies of 1,3-butadiene and its hydrogenation products were calculated over Pd(111) and PdNiPd(111) surfaces in order to compare and predict the butene selectivity. The activation barriers of each hydrogenation step were calculated for the estimation of hydrogenation activity over two kinds of metal surfaces.

The surfaces were modeled using a periodic 3 × 3 unit cell by four layers, and the calculations used a 3 × 3 × 1 Monkhorst-Pack k-point grid. The Pd-terminated bimetallic surface, designated as PdNiPd(111), was derived by replacing the second layer of Pd atoms with Ni atoms. During the calculation, the top two layers were allowed to move while the bottom two layers were fixed.

3.2.1 Adsorption Energy

Valcárcel et al. [64] reported some of the C4 adsorption geometries on Pd(111), as displayed in Fig. 3.2, while the current study optimized the C4 geometries on PdNiPd(111), as displayed in Fig. 3.3 [65]. As shown in the two figures, the C4 adsorption geometries resembles each other on Pd(111) and PdNiPd(111). The C4 molecules tend to adsorb on a Pd_4 region, with the π-bond or the C=C bond parallel with the surface.

The adsorption energies of 1,3-butadiene and its hydrogenation products are summarized in Table 3.1. The PdNiPd(111) surface exhibits a surface d-band center further away from the Fermi level and correspondingly lower binding energies for the adsorbed molecules, consistent with the reported rules by Nørskov [66]. On the PdNiPd(111) surface, 1-butene shows a very low binding energy (−0.13 eV), indicating that 1-butene should readily desorb from the surface after its formation rather than undergoing further hydrogenation. This suggests that 1,3-butadiene should be selectively hydrogenated to 1-butene rather than to butane. Similar to the current study, Gomez et al. [67] used DFT calculations and found that the adsorption energy of 1-butene was significantly lower on Pd_1Ni_3(111) than on Pd (111) and Pd_3Ni_1(111) surfaces. Based on this, they proposed that the Pd_1Ni_3(111) structure should give higher 1-butene selectivity.

3.2.2 Activation Barrier

As shown in the activation barrier of each step in Fig. 3.4, the hydrogenation of 1,3-butadiene to 1-butene on Pd(111) needs to overcome a relatively high activation barrier of 1.04 eV for the first step and 0.92 eV for the second step. In comparison,

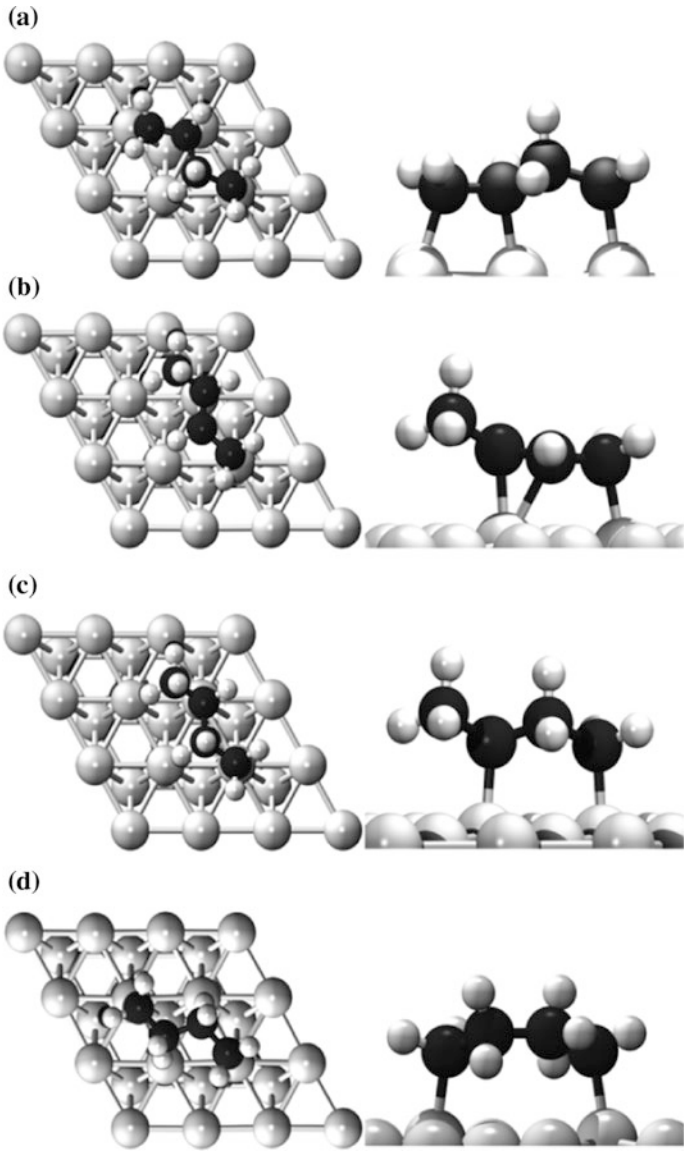

Fig. 3.2 Top and side views of optimized adsorption geometry of C4 species on Pd(111) surfaces: **a** 1-buten-4-yl **b** 2-buten-1-yl **c** butan-1,3-diyl **d** butan-1,4-diyl. Reprinted with permission from Ref. [64], Copyright (2005) American Chemical Society

lower reaction barriers are required on the PdNiPd(111) surface, with barriers for the first and second steps being 0.68 eV and 0.88 eV, respectively. The lower activation barriers on PdNiPd(111) suggest higher hydrogenation activity on the bimetallic surface.

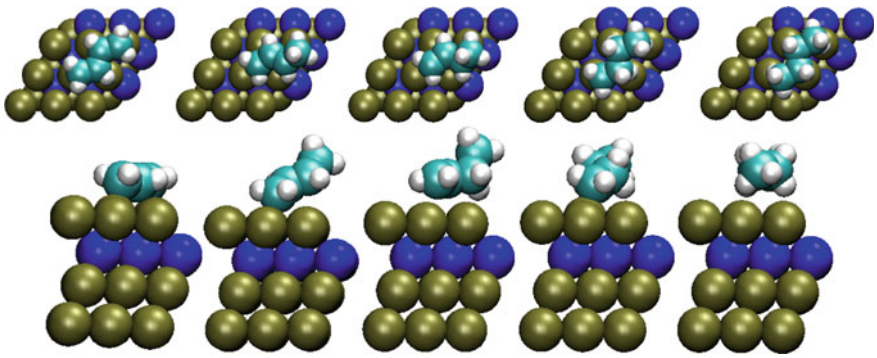

Fig. 3.3 Top and side views of optimized adsorption geometry of C_4H_6, C_4H_7, C_4H_8, C_4H_9, and C_4H_{10} molecules on PdNiPd(111) surfaces. Reprinted from Ref. [65], Copyright 2014, with permission from Elsevier

Table 3.1 Binding energies on Pd(111) and PdNiPd(111) surfaces. Reprinted from Ref. [65], Copyright 2014, with permission from Elsevier

Surface		Pd(111)	PdNiPd(111)
d-band center (eV)		−1.9	−2.25
Binding energy (eV)	C_4H_6	−1.49	−0.83
	C_4H_7	−1.62	−0.58
	C_4H_8	−0.55	−0.13
	C_4H_9	−1.58	−1.29
	C_4H_{10}	−0.11	−0.11

On Pd(111) surface:

$$C_4H_6 \underset{-H\ 0.64}{\overset{+H\ 1.04}{\rightleftharpoons}} C_4H_7 \underset{-H\ 0.49}{\overset{+H\ 0.92}{\rightleftharpoons}} C_4H_8 \underset{-H\ 0.49}{\overset{+H\ 1.01}{\rightleftharpoons}} C_4H_9 \underset{-H\ 1.05}{\overset{+H\ 0.87}{\rightleftharpoons}} C_4H_{10}$$

On PdNiPd(111) surface:

$$C_4H_6 \underset{-H\ 0.60}{\overset{+H\ 0.68}{\rightleftharpoons}} C_4H_7 \underset{-H\ 1.03}{\overset{+H\ 0.88}{\rightleftharpoons}} C_4H_8 \underset{-H\ 0.81}{\overset{+H\ 0.88}{\rightleftharpoons}} C_4H_9 \underset{-H\ 1.52}{\overset{+H\ 0.80}{\rightleftharpoons}} C_4H_{10}$$

Fig. 3.4 The reaction pathways for 1,3-butadiene hydrogenation on Pd(111) and PdNiPd(111) surfaces. The activation barriers are in eV. Reprinted from Ref. [65], Copyright 2014, with permission from Elsevier

3.3 UHV Results

3.3.1 Preparation of Single-Crystal Surfaces

In the UHV experiments, three single-crystal model surfaces will be used: Pd(111), NiPdPd(111), and PdNiPd(111). The Pd(111) surface was cleaned using sputtering–annealing cycles; the NiPdPd(111) was prepared by depositing Ni onto the Pd(111)

surface, while the surface was maintained at 300 K; the PdNiPd(111) surface was prepared by annealing the NiPdPd(111) surface to 600 K.

When preparing the NiPdPd(111) surface, the ratio of Ni and Pd peak intensities (I_{Ni}/I_{Pd}) from Auger measurements is plotted in Fig. 3.5a as a function of deposition time. Breaks were found at 4 min (point A) and 8 min (point B), suggesting that the deposition of the Ni atoms on the Pd(111) surface was in a layer-by-layer growth mode [68]. At point A, one layer of Ni atoms was deposited on the Pd(111) surface, referred to as the NiPdPd(111) surface.

After the preparation of the NiPdPd(111) surface, it was heated to higher temperatures, and Auger measurements were performed every 50 K [69]. The change in the Ni/Pd Auger peak ratio was plotted as a function of the surface temperature in Fig. 3.5b. The slope of the I_{Ni}/I_{Pd} curve changed when the surface was heated between 550 K (point C) and 650 K (point D), which indicated that Ni atoms started to diffuse into the Pd substrate [58, 70]. The observation of two distinct slopes in Fig. 3.5b suggested that two thermally induced diffusion regimes,

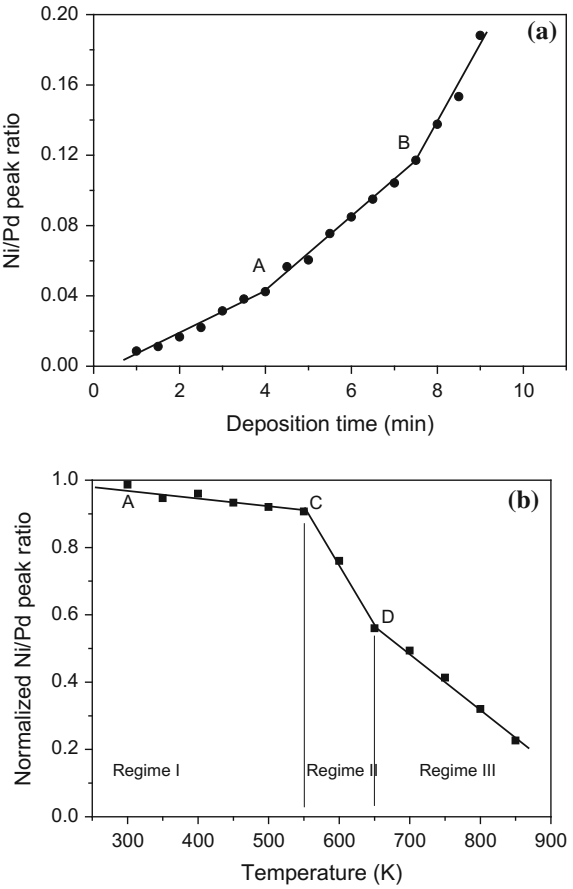

Fig. 3.5 **a** Deposition time versus AES Ni/Pd peak ratio and **b** thermal stability of the monolayer Ni surface (Regime I: NiPdPd(111) configuration; Regime II: transition from NiPdPd(111) to PdNiPd(111) configuration; Regime III: diffusion of Ni into bulk phase). Reprinted from Ref. [65], Copyright 2014, with permission from Elsevier

subsurface and bulk diffusion, might exist for the Ni/Pd(111) surface. Three regimes were found on the figure as the slope changes. Regime I, II, and III could be referred to the Ni-terminated surface, Ni diffusion into subsurface, and Ni diffusion into the bulk, respectively.

In the current chapter, the NiPd surface annealed to 600 K is referred to as the subsurface PdNiPd(111) structure in TPD measurements. However, the slope of Ni subsurface diffusion is greater than that of the Ni bulk diffusion, which is uncommon compared with the previous studies of metal/Pt(111) surfaces [71]. The only plausible explanation is that the decrease in the Ni AES signal is related to the term of $\exp[-d/\lambda]$, where d is the thickness of Pd layers screening the Ni atoms and λ the mean free path of Ni Auger electrons. Because the mean free path of the Ni (LMM) electrons is relatively large, it is possible that Ni can still be detected by AES, although at a reduced intensity of $\exp[-d/\lambda]$, even after Ni atoms diffuse several layers deep in the bulk. However, it is difficult to quantify the slope without knowing the rate and depth of Ni diffusion into the bulk Pd(111).

The surface structure and elemental composition of the 300 K and 600 K Ni/Pd(111) surfaces have been characterized using scanning tunneling microscopy (STM) and low-energy ion scattering (LEIS) [72], as shown in Figs. 3.6, 3.7, and 3.8. The STM images suggested that Ni monolayer deposition at 300 K and Ni diffusion into subsurface after annealing to 600 K formed a Pd-terminated surface. The LEIS results confirmed the thermally induced diffusion of Ni, leading to a Pd-terminated surface after annealing to 600 K. The PdNiPd(111) surface in the current work is the Pd-terminated surface, while the Ni has not been proved perfectly to stay in the second layer.

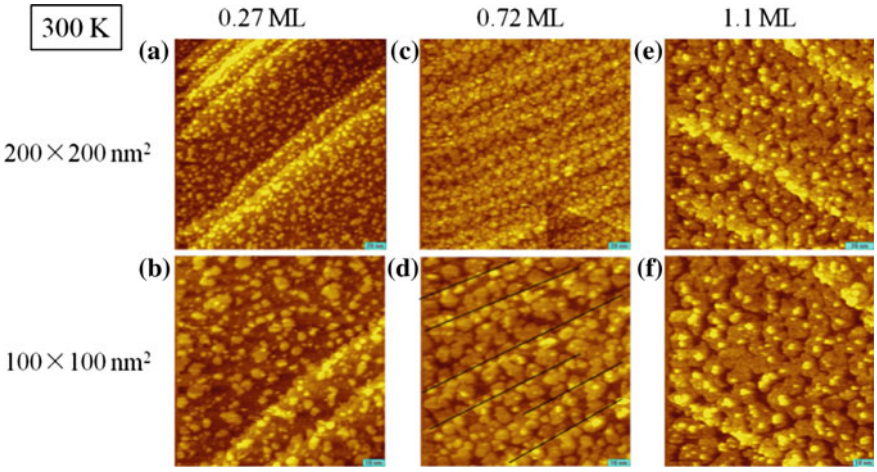

Fig. 3.6 STM images of as-deposited Ni/Pd(111) surfaces at three coverage at 300 K. Reprinted from Ref. [72], Copyright 2012, with permission from Elsevier

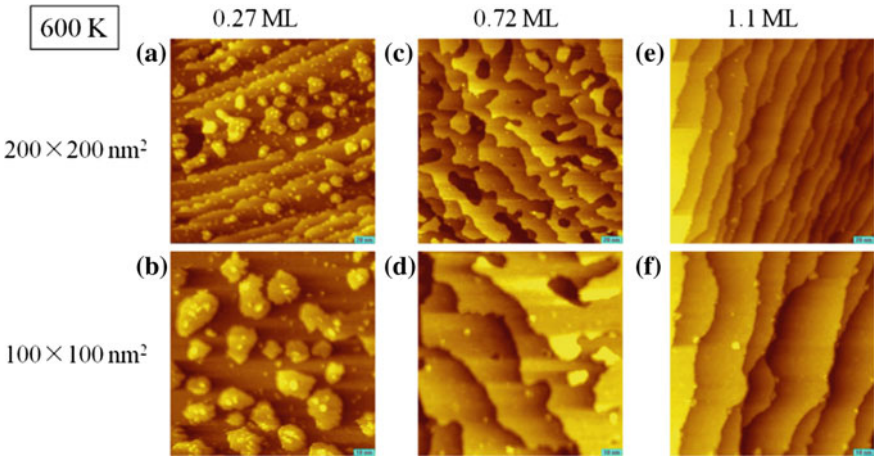

Fig. 3.7 STM images of Ni/Pd(111) surfaces after annealing to 600 K. Reprinted from Ref. [72], Copyright 2012, with permission from Elsevier

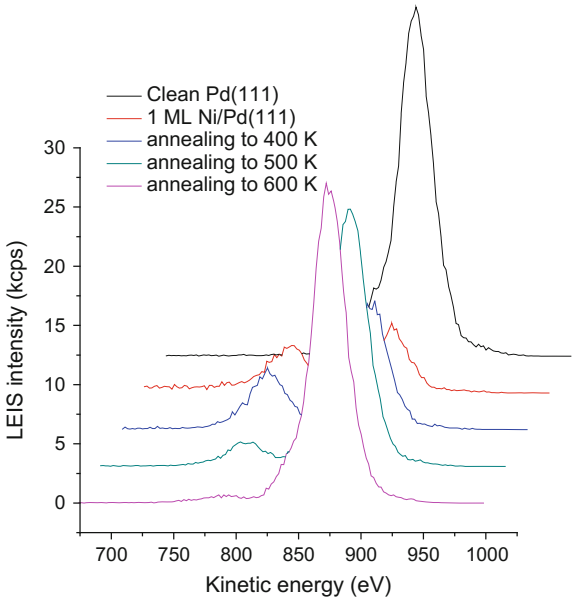

Fig. 3.8 LEIS intensity change of 1 ML Ni/Pd(111) surface before and after annealing up to 600 K

3.3.2 TPD Results

To verify the DFT results in Sect. 3.3.2, temperature programmed desorption (TPD) experiments of 1,3-butediene hydrogenation were performed on the Pd(111) and PdNiPd(111) surfaces. In the TPD experiment, 2.0 L 1,3-butadiene and 3.0 L hydrogen were introduced into the UHV chamber at 180 K, and the gas molecules

could adsorb on the surface of the as-prepared single crystal; the single crystal was then heated by a temperature program while a mass spectrometry was used to detect the desorbed gas intensities. The TPD results are displayed in Fig. 3.9. For comparison, the Ni-terminated, NiPdPd(111) surface was also studied.

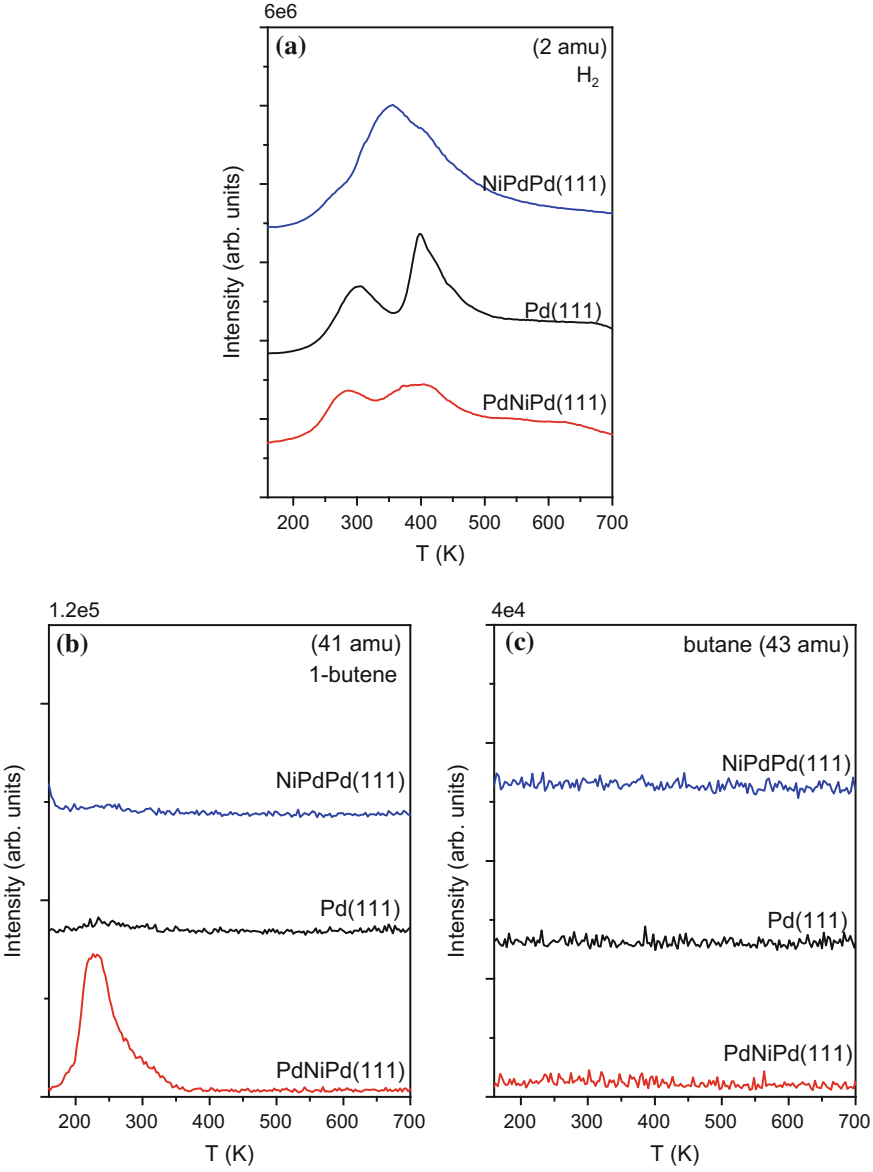

Fig. 3.9 TPD spectra of **a** 1-butene, and **b** butane following 2.0 L predosed H_2 and 2.0 L 1,3-butadiene on NiPdPd(111), Pd(111) and PdNiPd(111) surfaces. Reprinted from Ref. [65], Copyright 2014, with permission from Elsevier

Figure 3.9a shows the TPD spectra of hydrogen on the three surfaces. The hydrogen desorption peak areas indicate the amount of unreacted hydrogen on each surface. Two H_2 desorption peaks are observed at ~300 and ~400 K on both Pd (111) and PdNiPd(111) surfaces, which correspond to the subsurface hydrogen and surface hydrogen, respectively [73, 74]. On NiPdPd(111), only one desorption peak is found, indicating the surface Ni layer inhibits the hydrogen dissociation and diffusion into the bulk. Quantitative analysis of the hydrogen desorption peaks was made, as shown in Fig. 3.10 and Table 3.2. The peak areas of dissolved (subsurface) and adsorbed (surface) hydrogen on PdNiPd(111) are both smaller than their counterparts on Pd(111). The total area of hydrogen desorption peaks implies how much hydrogen was not reacted during the TPD experiment. As summarized in Table 3.2, the total peak areas of Pd(111) and NiPdPd(111) are similar while that of PdNiPd(111) is smaller, indicating more hydrogen was involved in the hydrogenation reaction during the TPD process.

In Fig. 3.9b, a desorption peak of 1-butene is observed around 230 K on the PdNiPd(111) surface, indicating the formation of 1-butene from the hydrogenation of 1,3-butadiene. In comparison, only a small peak around 230 K is observed from Pd(111), and no peak is observed from NiPdPd(111).

In Fig. 3.9c, no butane desorption peak is observed on the three surfaces, suggesting that there was no butane formed during the TPD experiments.

Based on the analysis of the total hydrogen amount and the butene formation amount, the TPD results demonstrate that the PdNiPd(111) bimetallic surface shows the highest activity for 1,3-butadiene hydrogenation, while the Pd(111) and NiPdPd(111) surfaces are not active. The 1,3-butadiene hydrogenation activities over the three surfaces follow the order of PdNiPd(111) > Pd(111) > NiPdPd(111). Furthermore, no butane formation is observed on the PdNiPd(11) surface, suggesting that the Pd-terminated bimetallic structure should have both high activity and selectivity toward 1-butene.

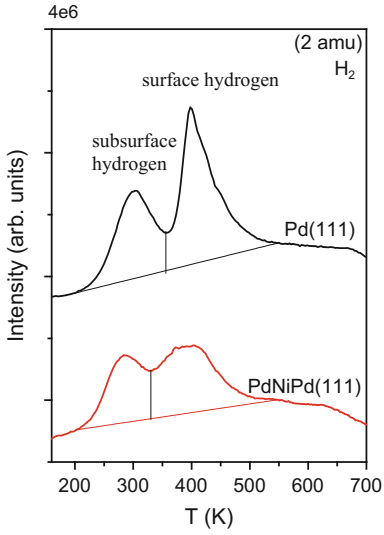

Fig. 3.10 TPD spectra of H_2 on Pd(111) and PdNiPd(111) surfaces

Table 3.2 Peak area analysis[a] of hydrogen species on Pd(111) and PdNiPd(111) surfaces

	Subsurface hydrogen	Surface hydrogen	Total
Pd(111)	5.5	8.9	14.4
PdNiPd(111)	4.0	6.4	10.4
NiPdPd(111)	–	–	14.6

[a]Non-dimensional peak surface area

It was reported in the literature that the subsurface hydrogen would compete with the surface adsorbed hydrogen in the reaction. For example, Valcarcel et al. [75] demonstrated that hydrogen dissolution was a major reason for the lower activity on Pd surfaces in a gas-phase static reactor, and the inhibition of Pd hydride formation in Pd_8Ni_{92} was the main reason for the activity improvement. Additionally, according to Rupprechter et al. [76], although the dissolved hydrogen could be available for surface hydrogenation, the reaction rate with dissolved hydrogen is much lower than with the surface adsorbed hydrogen. In the current study, the surface and dissolved hydrogen were analyzed quantitatively in Table 3.2. The surface hydrogen and the dissolved hydrogen on PdNiPd(111) are both ~25% lower than those on Pd(111), and the ratios of surface hydrogen to subsurface hydrogen are both approximately 1.6. Consequently, neither surface hydrogen nor subsurface hydrogen were inhibited on PdNiPd(111), as such the higher activity on PdNiPd(111) should not be attributed to the hydride effect.

Furthermore, Filhol et al. [77] reported the strain relaxation effect could contribute to the higher alkene hydrogenation activity on a Pd–Ni structure. Similar strain effects should also play a role in the higher hydrogenation activity on PdNiPd(111).

3.4 Characterization of Supported Catalysts

The surface science study from DFT calculations and UHV experiments shows consistently that the PdNiPd(111) surface possess higher activity and possibly higher 1-butene selectivity than the Pd(111) surface. Thus, it is predicted that the supported Pd–Ni bimetallic catalyst should also have better performance than the Pd monometallic catalyst. In the following sections, supported catalysts were synthesized by incipient wetness impregnation and were further characterized and tested for the 1,3-butadiene hydrogenation. γ–Al_2O_3 was selected as the catalyst support. The metal loading in the current study are 0.91% w.t. for Pd and 1.51% w.t. for Ni, with Pd/Ni atomic ratio of 1:3 on the bimetallic catalyst.

In the current section, Pd/γ–Al_2O_3, Ni/γ–Al_2O_3, and PdNi/γ–Al_2O_3 are characterized by TEM, CO-chemisorption, and XAFS, in order to obtain a better understanding of the structure of metal particles on the supported catalyst. The particle size distributions and average particle sizes were obtained from TEM.

The active sites were characterized by CO chemisorption. The XAFS measurement could not only provide important information on the metal coordination numbers and the bond distances on both monometallic and bimetallic catalysts, but also the oxidation changes before and after reduction.

3.4.1 TEM

The high-angle annular dark field (HAADF) TEM images of the catalysts are shown in Fig. 3.11. The particle size distributions were calculated by measuring horizontal particle diameters in several different images for each catalyst. The particle size distributions are relatively wide on the three catalysts, with the particle size ranging from 2 to 12 nm. The average particle sizes are calculated and are displayed in Table 3.3. The average particle sizes of PdNi/γ–Al_2O_3, Pd/γ–Al_2O_3 and Ni/γ–Al_2O_3 are 5.9, 5.1, and 5.2 nm, respectively. The particle size distributions and average particle sizes are similar on the three catalysts.

3.4.2 CO Chemisorption

The CO uptake values are 29.3, 15.2, and 12.3 μmol g^{-1} for PdNi/γ–Al_2O_3, Pd/γ–Al_2O_3, and Ni/γ–Al_2O_3, respectively, as shown in Table 3.3. The bimetallic catalyst has a higher value of CO uptake, indicating more active sites were formed.

3.4.3 XAFS

The Pd K-edge X-ray absorption near-edge structure (XANES) spectra and the extended X-ray absorption fine structure (EXAFS) spectra of the three catalysts are shown in Fig. 3.12.

Figure 3.12a shows the Pd K-edge XANES spectra of the Pd/γ–Al_2O_3 and PdNi/γ–Al_2O_3 catalysts before and after reduction, along with the spectra of the Pd foil for reference. The background-subtracted, edge-step normalized and k2-weighted Pd K-edge EXAFS data (χ(k)) are shown in R-space in Fig. 3.12b, along with the fits obtained using FEFF6 theory shown in Fig. 3.12c.

Careful examination of the Pd K-edge XANES and EXAFS reveals information regarding the extent of oxidation of the catalysts. Relatively intense peaks are presented in Fig. 3.12a at 24,350 eV prior to reduction and are attributed to the Pd–O bond, which is confirmed by the peaks at low radial distribution in

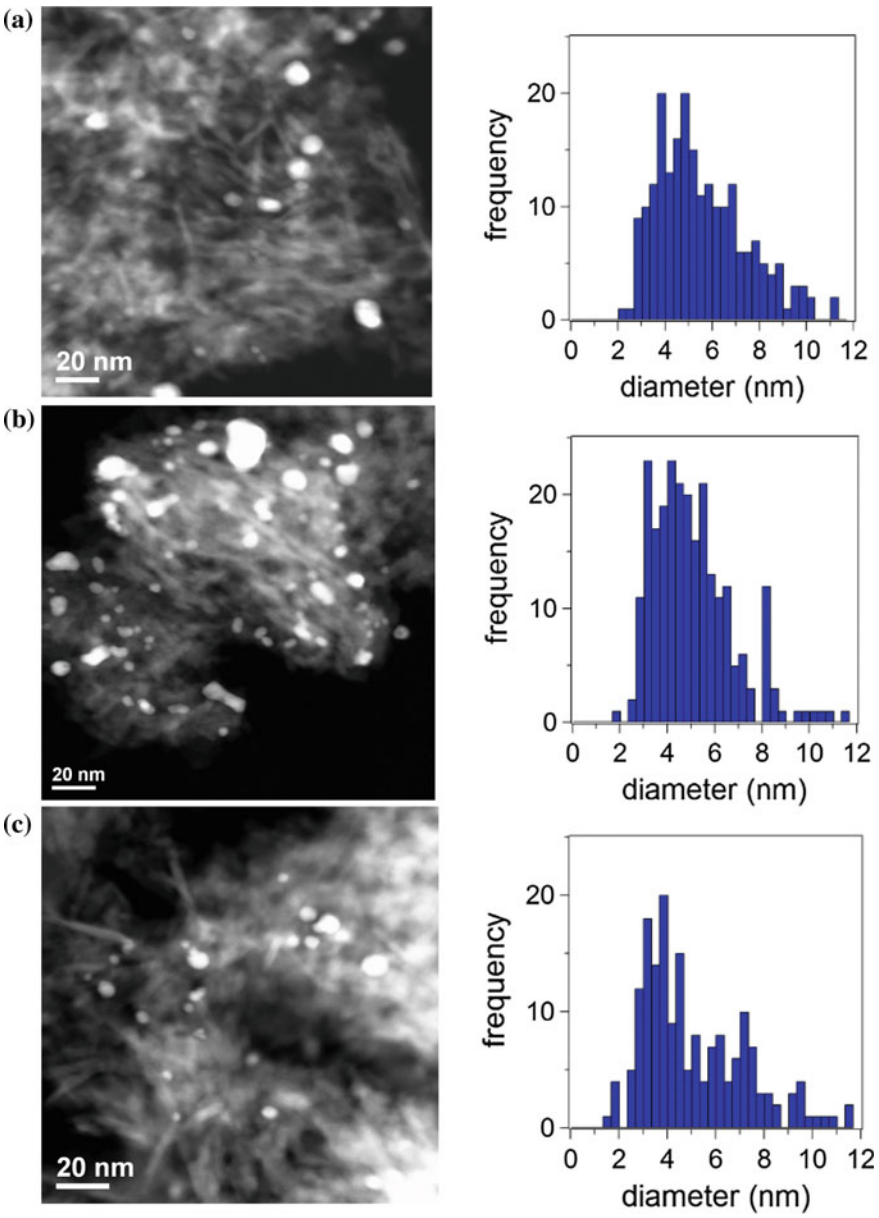

Fig. 3.11 HAADF TEM micrographs and particle size distributions for the catalysts: **a** PdNi/γ–Al_2O_3, **b** Pd/γ–Al_2O_3, **c** Ni/γ–Al_2O_3. Reprinted from Ref. [65], Copyright 2014, with permission from Elsevier

Table 3.3 Average particle size and CO chemisorption results on supported catalysts. Reprinted from Ref. [65], Copyright 2014, with permission from Elsevier

Catalyst	Average particle size (nm)	CO uptake (μmol g^{-1} cat)
PdNi/γ–Al_2O_3	5.9	29.3
Pd/γ–Al_2O_3	5.1	15.2
Ni/γ–Al_2O_3	5.2	12.3

Fig. 3.12b. After reduction in H_2, the spectra are more similar to that of the Pd foil in Fig. 3.12a, and the Pd–O peaks are not present in Fig. 3.12b. The Pd–O peaks are replaced by Pd–Ni peaks at slightly larger values of R. Together, these changes in the spectra indicate that Pd is in a metallic state after reduction in H_2.

Figure 3.12c presents the Fourier-transformed (R-space) data of the reduced catalysts and their associated fits from FEFF6. Fits were obtained by only including Pd–Pd and Pd–Ni contributions. The results from the fitting procedure are shown in Table 3.4. For both the Pd/γ–Al_2O_3 and PdNi/γ–Al_2O_3 catalysts, the Pd–Pd distances (2.83 and 2.79 Å, respectively) are larger than the bulk Pd–Pd distance (2.75 Å), possibly due to the formation of Pd hydride and the expansion of Pd–Pd bond [78, 79]. For the PdNi/γ–Al_2O_3 catalyst, the Pd–Pd distance is 2.79 Å, which is 0.04 Å smaller than the monometallic Pd–Pd distance (2.83 Å), while the Pd–Ni distance is 2.64 Å, which is 0.15 Å larger than the metallic Ni-Ni distance (2.49 Å). These changes in bond distance are most likely related to the strain of the larger Pd atoms residing on top of smaller Ni atoms. A similar effect was observed previously from EXAFS studies of the PtNi/γ–Al_2O_3 catalyst [49]. The EXAFS results confirm that Pd–Ni bimetallic bonds are formed in the catalysts because the bimetallic bond lengths are between that of either parent metal. In addition to the observed attenuation in bond lengths, the CN of Pd–Ni is 1.44, which indicates that bimetallic bonds are present in the Pd–Ni/γ–Al_2O_3 catalyst. During data fitting, good fits to the Pd K-edge experimental data could only be obtained by including both Pd–Pd and Pd–Ni contributions in the model, which further suggest that bimetallic bonds are present.

The overall coordination number is 9.77 on Pd/γ–Al_2O_3 and is 9.78 on PdNi/γ–Al_2O_3 (N(Pd−Pd) + N(Pd+Ni)). The similarity between the coordination numbers indicates that the metallic particles on each catalyst should be of similar size, consistent with the particle size statistics from TEM images as listed in Table 3.3. In the bimetallic catalyst, the ratio of Pd–Pd to Pd–Ni coordination numbers (CN (Pd−Pd):CN(Pd−Ni) = 8.34:1.44 = 5.79:1) is much larger than the atomic ratios of Pd:Ni (1:3). It implies that a considerable amount of remaining Ni atoms is located as monometallic Ni nanoparticles, dispersed across the γ–Al_2O_3 support, or is present in the form of $NiAl_2O_4$.

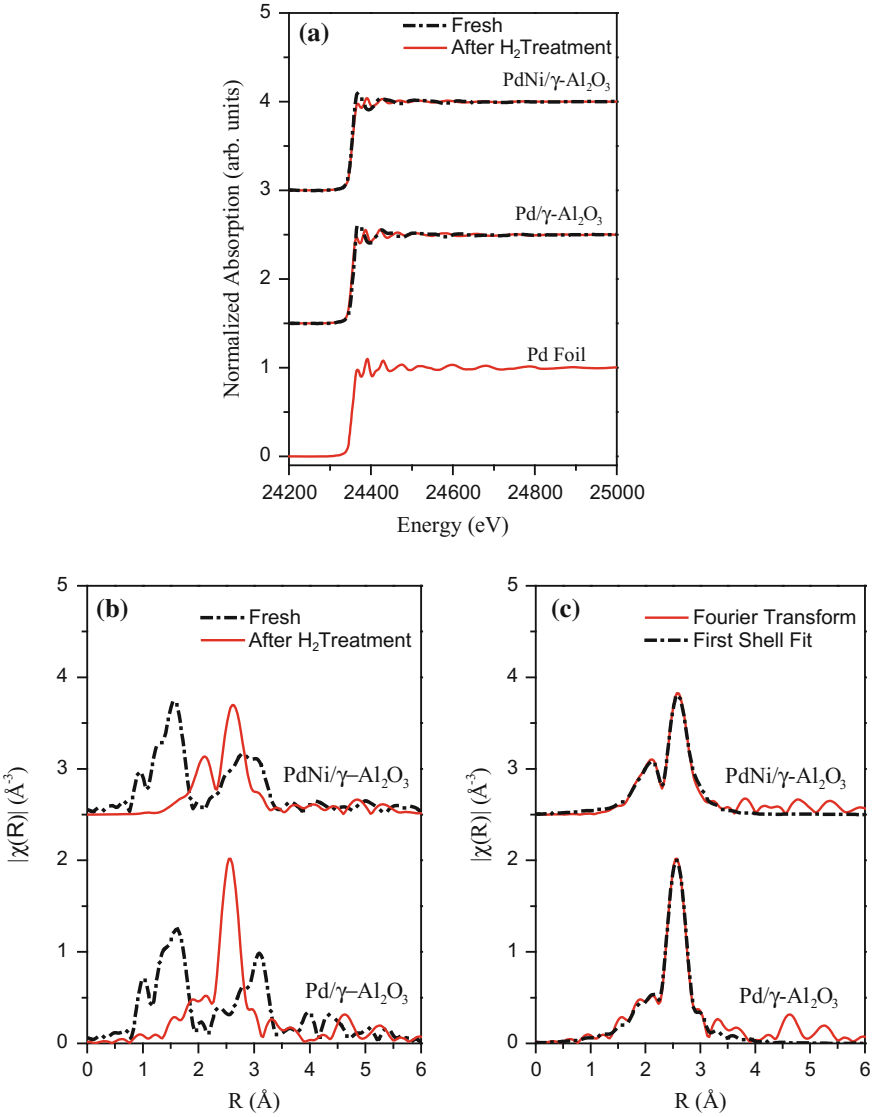

Fig. 3.12 **a** Pd K-edge XANES spectra before and after reduction **b** fourier transformed (magnitude) k^2 weighted EXAFS function ($\chi(k)$) before and after reduction **c** Pd K-edge Fourier transformed (magnitude) k^2 weighted EXAFS function ($\chi(k)$) after reduction with first shell fit. The Pd foil is included in (**a**) to serve as a reference for metallic Pd. Reprinted from ref. [65], Copyright 2014, with permission from Elsevier

Table 3.4 Summary of EXAFS analysis of Pd K-edge catalysts supported on γ–Al_2O_3. Reprinted from Ref. [65], Copyright 2014, with permission from Elsevier

Catalysts	Pd/γ–Al_2O_3	PdNi/γ–Al_2O_3
CN(Pd–Pd)	9.77 ± 0.38	8.34 ± 0.74
CN(Pd–Ni)	–	1.44 ± 0.50
R(Pd–Pd) (Å)	2.83 ± 0.002	2.79 ± 0.01
R(Pd–Ni) (Å)	–	2.64 ± 0.01
σ^2(Pd–Pd) (Å^2)	0.008 ± 0.001	0.010 ± 0.001
σ^2(Pd–Ni) (Å^2)	–	0.016 ± 0.004

3.5 Evaluation of Supported Catalysts

According to the characterization results of supported catalysts, the Pd–Ni bimetallic catalyst has similar particle size distribution and more active sites than the monometallic catalyst. Moreover, bimetallic bonds were found on Pd–Ni catalyst. In this section, the supported catalysts were tested in both batch and fixed-bed reactors. The batch reactor was equipped with an FT-IR in order to detect the gas-phase concentration with time, and the first-order kinetics could be estimated. The fixed-bed reactor was operated at steady state, which is similar to industrial reaction conditions; as a result, the steady-state catalytic activity and selectivity, as well as the catalyst stability could be tested.

3.5.1 Batch Reactor

In the batch reactor, the initial gas-phase concentration was 7.8 Torr C_4H_6, 17.2 Torr H_2, and 25 Torr He. The ratio of 1,3-butadiene and hydrogen was 1:2.2. Because the hydrogenation reaction is exothermic, helium was introduced into the chamber for dilution to reduce the instant temperature rise at the beginning of the reaction. The reaction was performed at 308 K. The catalyst loading was about 13.6 mg.

Figure 3.13 shows the changes in gas-phase concentrations of 1,3-butadiene, 1-butene, and *n*-butane with reaction time over the PdNi/γ–Al_2O_3, Pd/γ–Al_2O_3, and Ni/γ–Al_2O_3 catalysts. The Pd–Ni bimetallic catalyst exhibits a higher hydrogenation activity than both the Pd and Ni monometallic catalysts, as illustrated in the 1,3-butadiene consumption rates in Fig. 3.13a, which is consistent with the model surface studies. After two hours of reaction, 1,3-butadiene is completely converted over PdNi/γ–Al_2O_3, ∼80% is converted over Pd/γ–Al_2O_3, and only ∼7% over Ni/γ–Al_2O_3. Figures 3.13b, c show once again that the bimetallic catalyst outperforms the monometallic Pd and Ni catalysts. A broad peak of 1-butene appears between 40 and 60 min over PdNi/γ–Al_2O_3, which indicates the possibility of producing the maximum amount of 1-butene within a short contact time on the bimetallic catalyst.

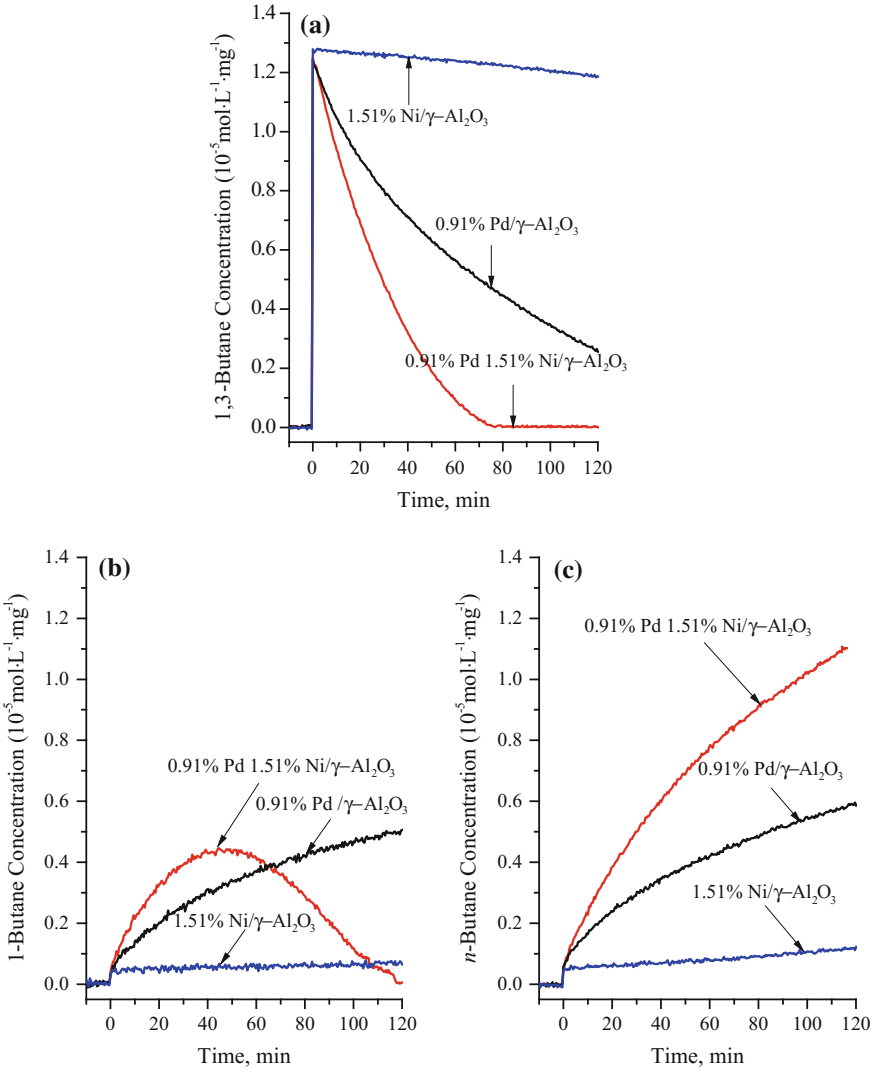

Fig. 3.13 The consumption of **a** 1,3-butadiene, production of **b** 1-butene, and production of **c** *n*-butane during the hydrogenation of 1,3-butadiene at 308 K. Reprinted from Ref. [65], Copyright 2014, with permission from Elsevier

To make a quantitative analysis, the hydrogenation reaction rates are estimated by a first-order rate law for the consumption of 1,3-butadiene. The fitting results of 1,3-butadiene consumption curves are shown in Fig. 3.14. Details are shown below:

1. First-order rate equation:

$$-r_A = -\frac{dC_A}{dt} = k \cdot C_A(t) \tag{3.1}$$

2. Integral equation of (3.1):

$$\frac{C_A(t)}{C_A(0)} = e^{-kt} \tag{3.2}$$

The rate constants normalized by catalyst weight, by CO uptake, and by total metal loadings are shown in Table 3.5. The rate constant of PdNi/γ–Al_2O_3, normalized by weight, is twice that of Pd/γ–Al_2O_3, while that of Ni/γ–Al_2O_3 is smaller by two orders of magnitude. This suggests that Ni/γ–Al_2O_3 is almost inactive for 1,3-butadiene hydrogenation. The rate constants normalized by CO uptake follow the same trend of PdNi/γ–Al_2O_3 > Pd/γ–Al_2O_3 > Ni/γ–Al_2O_3. The rate constant of PdNi/γ–Al_2O_3 normalized by CO uptake is only slightly larger than that of Pd/γ–Al_2O_3, and that of Ni/γ–Al_2O_3 is still smaller by orders of magnitude.

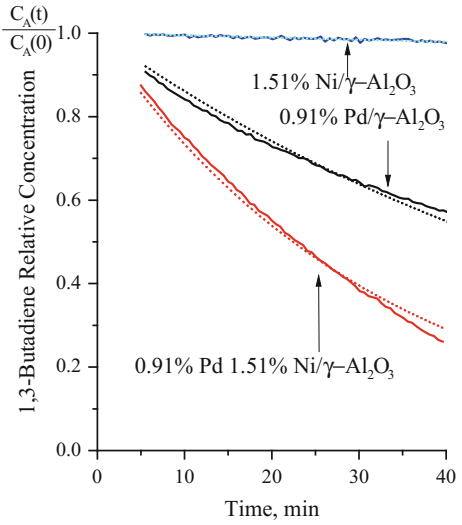

Fig. 3.14 Fitting results of 1,3-butadiene consumption curves based on first-order rate law (*dashed*)

Table 3.5 Normalized rate constant by first-order fitting. Reprinted from ref. [65], Copyright 2014, with permission from Elsevier

Catalysts	Normalized k_r (by weight) (min^{-1} g^{-1} cat)	Normalized k_r (by CO uptake) (10^{-2} min^{-1} μmol^{-1} CO)	Normalized k_r (by total metal loading) (10^{-3} min^{-1} g^{-1} metal)
PdNi/γ–Al_2O_3	2.32	7.92	9.59
Pd/γ–Al_2O_3	1.08	7.11	11.87
Ni/γ–Al_2O_3	0.038	0.31	0.25

According to the EXAFS results, not all Ni atoms are alloyed with Pd on the bimetallic catalyst. Some Ni particles are isolated on the support. These Ni particles have CO uptake values but barely contribute to hydrogenation activity. Therefore, the rate constants normalized by weight are more suitable for the activity comparison among the different catalysts. The higher rate constant of PdNi/γ–Al_2O_3 verifies the prediction of higher hydrogenation activity in the TPD results and the lower activation barrier in the DFT calculations on Pd-terminated PdNiPd(111) surface. Previous DFT calculations of Pd–Ni bimetallic systems have indicated that, in the presence of adsorbed hydrogen, the Pd-terminated surface is the thermodynamically stable structure [55, 80], which contributes to the good correlation between the supported catalysts and model surfaces.

3.5.2 *Fixed-Bed Reactor*

To verify the batch reactor results and to test the catalytic selectivity under steady-state conditions, 1,3-butadiene hydrogenation was performed in a fixed-bed reactor. The catalyst was mixed with quartz particles in a ratio of 1:29 (100 mg catalyst and 2.9 g quartz particles) in a fixed-bed reactor. Prior to the reaction, the catalysts were reduced in pure hydrogen at 450 °C for 3 h and then cooled to reaction temperature. The total flow rate of 1,3-butadiene and hydrogen was 9.6 mL/min, and the 1,3-butadiene to hydrogen ratio was 1:2.2 or 1:4. The flow rates of hydrogen, 1,3-butadiene, and nitrogen for each ratio are shown in Table 3.6. The reaction temperatures studied were from 40 to 100°C at intervals of ~20 °C. The catalyst was left on stream for 1.5 h at each temperature to achieve steady state.

The outlet stream was analyzed online by a gas chromatograph equipped with a FID detector (GC 7900, Techcomp Ltd.) and an HP–Al/S PLOT column (Agilent, 30 m × 0.53 μm). Only the C4 species (1,3-butadiene, 1-butene, trans-2-butene, cis-2-butene and butane) were observed in the outlet, with the gas-phase carbon balance being above 95%. The selectivity of each product was calculated by dividing its concentration by the total products. The total butene selectivity was obtained by summing the selectivities of all butene species.

The 1,3-butadiene conversions at different temperatures were plotted in Fig. 3.15 with hydrogen to 1,3-butadiene ratios of 2.2:1 and 4:1. For both H_2/C_4H_6 ratios, PdNi/γ–Al_2O_3 exhibits higher activity than Pd/γ–Al_2O_3 at all temperatures, while

Table 3.6 Flow rates of inlet gas phase (Unit: mL/min)

H_2/C_4H_6	H_2		C_4H_6		N_2	
	Flow rate (mL/min)	Partial pressure (Pa)	Flow rate (mL/min)	Partial pressure (Pa)	Flow rate (mL/min)	Partial pressure (Pa)
2.2:1	6.6	2837	3.0	1296	225.0	97192
4:1	7.7	3242	1.9	810	230.4	97273

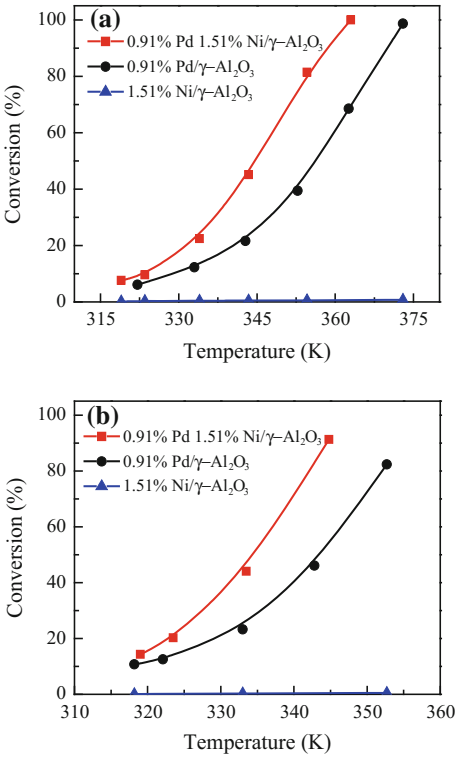

Fig. 3.15 Conversion of 1,3-butadiene in fixed-bed reactor at different temperatures. **a** H_2/C_4H_6 = 2.2:1; **b** H_2/C_4H_6 = 4:1. Reprinted from Ref. [65], Copyright 2014, with permission from Elsevier

$Ni/\gamma–Al_2O_3$ shows no hydrogenation activity below 100 °C, which is consistent with the batch reactor results. The ratio of hydrogen to 1,3-butadiene affects 1,3-butadiene conversion. Higher ratio enhances hydrogen to dissolve into the Pd bulk phase and plays a positive effect to the hydrogenation reaction.

To further evaluate the selective hydrogenation of 1,3-butadiene on different catalysts, the selectivities to total butene, 1-butene, *trans*-2-butene, and *cis*-2-butene were plotted in Figs. 3.16 and 3.17. The butene selectivities are independent of the

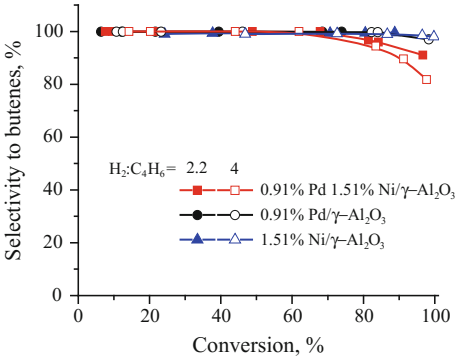

Fig. 3.16 Selectivity of total butene as a function of 1,3-butadiene conversion (*solid* H_2/C_4H_6 = 2.2:1; *hollow* H_2/C_4H_6 = 4:1)

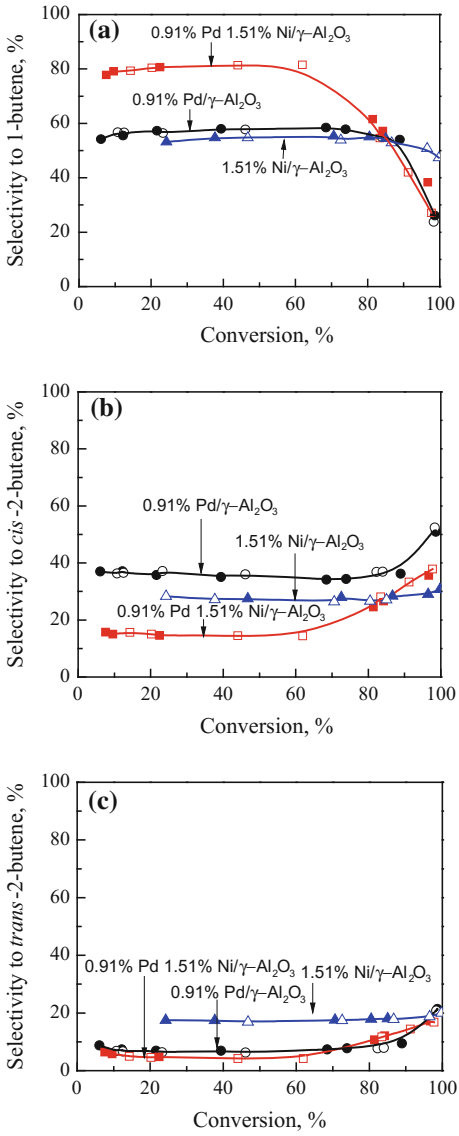

Fig. 3.17 Selectivities of **a** 1-butene **b** *trans*-2-butene and **c** *cis*-2-butene as a function of 1,3-butadiene conversion

H_2/C_4H_6 ratios. Similar product distribution and product selectivities are obtained for $H_2/C_4H_6 = 2.2$ and for $H_2/C_4H_6 = 4$. The total butene selectivity is 100% at conversions below 60% over the three catalysts. With increasing conversion toward 100%, the total butene selectivity decreases faster on $PdNi/\gamma–Al_2O_3$.

As shown in Fig. 3.17, the selectivity to 1-butene follows the order of $PdNi/\gamma–Al_2O_3 > Pd/\gamma–Al_2O_3–Ni/\gamma–Al_2O_3$, the selectivity to *trans*-2-butene follows the order of $Pd/\gamma–Al_2O_3 > Ni/\gamma–Al_2O_3 > PdNi/\gamma–Al_2O_3$, and the selectivity to

cis-2-butene follows the order of Ni/γ–Al_2O_3 > Pd/γ–Al_2O_3–PdNi/γ–Al_2O_3. As 1-butene is the most desirable product from 1,3-butadiene hydrogenation, PdNi/γ–Al_2O_3 is superior than Pd/γ–Al_2O_3 because it has higher hydrogenation activity and better performance in suppression of both complete hydrogenation and isomerization reactions.

On the invested three catalysts, the ratio of *trans*-2-butene and *cis*-2-butene does not change much at different conversions. Moreover, the selectivity at different H_2/C_4H_6 ratios falls on the same trend line, which indicates that the hydrogen partial pressure does not affect the selectivity.

The different selectivity on the three catalysts implies that the metallic effect plays the major role in affecting the formation of butene species, especially the desired 1-butene.

3.6 Discussion

Several parallels between model surfaces and supported catalysts can be drawn based on the results presented above. In the TPD experiments of model surfaces, the Pd-terminated PdNiPd(111) surface shows much higher activity for 1,3-butadiene hydrogenation than Pd(111) and NiPdPd(111) surfaces. This trend is consistent with DFT calculations, which show that the activation barrier for each hydrogenation step is lower on PdNiPd(111) than on Pd(111). The catalytic evaluation of the supported catalysts in both batch and fixed-bed reactors shows that PdNi/γ–Al_2O_3 exhibits higher activity than its monometallic catalysts, demonstrating an excellent correlation between model surfaces and supported catalysts. The selectivity also shows similarities between model surfaces and supported catalysts. The PdNiPd(111) surface does not produce butane from 1-butene under the UHV-TPD experimental conditions. DFT calculations show that 1-butene has much lower binding energy on PdNiPd(111) than on Pd(111), indicating a higher 1-butene selectivity due to its facile desorption from the PdNiPd(111) surface. Both DFT calculations and TPD experiments predict that the Pd-terminated bimetallic structure should give higher 1-butene selectivity than the monometallic catalysts. This is validated by the catalytic evaluation of supported catalysts using the fixed-bed reactor, where PdNi/γ–Al_2O_3 shows a higher 1-butene selectivity over Pd/γ–Al_2O_3 at similar 1,3-butadiene conversions.

The results in the present work successfully bridge the “pressure gap” and “materials gap” between surface science studies under UHV conditions and reactor evaluations of supported catalysts under catalytic conditions. Equally important, this chapter reports a more effective catalyst for the selective hydrogenation of 1,3-butadiene. The PdNi/γ–Al_2O_3 catalyst has both higher hydrogenation activity and higher selectivity to 1-butene, which is the most desirable product in the purification of butene streams.

However, an inconsistency has been found between model surfaces and supported catalysts. The activity increase by the addition of Ni is not as significant in

supported catalysts as suggested from surface science studies. This is most likely due to the relatively low degree of bonding between Ni and Pd in the supported catalysts. According the EXAFS results, the coordination number of Pd–Ni is only 1.44, which is much lower than common bimetallic catalysts [81]. A similar coordination number of 1.35 is found on 0.18% Pd-1.5% Ni/γ–Al_2O_3 (atomic ratio 1:15; EXAFS results not shown), indicating the difficulty of Ni insertion into Pd nanoparticles. To better understand the bimetallic effect and to promote the formation of Pd–Ni bimetallic bonds, Pd–Ni nanoparticle structures on other oxide supports should be further explored.

Furthermore, according to the DFT results by Goda et al. [62] and Wang [63], the Pd–Ni bimetallic catalyst might have higher activity and higher ethylene selectivity than the Pd monometallic catalyst. The Pd/γ–Al_2O_3 and PdNi/γ–Al_2O_3 were tested in the fixed-bed reactor for the hydrogenation of acetylene and the results are shown in Fig. 3.18. The Pd loading in the acetylene experiment was 0.1% w.t. and the Pd/Ni atomic ratio was 1:3.

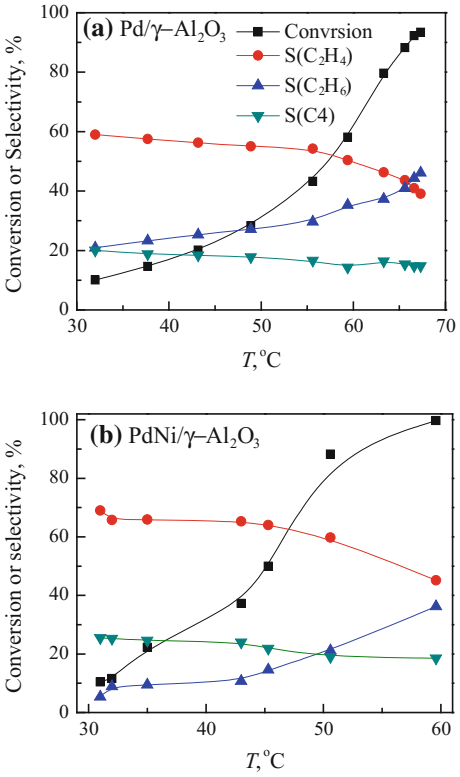

Fig. 3.18 Catalytic behavior of **a** Pd/γ–Al_2O_3 and **b** PdNi/γ–Al_2O_3 for acetylene hydrogenation (GHSV = 40,000 ml g cat^{-1} h^{-1}, H_2/C_2H_2 = 6)

As shown in Fig. 3.18, PdNi/γ–Al_2O_3 and Pd/γ–Al_2O_3 exhibit similar activity under room temperature. When the reaction temperature is higher than 35 °C, the hydrogenation activity on PdNi/γ–Al_2O_3 is higher than that on Pd/γ–Al_2O_3. At lower acetylene conversion, the selectivity to ethylene on PdNi/γ–Al_2O_3 is about 65%, while that on Pd/γ–Al_2O_3 is about 60%. With increasing conversion, the selectivity to ethylene decreases slowly on both catalysts. When the acetylene conversion increases to 88%, the selectivity to ethylene on PdNi/γ–Al_2O_3 decreases to 60% while that on Pd/γ–Al_2O_3 decreases to 44%. When the acetylene conversion increases to about 100%, the selectivity to ethylene on both catalysts decreases to about 40%.

The fixed-bed reactor results indicate that the PdNi/γ–Al_2O_3 has higher hydrogenation activity and higher ethylene selectivity than Pd/γ–Al_2O_3, which is consistent with the DFT calculation results [62, 63]. This once again proves the possibility of design supported catalyst from model surfaces and the better performance of Pd–Ni bimetallic catalyst in selective hydrogenation of acetylene and 1,3-butadiene.

3.7 Conclusion

Hydrogenation of 1,3-butadiene has been studied on Pd–Ni bimetallic catalysts using a combination of DFT calculations and TPD experiments on model surfaces and reactor evaluation over supported catalysts. The results show that the Pd–Ni bimetallic structure has higher hydrogenation activity than its monometallic counterparts. The activity of the catalysts follows the trend of Pd–Ni > Pd > Ni. The selectivity is evaluated with supported catalysts in both batch and fixed-bed reactors. The Pd–Ni, Pd and Ni catalysts supported on γ–Al_2O_3 show similar total selectivity to butenes, while Pd–Ni/γ–Al_2O_3 gives the highest 1-butene selectivity at similar conversions. The high hydrogenation activity and 1-butene selectivity make PdNi/γ–Al_2O_3 a better catalyst for 1,3-butadiene removal than the Pd monometallic catalyst. The good correlation between model surfaces and supported catalysts demonstrates the feasibility of designing selective hydrogenation catalysts using well-defined single-crystal surfaces. The Pd–Ni bimetallic catalyst also shows better performance in acetylene hydrogenation. The idea of the catalyst design is shown in Fig. 3.19.

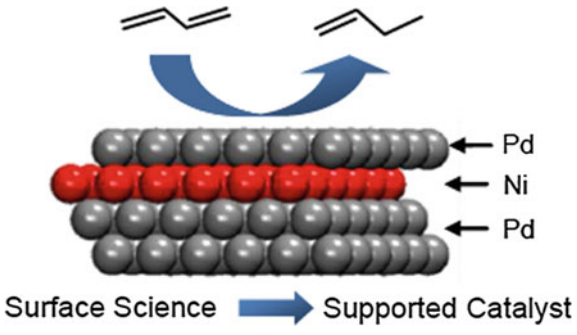

Fig. 3.19 New concept for catalyst design

References

1. Ahn IY, Lee JH, Kim SK et al (2009) Three-stage deactivation of Pd/SiO_2 and Pd–Ag/SiO_2 catalysts during the selective hydrogenation of acetylene. Appl Catal A-Gen 360(1):38–42
2. Zhang QW, Li J, Liu XX et al (2000) Synergetic effect of Pd and Ag dispersed on Al_2O_3 in the selective hydrogenation of acetylene. Appl Catal A-Gen 197(2):221–228
3. Khan NA, Uhl A, Shaikhutdinov S et al (2006) Alumina supported model Pd–Ag catalysts: A combined STM, XPS. TPD and IRAS study. Surf Sci 600(9):1849–1853
4. Khan NA, Shaikhutdinov S, Freund HJ (2006) Acetylene and ethylene hydrogenation on alumina supported Pd–Ag model catalysts. Catal Lett 108(3–4):159–164
5. Sheth PA, Neurock M, Smith CM (2005) First-principles analysis of the effects of alloying Pd with Ag for the catalytic hydrogenation of acetylene-ethylene mixtures. J Phys Chem B 109 (25):12449–12466
6. Ma Y, Diemant T, Bansmann J et al (2011) The interaction of CO with PdAg/Pd(111) surface alloys-A case study of ensemble effects on a bimetallic surface. Phys Chem Chem Phys 13 (22):10741–10754
7. Gonzalez S, Neyman KM, Shaikhutdinov S et al (2007) On the promoting role of Ag in selective hydrogenation reactions over Pd–Ag bimetallic catalysts: a theoretical study. J Phys Chem C 111(18):6852–6856
8. Mei D, Neurock M, Smith CM (2009) Hydrogenation of acetylene-ethylene mixtures over Pd and Pd–Ag alloys: first-principles-based kinetic Monte Carlo simulations. J Catal 268(2): 181–195
9. Pachulski A, Schodel R, Claus P (2011) Performance and regeneration studies of Pd–Ag/Al_2O_3 catalysts for the selective hydrogenation of acetylene. Appl Catal A-Gen 400 (1–2):14–24
10. Lu FF, Sun DH, Huang JL et al (2014) Plant-mediated synthesis of Ag-Pd alloy nanoparticles and their application as catalyst toward selective hydrogenation. ACS Sustain Chem Eng 2 (5):1212–1218
11. Wei HH, Yen CH, Lin HW et al (2013) Synthesis of bimetallic Pd–Ag colloids in CO_2-expanded hexane and their application in partial hydrogenation of phenylacetylene. J Supercrit Fluids 81:1–6
12. Redjala T, Remita H, Apostolescu G et al (2006) Bimetallic Au-Pd and Ag-Pd clusters synthesised by gamma or electron beam Radiolysis and study of the reactivity/structure relationships in the selective hydrogenation of buta-1,3-diene. Oil Gas Sci Technol 61 (6):789–797
13. Sarkany A (1997) Semi-hydrogenation of 1,3-butadiene over Pd–Ag/alpha–Al_2O_3 poisoned by hydrocarbonaceous deposits. App Catal A-Gen 165(1–2):87–101
14. Sarkany A (1997) Self-poisoning and aging of Pd–Ag/Al_2O_3 in semi-hydrogenation of 1,3-butadiene: effects of surface inhomogeneity caused by hydrocarbonaceous deposits. In: Bartholomew CH, Fuentes GA (eds) Catalyst deactivation 1997, vol 111. Studies in Surface Science and Catalysis, pp 111–118
15. Zhang YY, Diao WJ, Williams CT et al (2014) Selective hydrogenation of acetylene in excess ethylene using Ag- and Au-Pd/SiO_2 bimetallic catalysts prepared by electroless deposition. Appl Catal A-Gen 469:419–426
16. Pei GX, Liu XY, Wang AQ et al (2014) Promotional effect of Pd single atoms on Au nanoparticles supported on silica for the selective hydrogenation of acetylene in excess ethylene. New J Chem 38(5):2043–2051
17. Sarkany A, Horvath A, Beck A (2002) Hydrogenation of acetylene over low loaded Pd and Pd–Au/SiO_2 catalysts. App Catal A-Gen 229(1–2):117–125
18. Kittisakmontree P, Yoshida H, Fujita S et al (2015) The effect of TiO_2 particle size on the characteristics of Au-Pd/TiO_2 catalysts. Catal Comm 58:70–75
19. Wang Z, Zhang K, Yang K et al (2014) Effect of alkali metal modification on selective hydrogenation of isoprene on Pd–Au/Al_2O_3 catalysts. PetroProcess Petrochem 45(12):38–42

20. Zhang K, Wang Z, Ze B et al (2014) Selective hydrogenation of isoprene on Pd–Au/Al_2O_3 catalysts modified with Bi. Petrochem Tech 43(2):132–137
21. El Kolli N, Delannoy L, Louis C (2013) Bimetallic Au-Pd catalysts for selective hydrogenation of butadiene: Influence of the preparation method on catalytic properties. J Catal 297:79–92
22. Kittisakmontree P, Pongthawornsakun B, Yoshida H et al (2013) The liquid-phase hydrogenation of 1-heptyne over Pd–Au/TiO_2 catalysts prepared by the combination of incipient wetness impregnation and deposition-precipitation. J Catal 297:155–164
23. Pongthawornsakun B, Fujita SI, Arai M et al (2013) Mono- and bi-metallic Au-Pd/TiO_2 catalysts synthesized by one-step flame spray pyrolysis for liquid-phase hydrogenation of 1-heptyne. Appl Catal A-Gen 467:132–141
24. Piccolo L, Piednoir A, Bertolini JC (2005) Pd–Au single-crystal surfaces: segregation properties and catalytic activity in the selective hydrogenation of 1,3-butadiene. Surf Sci 592 (1–3):169–181
25. Miura H, Terasaka M, Oki K et al (1993) Preparation of eggshell type Pd–Ag and Pd–Au catalysts by selective deposition and hydrogenation of 1,3-butadiene. Stud Surf Sci Catal 75:2379–2382
26. Wang ZQ, Zhou ZM, Zhang R et al (2014) Selective hydrogenation of phenylacetylene over Pd–Cu/γ–Al_2O_3 catalysts. Acta Phys-Chim Sin 30(12):2315–2322
27. McCue AJ, McRitchie CJ, Shepherd AM et al (2014) Cu/Al_2O_3 catalysts modified with Pd for selective acetylene hydrogenation. J Catal 319:127–135
28. Kim SK, Lee JH, Ahn IY et al (2011) Performance of Cu-promoted Pd catalysts prepared by adding Cu using a surface redox method in acetylene hydrogenation. Appl Catal A-Gen 401 (1–2):12–19
29. Kang M, Song MW, Kim KL (2002) SMSI effect on ceria supported Cu-Pd catalysts in the hydrogenation of 1,3-butadiene. React Kinet Catal Lett 75(1):177–183
30. Cooper A, Bachiller-Baeza B, Anderson JA et al (2014) Design of surface sites for the selective hydrogenation of 1,3-butadiene on Pd nanoparticles: Cu bimetallic formation and sulfur poisoning. Catal Sci Tech 4(5):1446–1455
31. Insorn P, Suriyaphaparkorn K, Kitiyanan B (2013) Selective hydrogenation of 1-hexyne using Pd–Cu and Pd-W supported on alumina catalysts. In: 11th International conference on chemical and process engineering, Pts 1–4, vol 32, pp 847–852
32. Guczi L, Schay Z, Stefler G et al (1999) Pumice-supported Cu-Pd catalysts: influence of copper on the activity and selectivity of palladium in the hydrogenation of phenylacetylene and but-1-ene. J Catal 182(2):456–462
33. Mashkovsky IS, Baeva GN, Stakheev AY et al (2014) Novel Pd–Zn/C catalyst for selective alkyne hydrogenation: evidence for the formation of Pd–Zn bimetallic alloy particles. Mendeleev Comm 24(6):355–357
34. Tew MW, Emerich H, van Bokhoven JA (2011) Formation and characterization of PdZn alloy: a very selective catalyst for alkyne semihydrogenation. J Phys Chem C 115(17): 8457–8465
35. Osswald J, Giedigkeit R, Jentoft RE et al (2008) Palladium-gallium intermetallic compounds for the selective hydrogenation of acetylene—Part I: preparation and structural investigation under reaction conditions. J Catal 258(1):210–218
36. Osswald J, Kovnir K, Armbruester M et al (2008) Palladium-gallium intermetallic compounds for the selective hydrogenation of acetylene—Part II: surface characterization and catalytic performance. J Catal 258(1):219–227
37. Kovnir K, Osswald J, Armbruester M et al (2006) PdGa and Pd_3Ga_7: highly-selective catalysts for the acetylene partial hydrogenation. In: Scientific bases for the preparation of heterogeneous catalysts, proceedings of the 9th international symposium, vol 162, pp 481–488
38. Armbruester M, Wowsnick G, Friedrich M et al (2011) Synthesis and catalytic properties of nanoparticulate intermetallic Ga-Pd compounds. J Am Chem Soc 133(23):9112–9118

39. Kovnir K, Armbruester M, Teschner D et al (2009) In situ surface characterization of the intermetallic compound PdGa—a highly selective hydrogenation catalyst. Surf Sci 603 (10–12):1784–1792
40. Ota A, Armbruester M, Behrens M et al (2011) Intermetallic compound Pd_2Ga as a selective catalyst for the semi-hydrogenation of acetylene: from model to high performance systems. J Phys Chem C 115(4):1368–1374
41. He Y, Liang L, Liu Y et al (2014) Partial hydrogenation of acetylene using highly stable dispersed bimetallic Pd–Ga/MgO–Al_2O_3 catalyst. J Catal 309:166–173
42. Yang Z, Li X, Wu X (2001) Present situation of gallium production and its application prospect. World Nonferrous Metals 08:9–11
43. Daley SP, Utz AL, Trautman TR et al (1994) Ethylene hydrogenation on Ni(111) by bulk hydrogen. J Am Chem Soc 116(13):6001–6002
44. Pena JA, Herguido J, Guimon C et al (1996) Hydrogenation of acetylene over Ni/$NiAl_2O_4$ catalyst: Characterization, coking, and reaction studies. J Catal 159(2):313–322
45. Keane MA (1997) The hydrogenation of o-, m-, and p-xylene over Ni/SiO_2. J Catal 166 (2):347–355
46. Song MW, Kang M, Kim TW et al (2001) The enhancement of 1-butene selectivity in the hydrogenation of 1,3-butadiene over K-Ni catalysts. J Chem Eng Japan 34(11):1407–1414
47. Liu T, Jin Y, Wei M et al(2003) Selective hydrogenation of FCC light gasoline on the Ni-La/Al_2O_3 Catalyst. J Petrochem Universities 16(4):24–26,34
48. Lonergan WW, Xing XJ, Zheng RY et al (2011) Low-temperature 1,3-butadiene hydrogenation over supported Pt/3d/γ–Al_2O_3 bimetallic catalysts. Catal Today 160(1):61–69
49. Lonergan WW, Vlachos DG, Chen JG (2010) Correlating extent of Pt–Ni bond formation with low-temperature hydrogenation of benzene and 1,3-butadiene over supported Pt/Ni bimetallic catalysts. J Catal 271(2):239–250
50. Qi S, Yu W, Lonergan WW et al (2010) General trends in the partial and complete hydrogenation of 1,4-cyclohexadiene over Pt–Co, Pt–Ni and Pt–Cu bimetallic catalysts. ChemCatChem 2(6):625–628
51. Qi S, Yu W, Lonergan WW et al (2010) Low-temperature hydrogenation and dehydrogenation of 1, 3-cyclohexadiene on Pt/Ni bimetallic catalysts. Chin J Catal 31(8):955–960
52. Lonergan WW, Wang T, Vlachos DG et al (2011) Effect of oxide support surface area on hydrogenation activity: Pt/Ni bimetallic catalysts supported on low and high surface area Al_2O_3 and ZrO_2. App Catal A-Gen 408(1–2):87–95
53. Lonergan WW, Xing X, Zheng R et al (2011) Low-temperature 1,3-butadiene hydrogenation over supported Pt/3d/γ–Al_2O_3 bimetallic catalysts. Catal Today 160(1):61–69
54. Qi S, Cheney BA, Zheng R et al (2011) The effects of oxide supports on the low temperature hydrogenation activity of acetone over Pt/Ni bimetallic catalysts on SiO_2, γ–Al_2O_3 and TiO_2. App Catal A-Gen 393(1–2):44–49
55. Yu W, Porosoff MD, Chen JG (2012) Review of Pt-based bimetallic catalysis: from model surfaces to supported catalysts. Chem Rev 112(11):5780–5817
56. Miegge P, Rousset JL, Tardy B et al (1994) Pd_1Ni_{99} and Pd_5Ni_{95}—Pd surface segregation and reactivity for the hydrogenation of 1,3-butadiene. J Catal 149(2):404–413
57. Saint-Lager MC, Jugnet Y, Dolle P et al (2005) Pd_8Ni_{92}(110) surface structure from surface X-ray diffraction: Surface evolution under hydrogen and butadiene reactants at elevated pressure. Surf Sci 587(3):229–235
58. Michel AC, Lianos L, Rousset JL et al (1998) Surface characterization and reactivity of Pd_8Ni_{92}(111) and (110) alloys. Surf Sci 416(1–2):288–294
59. Hermann P, Tardy B, Jugnet Y et al (1996) Surface characterisation and reactivity of a Pd 0.5 monolayer deposit on Ni(110). Catal Lett 36(1–2):9–13
60. Hermann P, Guigner JM, Tardy B et al (1996) The Pd/Ni(110) bimetallic system: surface characterisation by LEED, AES, XPS, and LEIS techniques; new insight on catalytic properties. J Catal 163(1):169–175
61. Porte L, Phaner-Goutorbe M, Guigner JM et al (1999) Structuring and catalytic activity of palladium thin layers deposited on the Ni(110) surface. Surf Sci 424(2–3):262–270

62. Goda AM, Barteau MA, Chen JG (2006) Correlating electronic properties of bimetallic surfaces with reaction pathways of C-2 hydrocarbons. J Phys Chem B 110(24):11823–11831
63. Wang X (2013) A DFT study of selective hydrogenaion of acetylene over Pd–Ni bimetallic surface and defect Pd(111) surface. Dissertation, Beijing University of Chemical Technology
64. Valcárcel A, Clotet A, Ricart JM et al (2005) Selectivity control for the catalytic 1,3-butadiene hydrogenation on Pt (111) and Pd (111) surfaces: radical versus closed-shell intermediates. J Phys Chem B 109(29):14175–14182
65. Hou R, Yu W, Porosoff MD et al (2014) Selective hydrogenation of 1,3-butadiene on Pd–Ni bimetallic catalyst: from model surfaces to supported catalysts. J Catal 316:1–10
66. Liu P, Norskov JK (2001) Ligand and ensemble effects in adsorption on alloy surfaces. Phys Chem Chem Phys 3(17):3814–3818
67. Gomez G, Belelli PG, Cabeza GF et al (2010) The adsorption of 1,3-butadiene on Pd/Ni multilayers: the interplay between spin polarization and chemisorption strength. J Solid State Chem 183(12):3086–3092
68. Nascente PA, Carazzolle M, de Siervo A et al (2008) Crystallographic structure of ultra-thin films of Pd on Ni(111) and Ni on Pd(111) studied by photoelectron diffraction. J Mol Catal A-Chem 281(1):3–8
69. Cumpson PJ, Seah MP (1997) Elastic scattering corrections in AES and XPS.2. Estimating attenuation lengths and conditions required for their valid use in overlayer/substrate experiments. Surf Interface Anal 25(6):430–446
70. Carazzolle M, Maluf S, de Siervo A et al (2007) Surface composition and structure of nickel ultra-thin films deposited on Pd (111). J Electron Spectrosc 156:405–408
71. Kitchin JR, Khan NA, Barteau MA et al (2003) Elucidation of the active surface and origin of the weak metal-hydrogen bond on Ni/Pt (111) bimetallic surfaces: a Surf Sci and density functional theory study. Surf Sci 544(2):295–308
72. Fu J, Yang X, Menning CA et al (2016) Composition, structure and stability of surfaces formed by Ni deposition on Pd (111). Surf Sci 646:56–64
73. Shaikhutdinov S, Heemeier M, Bäumer M et al (2001) Structure-reactivity relationships on supported metal model catalysts: adsorption and reaction of ethene and hydrogen on $Pd/Al_2O_3/NiAl$ (110). J Catal 200(2):330–339
74. Farias D, Patting M, Rieder K (1997) Helium diffraction investigations of the transition of chemisorbed hydrogen into subsurface sites on palladium surfaces. Phys Status Solidi A 159 (1):255–262
75. Valcarcel A, Morfin F, Piccolo L (2009) Alkene hydrogenation on metal surfaces: why and when are Pd overlayers more efficient catalysts than bulk Pd? J Catal 263(2):315–320
76. Rupprechter G, Somorjai GA (1997) Palladium-catalyzed hydrogenation without hydrogen: the hydrodechlorination of chlorofluorocarbons with solid state hydrogen over the palladium (111) crystal surface and its implications. Catal Lett 48(1–2):17–20
77. Filhol JS, Simon D, Sautet P (2004) Understanding the high activity of a nanostructured catalyst obtained by a deposit of Pd on Ni: First principle calculations. J Am Chem Soc 126 (10):3228–3233
78. Tew MW, Janousch M, Huthwelker T et al (2011) The roles of carbide and hydride in oxide-supported palladium nanoparticles for alkyne hydrogenation. J Catal 283(1):45–54
79. Hou R, Wang T, Lan X (2013) Enhanced selectivity in the hydrogenation of acetylene due to the addition of a liquid phase as a selective solvent. Ind Eng Chem Res 52(37):13305–13312
80. Menning CA, Chen JG (2009) General trend for adsorbate-induced segregation of subsurface metal atoms in bimetallic surfaces. J Chem Phys 130(17):363–366
81. Porosoff MD, Chen JG (2013) Trends in the catalytic reduction of CO_2 by hydrogen over supported monometallic and bimetallic catalysts. J Catal 301:30–37

Chapter 4
Effect of Oxide Supports on Pd–Ni Bimetallic Catalysts for 1,3-Butadiene Hydrogenation

4.1 Introduction

In Chap. 3, the Pd-terminated, PdNiPd (111) surface was demonstrated to be more active and more selective to 1-butene than the Pd (111) surface for the hydrogenation of 1,3-butadiene using UHV-TPD experiments and DFT calculations. The better performance of the Pd–Ni bimetallic surface was verified on γ-Al_2O_3-supported catalysts [1]. Similar results were obtained for acetylene hydrogenation.

Support is one of the most important factors on supported catalysts. The surface area, pore structure, acidity and the support–metal interaction can affect the catalytic performance.

In industry, it is important to identify a proper support for the Pd–Ni bimetallic catalyst, with respect to the catalytic activity and selectivity. The interaction between the oxide supports and metal particles was previously shown to have a significant effect on the catalyst activity for hydrogenation reactions [2]. For the hydrogenation of acetone over the Pt–Ni bimetallic catalysts, Qi et al. [3] reported that PtNi/SiO_2 had much higher activity than PtNi/γ-Al_2O_3 and PtNi/TiO_2. For the hydrogenation of 1,3-butadiene, Lonergan et al. [4] reported that the activity of Pt–Ni catalysts were similar on γ-Al_2O_3, α-Al_2O_3 and low surface area (LSA)-ZrO_2, while Pt–Ni supported on high-surface area (HSA)-ZrO_2 showed much lower activity due to the strong metal–support interaction (SMSI). It was also reported that Pt–Ni/TiO_2 showed much lower activity than Pt–Ni/γ-Al_2O_3 due to the SMSI between the Pt particles and TiO_2 [5]. Lee et al. [6] further found that by forming strong interaction of Pd with TiO_2, the 1,3-butadiene hydrogenation activity was decreased and the 1-butene selectivity was improved by the inhibition of 1-butene isomerization.

R. Hou, *Catalytic and Process Study of the Selective Hydrogenation of Acetylene and 1,3-Butadiene*, Springer Theses, DOI 10.1007/978-981-10-0773-6_4

According to the literature above, the SMSI effect inhibits the hydrogenation activity of the Pt-based catalysts. In this work, the Pd–Ni bimetallic catalysts on several commonly used oxide supports were synthesized for the hydrogenation of 1,3-butadiene to study the support effect on the hydrogenation activity and selectivity. The supports are γ-Al_2O_3, SiO_2, ZrO_2, CeO_2, and TiO_2. Transmission electron microscopy (TEM), CO chemisorptions, temperature programmed desorption (TPR), and extended X-ray absorption fine structure (EXAFS) were used to characterize the catalysts. The bimetallic catalysts on different supports were further evaluated in a flow reactor equipped with a gas chromatograph (GC).

Another motivation to study the support effect is that the extent of Pd–Ni bimetallic bond formation in PdNi/γ-Al_2O_3 was relatively small. The Pd–Ni coordination number was only 1.4 because most Ni atoms existed either in the form of $NiAl_2O_4$ or as Ni monometallic nanoparticles. It is very likely that the Pd–Ni bimetallic effect would be more pronounced by increasing the extent of Pd–Ni bimetallic bond formation. One possible way to increase the Pd–Ni coordination number is using oxide supports other than γ-Al_2O_3 on which the active metal would not form the spinel species.

4.2 Catalyst Characterization

The catalysts used in this chapter are supported Pd–Ni bimetallic catalysts similar as those reported in Chap. 3, with Pd loading of 0.91 wt%. and Ni loading of 1.51 wt%. The Pd/Ni ratio is 1:3.

4.2.1 TEM

High-angle annular dark field (HAADF) TEM images are presented in Fig. 4.1 for the Pd–Ni catalysts. The average particle sizes are summarized in Table 4.1. Except Pd-Ni/CeO_2, all catalysts show similar average particle sizes and broad particle size distributions, ranging from $\sim$1 nm up to at least 15 nm, while PdNi/CeO_2 has a much narrower particle size distribution and smaller average particle size of $\sim$3 nm, likely due to the partial alloying of Pd with Ce which has been reported by Bernal et al. [7].

4.2.2 CO Chemisorption

The CO-uptake values are shown in Table 4.2. The CO chemisorption results are consistent with the TEM results. The Pd–Ni catalysts supported on the investigated supports exhibit similar CO-uptake values, except that PdNi/CeO_2 has a much

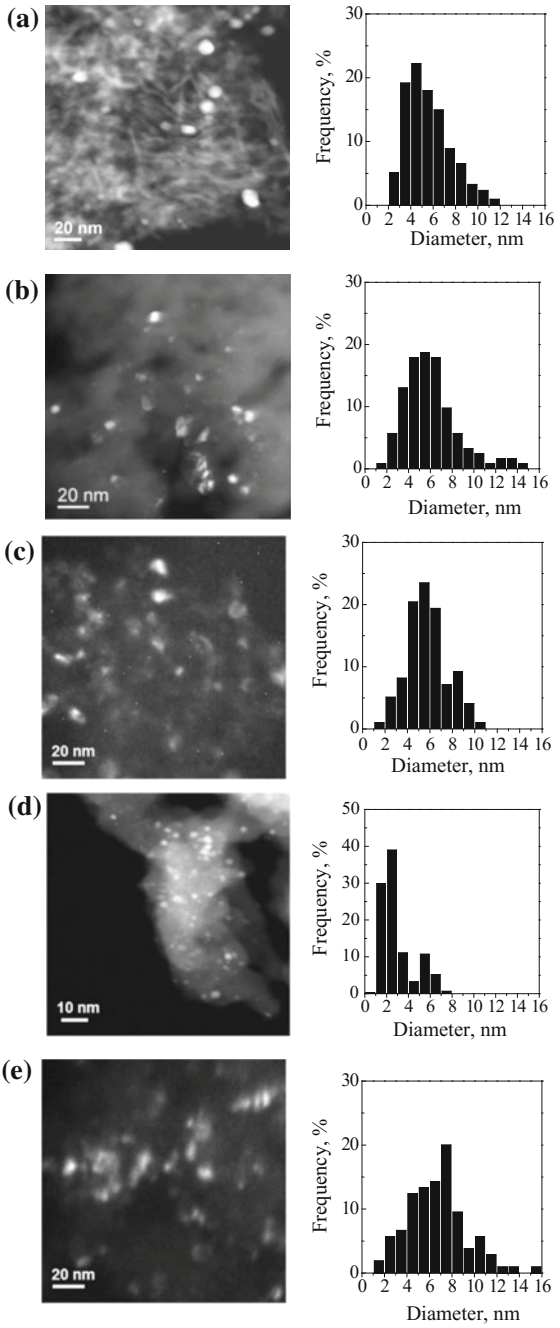

Fig. 4.1 HAADF TEM images and particle size distributions of Pd–Ni catalysts supported on **a** γ-Al_2O_3, **b** SiO_2, **c** ZrO_2, **d** CeO_2, and **e** TiO_2

Table 4.1 Summary of average particle sizes for supported Pd–Ni catalysts

Catalyst	Average particle size (nm)
Al_2O_3	5.9
SiO_2	6.3
CeO_2	3.1
TiO_2	6.7
ZrO_2	5.9

Table 4.2 Summary of CO uptakes for supported Pd–Ni catalysts

Catalyst	CO uptake (μmol/g)	CO uptake/$\overline{D}_p$
Al_2O_3	15.7	2.7
SiO_2	10.1	1.6
CeO_2	36.8	11.9
TiO_2	9.3	1.4
ZrO_2	16.1	2.7

higher CO uptake. Combining the TEM and CO-uptake results, the values of CO uptake/$\overline{D}_p$, where $\overline{D}_p$ is the average particle size, are also summarized in Table 4.2. As shown in the table, the CO uptake/$\overline{D}_p$ values are similar on Al_2O_3, SiO_2, TiO_2, and ZrO_2 (1.4–2.7), while that on CeO_2 is much higher (11.9).

4.2.3 Temperature Programmed Reduction (TPR)

The TPR spectra of the Pd–Ni catalysts are shown in Fig. 4.2, along with the Ni/SiO_2. The reduction peaks of PdNi/SiO_2 and Ni/SiO_2 are similar with each other, while the reduction temperature of PdNi/SiO_2 is slightly lower than that of Ni/SiO_2,

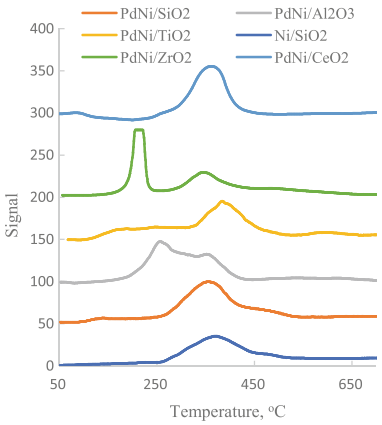

Fig. 4.2 TPR spectra of Pd–Ni catalysts along with Ni/SiO_2

indicating that the formation of bimetallic bond lowers the required reduction temperature slightly.

The reduction temperature for each TPR spectra peaks are below 450 °C, as a result, the reduction temperature (450 °C) chosen for experiment was sufficient to reduce the Pd–Ni bimetallic catalysts.

Moreover, the reduction temperature of $PdNi/CeO_2$ and $PdNi/TiO_2$ is higher than that of $PdNi/SiO_2$, implying the possibility of SMSI formation on CeO_2 and TiO_2. Two reduction peaks are observed on the TPR spectra of $PdNi/ZrO_2$, $PdNi/TiO_2$, and $PdNi/Al_2O_3$, indicating the existence of two oxide states.

4.2.4 XAFS

Figure 4.3a shows the Pd K-edge X-ray absorption near-edge structure (XANES) spectra of the PdNi catalysts supported on γ-Al_2O_3, SiO_2, TiO_2, and CeO_2 [8]

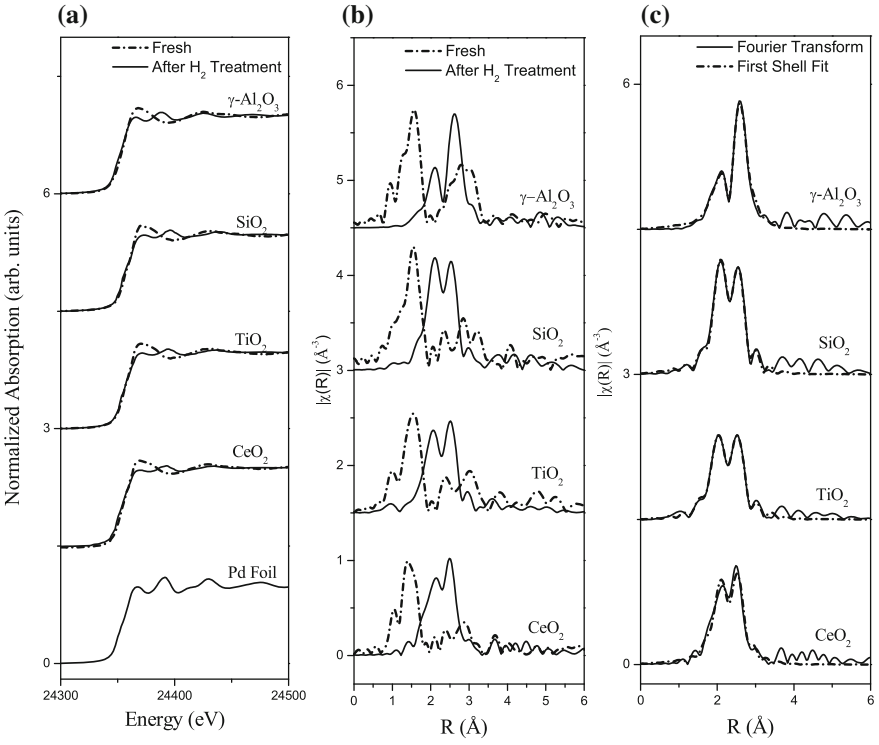

Fig. 4.3 **a** Pd K-edge XANES spectra before and after reduction; **b** Fourier-transformed (magnitude) k^2-weighted EXAFS function (χ(k)) before and after reduction; **c** Pd K-edge Fourier-transformed (magnitude) k^2-weighted EXAFS function (χ(k)) after reduction with first shell fit

before and after reduction, along with the spectra of the Pd foil for reference. The background-subtracted, edge-step normalized, and k^2-weighted Pd K-edge EXAFS data ($\chi(k)$) are shown in R-space in Fig. 4.3b, along with the fits obtained using FEFF6 theory shown in Fig. 4.3c. The ZrO_2 supported catalyst is not included because of the poor quality of EXAFS data, likely due to the high background absorbance of Zr (17998 eV) in the range of Pd (24350 eV).

Examination of the Pd K-edge XANES and EXAFS reveals information regarding the extent of oxidation of the samples. Relatively intense peaks are present in Fig. 4.3a at 24350 eV prior to reduction and are attributed to the Pd–O bond, which is confirmed by the peaks at low radial distribution in Fig. 4.3b. After reduction in H_2, the spectra are similar to that of the Pd foil in Fig. 4.3a, and the Pd–O peaks are no longer present in Fig. 4.3b. The Pd–O peaks are replaced by Pd–Ni peaks at slightly larger values of R. These changes in the spectra indicate that Pd is in a metallic state after reduction in H_2.

Figure 4.3c presents the Fourier-transformed (R-space) data of the reduced catalysts and the associated fits from FEFF6 by including only Pd–Pd and Pd–Ni contributions. The results from the fitting are shown in Table 4.3. The coordination numbers reveal that bimetallic Pd–Ni bonds are formed in all four catalysts. Table 4.3 also compares the value of N(Pd–Ni)/[(N(Pd–Ni) + N(Pd-Pd)], which can be used to compare the general trend in the extent of Pd–Ni bimetallic formation. The values are similar on PdNi/CeO_2, PdNi/TiO_2, and PdNi/SiO_2, with PdNi/γ-Al_2O_3 showing a significantly lower value. Such comparison indicates that the extent of Pd–Ni bimetallic formation is much lower on γ-Al_2O_3 than on the other three supports. The relatively small amount of bimetallic bond formation on γ-Al_2O_3 is because a large fraction of Ni atoms forms $NiAl_2O_4$ with the support. For all Pd–Ni catalysts, the EXAFS results show that the Pd–Pd distances are smaller than the Pd–Pd distance on the monometallic catalyst (2.83 Å), while the Pd–Ni distances are larger than the metallic Ni-Ni distance (2.49 Å). These results suggest that Pd–Ni bimetallic bonds are formed on the catalysts because the bimetallic bond lengths are between that of either parent metal. In addition, good

Table 4.3 Summary of EXAFS analysis of Pd K-edge for supported Pd–Ni catalysts

Catalysts	CeO_2	TiO_2	SiO_2	γ-Al_2O_3
N(Pd–Pd)	4.6 ± 0.4	5.1 ± 0.4	5.8 ± 0.5	8.3 ± 0.7
N(Pd–Ni)	2.3 ± 0.3	2.6 ± 0.7	3.5 ± 0.6	1.4 ± 0.5
R(Pd–Pd) (Å)	2.71 ± 0.01	2.71 ± 0.01	2.70 ± 0.01	2.79 ± 0.01
R(Pd–Ni) (Å)	2.59 ± 0.01	2.58 ± 0.01	2.59 ± 0.01	2.64 ± 0.01
σ^2 (Pd–Pd) ($Å^2$)	0.008 ± 0.001	0.008 ± 0.003	0.007 ± 0.001	0.010 ± 0.001
σ^2 (Pd–Ni) ($Å^2$)	0.007 ± 0.001	0.009 ± 0.001	0.008 ± 0.002	0.016 ± 0.004
N(Pd–Ni) + N (Pd–Pd)	6.9	7.7	9.3	9.7
N(Pd–Ni)/[N(Pd–Ni) + N(Pd–Pd)]	0.33	0.34	0.38	0.14

fits to the Pd K-edge experimental data could only be obtained by including both Pd–Pd and Pd–Ni contributions in the model, strongly suggesting that bimetallic bonds are present.

In principle, the total coordination numbers from the EXAFS measurements, such as the sum of N(Pd–Pd) and N(Pd-Ni), should correlate with the TEM analysis of particle size. However, quantitatively such correlation is valid only when the particles are uniform, both in physical size and chemical composition. The TEM images reveal that the metals particles have a relatively wide range of size distribution. Therefore, TEM results are more reliable and more direct than EXAFS for particle size estimation. The TEM results are also consistent with the trend in the metal dispersion from the CO chemisorption measurements. For example, among the bimetallic catalysts on the four oxide supports, $PdNi/CeO_2$ is characterized by the smallest particle size in TEM images and the highest metal dispersion in CO chemisorption measurements.

4.3 Catalyst Evaluation

The Pd–Ni bimetallic catalysts were tested in a flow reactor. Firstly, the Pd–Ni bimetallic effects were verified using two supports (γ-Al_2O_3 and SiO_2) based on the previous results in Chap. 3. Then, the oxide support effect was investigated on the synthesized Pd–Ni bimetallic catalysts. The flow rates of gases in the catalyst evaluation were as follows: H_2 7.7 mL/min, 1,3-butadiene 1.9 mL/min. The ratio of H_2/C_4H_6 was 4:1. Experiments were carried out in the temperature range of 30–110 °C. The other experimental conditions were the same as in Chap. 3.

4.3.1 Bimetallic Effect

The Pd–Ni bimetallic effect was investigated on γ-Al_2O_3- and SiO_2-supported monometallic and bimetallic catalysts. The Pd catalysts and Pd–Ni bimetallic catalysts were evaluated for the selective hydrogenation of 1,3-butadiene at different temperatures, and the results are shown in Figs. 4.4 and 4.5. The conversions of 1,3-butadiene are plotted as a function of temperature in Fig. 4.4a, b, and the selectivities to butenes and 1-butene are plotted as a function of conversion in Fig. 4.5a, b, respectively. The Pd–Ni bimetallic catalysts on both supports show higher conversions and higher 1-butene selectivity than the Pd monometallic catalysts. At low temperature range (40–50 °C), there is no much difference between the activities of monometallic and bimetallic catalysts. With increasing temperature, the conversion over Pd–Ni catalyst increases faster than over the Pd catalyst. It is possible that under low temperatures, there is considerable β-PdH_x formation over the Pd-based catalysts and the β-PdH_x enhances the hydrogenation activity. According to the UHV results in Chap. 3, β-PdH_x exists on both mono- and

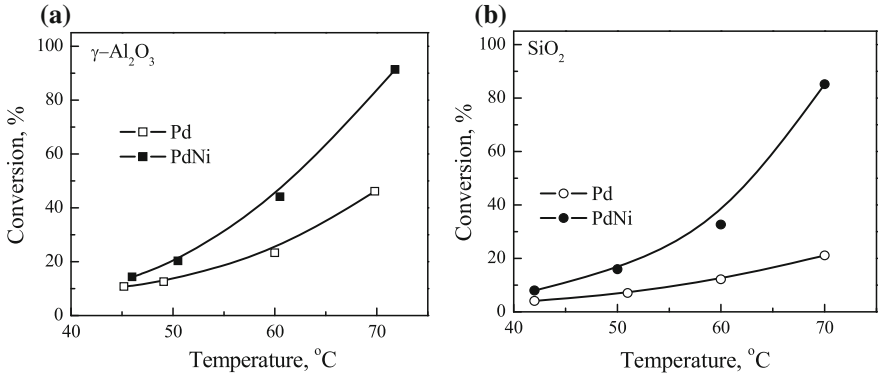

Fig. 4.4 Conversions of 1,3-butadiene in flow reactor as a function of temperatures for the comparison of Pd and Pd–Ni catalysts on **a** γ-Al_2O_3 and **b** SiO_2

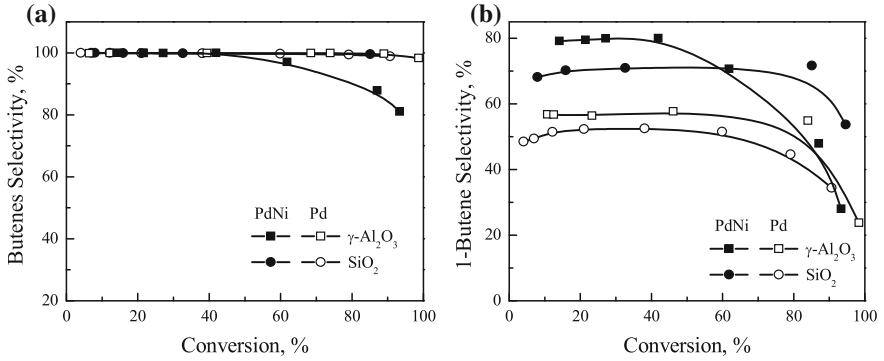

Fig. 4.5 Selectivities to **a** butenes and **b** 1-butene as a function of conversion of Pd–Ni (*solid*) and Pd (*hollow)*

bimetallic catalysts. As a result, the activities do not differ much from each other on the two catalysts. Under higher temperatures, the formation of β-PdH_x decreases and the bimetallic effect is more significant.

By comparing Fig. 4.4a, b, it could be seen that the Pd–Ni bimetallic effect is more pronounced on SiO_2 than on γ-Al_2O_3. The reason could be attributed to the higher coordination number on PdNi/SiO_2, which indicates there is more Pd–Ni bond formation on SiO_2.

Furthermore, the activity of Pd/γ-Al_2O_3 is higher than Pd/SiO_2. Because the particle size distributions are similar on the two catalysts according to the TEM results, the different activities should not come from the metal dispersion. As reported, acidity on the support could enhance the hydrogenation activity [9–11]. It is possible that the higher activity on γ-Al_2O_3 comes from the acidity effect.

The selectivity to 1-butene is generally higher on the Pd–Ni bimetallic catalysts than on the Pd catalysts, indicating that the formation of the Pd–Ni bimetallic bond plays a major role in the enhancement of 1-butene selectivity. At conversions below 50%, the selectivity to 1-butene is –20% higher on PdNi/γ-Al_2O_3 than on Pd/γ-Al_2O_3. Note that on PdNi/γ-Al_2O_3, the 1-butene selectivity decreases rapidly with increasing 1,3-butadiene conversion above 50%, while on Pd/γ-Al_2O_3 it decreases more slowly. Nevertheless, the 1-butene selectivity on PdNi/γ-Al_2O_3 remains higher than that on Pd/γ-Al_2O_3 at conversions below 90% and is similar to that on Pd/γ-Al_2O_3 at conversion above 90%. The possible explanation could attribute to the local concentration of the C4 species. At conversions above 90%, the concentration of 1-butene on PdNi/γ-Al_2O_3 becomes very high and the 1,3-butadiene concentration becomes very low. The high concentration ratio of 1-butene and 1,3-butadiene likely enhances the coverage of 1-butene on the surface of Pd–Ni, leading to further hydrogenation and isomerization reactions. As a result, the 1-butene selectivity decreases to the same value with Pd/γ-Al_2O_3 at high 1,3-butadiene conversions. Moreover, the difference between the Pd–Ni and Pd catalysts is larger on SiO_2 than on γ-Al_2O_3. The greater enhancement is most likely from the different extent of Pd–Ni bimetallic bonding. As summarized in Table 4.3, the coordination number of Pd–Ni on SiO_2 is 3.5, which is about 2.5 times larger than that on γ-Al_2O_3.

4.3.2 Hydrogenation Activity

The Pd–Ni bimetallic catalysts on different supports were evaluated, and the activity results are summarized in Figs. 4.6 and 4.7. Figure 4.6 shows the 1,3-butadiene conversion on different catalysts as a function of reaction temperature. Based on catalyst weight, the activity of the Pd–Ni bimetallic catalysts follows the trend of CeO_2 > γ-Al_2O_3–SiO_2 > ZrO_2 > TiO_2. However, after normalized by CO uptake, the turnover frequencies (TOFs, calculated using the data with conversions below 20%) as shown in Fig. 4.7 are similar among the five catalysts, and the logarithm of

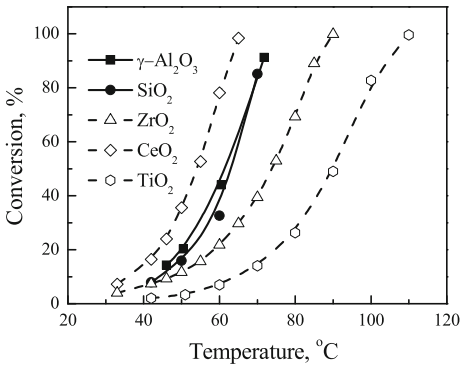

Fig. 4.6 Conversions of 1,3-butadiene in flow reactor at different temperatures for the comparison of Pd–Ni bimetallic catalysts on different supports

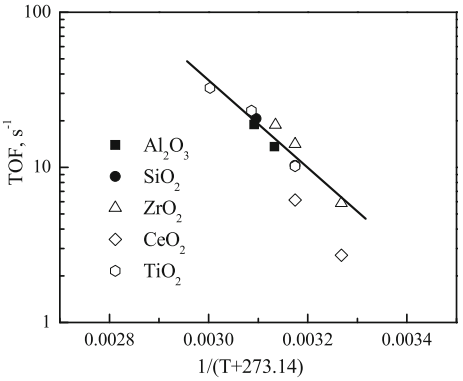

Fig. 4.7 TOFs of 1,3-butadiene in flow reactor at different temperatures for the comparison of Pd–Ni bimetallic catalysts on different supports

TOFs shows a linear relationship with the offset reciprocal of the reaction temperatures, except that the TOF value of $PdNi/CeO_2$ is lower than the trend line. The results demonstrate that the bimetallic catalysts on different supports display similar apparent hydrogenation activity regardless of the support nature, suggesting the presence of similar bimetallic active sites on the different oxide supports.

The exception of $PdNi/CeO_2$'s TOF value implies that it is less active than the other Pd–Ni bimetallic catalysts based on one active site. The different performance is consistent with the TEM and the CO-uptake results as discussed in Sect. 4.2. The metal particles are much smaller on $PdNi/CeO_2$, and the metal is more dispersed. The higher dispersion might contribute to the lower TOF on $PdNi/CeO_2$.

4.3.3 Selectivity

The selectivities to different butene products on the Pd–Ni bimetallic catalysts are shown in Figs. 4.8 and 4.9. Figure 4.8 compares the selectivities to butenes on different supports. The butenes selectivities are all close to 100% at conversions

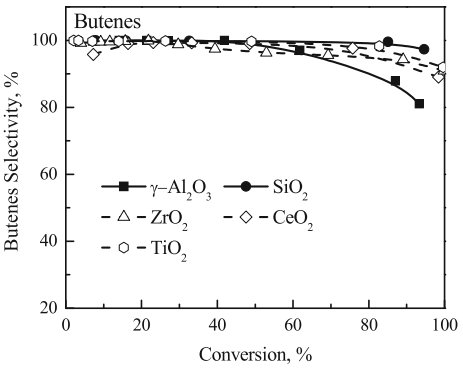

Fig. 4.8 Selectivities to butenes over Pd–Ni bimetallic catalysts on different supports

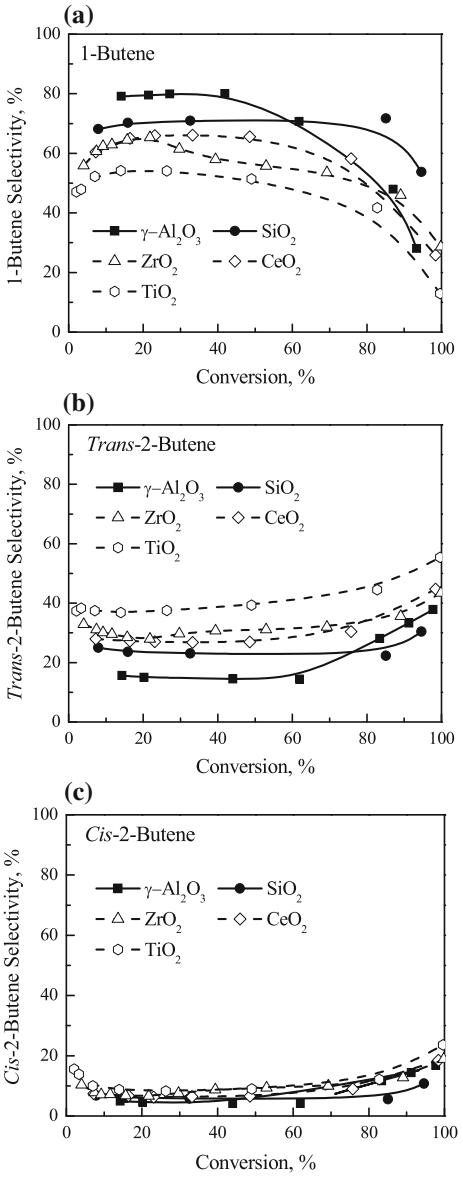

Fig. 4.9 Selectivities to **a** 1-butene, **b** *trans*-2-butene, and **c** *cis*-2-butene over Pd–Ni bimetallic catalysts on different supports

lower than 80%; when the conversion approaches 100%, the selectivity decreases slightly over SiO_2, CeO_2, ZrO_2, and TiO_2, but to a greater extent over PdNi/γ-Al_2O_3.

The selectivities to 1-butene, *trans*-2-butene, and *cis*-2-butene are plotted as a function of conversion in Fig. 4.9a–c, respectively. No isobutene was detected during the reaction. Among all the catalysts, the γ-Al_2O_3-supported catalyst gives

the highest 1-butene selectivity. At conversions lower than 25%, the selectivity to 1-butene over the Pd–Ni bimetallic catalysts on different supports follows the trend of γ-Al_2O_3 > SiO_2 > CeO_2–ZrO_2 > TiO_2. With increasing conversion, the general trend changes. The 1-butene selectivity on PdNi/ZrO_2 decreases slightly when the conversion increases above 25%, and it falls between those on PdNi/CeO_2 and PdNi/TiO_2. When the 1,3-butadiene conversion further increases to 100%, the selectivity to 1-butene on γ-Al_2O_3-supported catalysts decreases rapidly, while that on SiO_2-supported catalyst decreases only slightly.

The selectivity to *trans*-2-butene shown in Fig. 4.9b follows the trend of TiO_2 > CeO_2–ZrO_2 > SiO_2 > γ-Al_2O_3, which is opposite to that of the selectivity to 1-butene. The selectivity to *cis*-2-butene is similar on different supports, as shown in Fig. 4.9c. Because the hydrogenation of 1,3-butadiene only produces 1-butene in a batch reactor as reported before [1], it is very likely that 1,3-butadiene is firstly hydrogenated to 1-butene, and then 1-butene isomerizes to *trans*- and *cis*-2-butenes in the flow reactor. The opposite trend in the selectivities to 1-butene and *trans*-2-butene suggests that most 1-butene isomerizes into *trans*-2-butene. Based on the conclusion above, the oxide support appears to play an important role in the isomerization of 1-butene to *trans*-2-butene.

4.4 Discussion

4.4.1 Bimetallic Effect

The better performance of the Pd–Ni bimetallic catalysts has been previously demonstrated on single-crystal surfaces by both density functional theory (DFT) calculations and surface science experiments, and further verified on the γ-Al_2O_3-supported catalysts using both batch and flow reactors [1]. The present study further confirms the trend by supporting Pd–Ni and Pd onto γ-Al_2O_3 and SiO_2. The bimetallic catalysts show enhancement in both hydrogenation activity and 1-butene selectivity. Moreover, the larger coordination number of Pd–Ni on SiO_2 indicates a greater extent of Pd–Ni bond formation, which is consistent with the greater activity enhancement of PdNi/SiO_2 than PdNi/γ-Al_2O_3 compared with their Pd monometallic counterparts.

4.4.2 Support Effect

4.4.2.1 Activity

The characterization results from CO chemisorption and TEM are consistent in that PdNi/CeO_2 has higher CO uptake and more uniform small metal particles. The

other Pd–Ni-supported catalysts show similar particle size distributions and similar CO-uptake values. Normalized by CO uptake, the Pd–Ni bimetallic catalysts show similar activity regardless of the support types except that $PdNi/CeO_2$ shows a slightly lower activity.

Boitiaux et al. [12] reported that the 1,3-butadiene hydrogenation activity strongly depended on the metal dispersion on the Pd monometallic catalysts. The hydrogenation activity was similar when the Pd metal dispersion is lower than 20% and decreased with increasing metal dispersion at above 20%, regardless of the support types (γ-Al_2O_3, α-Al_2O_3, and SiO_2). Goetz et al. [13] also reported that large Pd particles ($\sim$6–7 nm) exhibited higher TOF than small Pd particles ($\sim$3 nm). These conclusions are consistent with the results in the current study for the Pd–Ni bimetallic catalysts. All the investigated Pd–Ni bimetallic catalysts exhibit similar metal dispersions lower than 20% except $PdNi/CeO_2$, and they display similar TOFs regardless of the support types. The higher metal dispersion on $PdNi/CeO_2$ results in slightly lower TOF, which is likely due to the exposure of less active sites on small bimetallic nanoparticles [12]. The electronic effect of the small metal particles makes 1,3-butadiene bind more strongly on the catalyst and accordingly decreases the hydrogenation activity [14].

However, the observation of similar TOF values on different oxide supports is different from the previous study on Pt-Ni bimetallic catalysts [4, 5]. It was reported that the activity of Pt–Ni bimetallic catalysts normalized by CO uptake was higher on γ-Al_2O_3 than on ZrO_2 [4] and TiO_2 [5] for the hydrogenation of 1,3-butadiene in a batch reactor. Moreover, Boitiaux et al. [15] and Primet et al. [16] have demonstrated that the hydrogenation activity of 1,3-butadiene was insensitive to the metal dispersions for Pt catalysts. Because the different activities among the Pt–Ni bimetallic catalysts [4, 5] are not from the metal dispersion [15, 16], they are possibly from the strong metal–support interaction (SMSI) between the small Pt–Ni nanoparticles and the oxide supports. Even though Pd–Ni might also have SMSI with the corresponding oxide supports, the interaction of Pd with ZrO_2 and TiO_2 might be different from that of Pt with ZrO_2 and TiO_2.

4.4.2.2 Selectivity

The selectivity to 1-butene over the Pd–Ni bimetallic catalysts on different supports follows the trend of γ-Al_2O_3 > SiO_2 > CeO_2–ZrO_2 > TiO_2 at low conversion of 1,3-butadiene. The different performance reflects the different support modification on Pd–Ni bimetallic catalysts. However, the selectivity performance varies at different 1,3-butadiene conversions.

It has been reported that the selectivities to butene species were independent of the metal dispersion [12]; therefore, the nature of supports, as well as the interaction between metal and support, should be responsible for the different performance in 1-butene selectivity among Pd–Ni catalysts on different supports. Several support effects, i.e., metal-support interaction, oxide defect, and geometric/electronic effect, could affect the selectivity in 1,3-butadiene hydrogenation.

SMSI has been reported to exist on the TiO_2-, CeO_2-, and ZrO_2-supported catalysts if reduced at temperatures higher than 500 °C [7, 17, 18], and that the SiO_2- and Al_2O_3-supported catalysts exhibit weaker metal–support interactions [2, 18, 19]. By forming bimetallic bond, the required reduction temperature for SMSI could be reduced (see Fig. 3 in Ref. [20]). As a result, the Pd–Ni bimetallic catalysts on TiO_2, CeO_2, and ZrO_2 probably present SMSI. The results show that the catalysts on the oxide supports with possible SMSI or possible oxide defects generally give lower 1-butene selectivity. The trend of 1-butene selectivity indicates that the possible SMSI effect decreases the 1-butene selectivity for the Pd–Ni bimetallic catalysts. The difference in 1-butene selectivity might also come from the oxide defects. TiO_2 and CeO_2 are reducible supports, and high-surface area ZrO_2 may have oxygen defects during reaction. The apparent correlation between the oxygen defects and the lower 1-butene selectivity suggests that the oxygen defects are also a possible reason for the lower 1-butene selectivity.

Different support might also affect the geometric and electronic properties on the Pd–Ni bimetallic catalysts [21]. According to the EXAFS results, the coordination numbers of Pd–Ni on different supports are different, leading to different particle composition on Pd–Ni bimetallic particles. On the other hand, TEM results revealed that the particle sizes were similar on all supports except on CeO_2. The EXAFS and TEM results suggest that the bimetallic composition, not the physical size of the particles, plays a significant role for the selectivity in 1,3-butadiene hydrogenation.

4.5 Conclusion

Hydrogenation of 1,3-butadiene has been studied on the Pd–Ni bimetallic catalysts supported on γ-Al_2O_3, SiO_2, CeO_2, ZrO_2, and TiO_2 using a fixed-bed reactor. The Pt–Ni bimetallic catalysts on γ-Al_2O_3 and SiO_2 are compared with the Pd catalysts to study the bimetallic synergy effect. The results show that the Pd–Ni bimetallic catalysts have both higher hydrogenation activity and higher 1-butene selectivity than the Pd catalysts. The bimetallic synergy effect is more significant on SiO_2 than on γ-Al_2O_3, i.e., the enhancement by Ni addition is greater on SiO_2 than on γ-Al_2O_3, which is consistent with the greater extent of Pd–Ni bimetallic bond formation on SiO_2.

The chemical nature of the supports influences the bimetallic metal particle structures but does not affect the hydrogenation activity. Only the metal particle size affects the turnover frequency. On the other hand, the 1-butene selectivity depends on the nature of supports. The possible SMSI effect and oxygen defects are the possible reasons for the lower 1-butene selectivity on PdNi/CeO_2, PdNi/ZrO_2 and PdNi/TiO_2.

References

1. Hou R, Yu W, Porosoff MD et al (2014) Selective hydrogenation of 1,3-butadiene on PdNi bimetallic catalyst: from model surfaces to supported catalysts. J Catal 316:1–10
2. Kang JH, Shin EW, Kim WJ et al (2002) Selective hydrogenation of acetylene on TiO_2-added Pd catalysts. J Catal 208(2):310–320
3. Qi S, Cheney BA, Zheng R et al (2011) The effects of oxide supports on the low temperature hydrogenation activity of acetone over Pt/Ni bimetallic catalysts on SiO_2, γ-Al_2O_3 and TiO_2. App Catal A Gen 393(1–2):44–49
4. Lonergan WW, Wang T, Vlachos DG et al (2011) Effect of oxide support surface area on hydrogenation activity: Pt/Ni bimetallic catalysts supported on low and high surface area Al_2O_3 and ZrO_2. App Catal A Gen 408(1–2):87–95
5. Wang T, Mpourmpakis G, Lonergan WW et al (2013) Effect of oxide supports in stabilizing desirable Pt–Ni bimetallic structures for hydrogenation and reforming reactions. Phys Chem Chem Phys 15(29):12156–12164
6. Lee DC, Kim JH, Kim WJ et al (2003) Selective hydrogenation of 1,3-butadiene on TiO_2-modified Pd/SiO_2 catalysts. App Catal A Gen 244(1):83–91
7. Bernal S, Calvino J, Cauqui M et al (1999) Some recent results on metal/support interaction effects in NM/CeO_2 (NM: noble metal) catalysts. Catal Today 50(2):175–206
8. Porosoff MD, Chen JG (2013) Trends in the catalytic reduction of CO_2 by hydrogen over supported monometallic and bimetallic catalysts. J Catal 301:30–37
9. Chen M, Qian X, Chu W et al (2006) Support effect on the Pd-based catalyst in selective hydrogenation. Petro Acta Petrol Sin 02:20–26
10. Zhu S, Hou R, Wang T (2012) Effects of supports and promoter Ag on Pd catalysts for selective hydrogenation of acetylene. Chin J Process Eng 12(3):489–496
11. Feng JT, Ma XY, Evans DG et al (2011) Enhancement of metal dispersion and selective acetylene hydrogenation catalytic properties of a supported Pd catalyst. Ind Eng Chem Res 50 (4):1947–1954
12. Boitiaux JP, Cosyns J, Vasudevan S (1983) Hydrogenation of highly unsaturated hydrocarbons over highly dispersed palladium catalyst: part I: behaviour of small metal particles. Appl Catal 6(1):41–51
13. Goetz J, Volpe MA, Touroude R (1996) Low-loaded Pd/α-Al_2O_3 catalysts: influence of metal particle morphology on hydrogenation of buta-1,3-diene and hydrogenation and isomerization of but-1-ene. J Catal 164(2):369–377
14. Lonergan WW, Xing X, Zheng R et al (2011) Low-temperature 1,3-butadiene hydrogenation over supported Pt/3d/γ-Al_2O_3 bimetallic catalysts. Catal Today 160(1):61–69
15. Boitiaux JP, Cosyns J, Robert E (1987) Liquid phase hydrogenation of unsaturated hydrocarbons on palladium, platinum and rhodium catalysts. Part I: kinetic study of 1-butene, 1,3-butadiene and 1-butyne hydrogenation on platinum. Appl Catal 32:145–168
16. Primet M, Elazhar M, Guenin M (1990) Influence of the support towards platinum catalyzed 1,3-butadiene hydrogenation. Appl Catal 58(2):241–253
17. Tauster S, Fung S, Garten R (1978) Strong metal-support interactions: group 8 noble metals supported on titanium dioxide. J Am Chem Soc 100(1):170–175
18. Benvenutti EV, Franken L, Moro CC et al (1999) FTIR study of hydrogen and carbon monoxide adsorption on Pt/TiO_2, Pt/ZrO_2, and Pt/Al_2O_3. Langmuir 15(23):8140–8146
19. Tauster SJ, Fung SC (1978) Strong metal-support interactions: occurrence among the binary oxides of groups IIA–VB. J Catal 55(1):29–35
20. Kang M, Song MW, Kim KL (2002) SMSI effect on ceria supported Cu-Pd catalysts in the hydrogenation of 1, 3-butadiene. React Kinet Catal Lett 75(1):177–183
21. Haller GL, Resasco DE (1989) Metal-support interaction: group VIII metals and reducible oxides. Adv Catal 36:173–235

Chapter 5
Replacing Precious Metals with Carbide Catalysts for Hydrogenation Reactions

5.1 Introduction

Pd–Ni bimetallic catalysts have been shown as more efficient catalyst for selective hydrogenation than the monometallic Pd catalyst. However, there is still precious component Pd in the catalyst, and the catalyst cost is still high. The current chapter will design non-precious catalyst for selective hydrogenation for dienes.

In manufacturing polymers, the catalytic hydrogenation of dienes is widely used for the purification of olefin stream. The hydrogenation catalysts commonly utilize supported precious metals, such as Pd [1–3]-, Pt [4–6]-, Rh [7]-, or Au [8, 9]-based catalysts. The precious metal catalysts have shown high activity; however, their high cost and limited abundance are potential concerns for industrial applications. By forming bimetallic structures with a non-precious metal, the precious metal-based catalysts could be enhanced in activity, thus lowering the catalyst cost. For example, by alloying Ni with Pd [10] or Pt [11, 12], the activity in 1,3-butadiene hydrogenation could be increased. Recently, Studt et al. [13] predicted using DFT calculation that Ni–Zn bimetallic catalysts should have good selectivity in the hydrogenation of acetylene and the prediction was verified by experiments [14, 15]; however, the activity of the Ni–Zn catalyst is much lower than the Pd-based catalyst. In a surface science study, the $Al_{13}Fe_4$ surface [16] was found to be active in 1,3-butadiene hydrogenation under ultra-high vacuum environment, demonstrating the feasibility of using non-precious metal catalysts for diene hydrogenation.

Another class of non-precious metal hydrogenation catalysts are carbides of early transition metals, which often show similar catalytic properties to precious metals [17, 18]. Kitchin et al. [19] compared the d-band structure of Pt(111) and Mo_2C by DFT calculation. As shown in Fig. 5.1, the d-band structures exhibited similarities close to the Fermi level for the Mo-terminated Mo_2C surface and Pt(111). Some literatures have reported the unique performance of Mo_2C for hydrogenation reactions. For example, molybdenum carbide (Mo_2C) was found to

R. Hou, *Catalytic and Process Study of the Selective Hydrogenation of Acetylene and 1,3-Butadiene*, Springer Theses, DOI 10.1007/978-981-10-0773-6_5

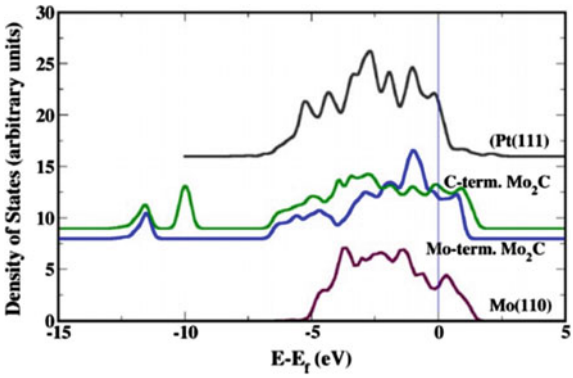

Fig. 5.1 Comparison of d-band structures of Pt(111), β-Mo_2C surfaces, and Mo (110). Reprinted from Ref. [19], Copyright 2005, with permission from Elsevier

be active in hydrogenation-related reactions, such as hydrodeoxygenation (HDO) [20–22], hydrodesulfurization (HDS) [22–24], and aromatic compound hydrogenations [22, 25–28]. However, to the best of our knowledge non-precious metal carbides have not been explored for the hydrogenation of dienes.

Moreover, according to previous studies [10, 11], the addition of Ni into the precious metal catalysts would enhance the catalytic performance in the hydrogenation of 1,3-butadiene. Therefore, Ni-modified Mo_2C was also studied in the current paper to further explore the enhancement by Ni addition.

In the current study, we explored the possibility of replacing precious metals by molybdenum carbide (Mo_2C) for the hydrogenation of 1,3-butadiene, 1,3-cyclohexadiene (1,3-CHD), and 1,4-cyclohexadiene (1,4-CHD) in a batch reactor, using a supported Pd/SiO_2 catalyst as a reference for comparison. Selective hydrogenation of 1,3-butadiene is an important reaction in industry for the purification of butene stream [29], while 1,3- and 1,4-CHDs are important reaction intermediates for hydrogen storage through hydrogenation–dehydrogenation of cyclic hydrocarbons [30]. The Mo_2C catalyst was further modified by Ni to determine the effect of metal modification on the hydrogenation activity and selectivity of 1,3-butadiene.

5.2 Catalyst Characterization

The as-synthesized (details in Chap. 2) Mo_2C was characterized by SEM, TEM, XRD, and N_2-physisorption.

Figure 5.2 presents the SEM image of Mo_2C. As shown in the figure, the prepared Mo_2C is flat on the surface with little pore structure. The Mo_2C particle is on millimeter scale. The particle sizes of Mo_2C and Ni/Mo_2C are 0.5–1.5 μm.

Figure 5.3 displays the TEM image of Mo_2C. The lattice parameters were measured on the image. The exposed 0.23 and 0.26 nm lattices correspond to the (101) and (100) facet on Mo_2C, respectively.

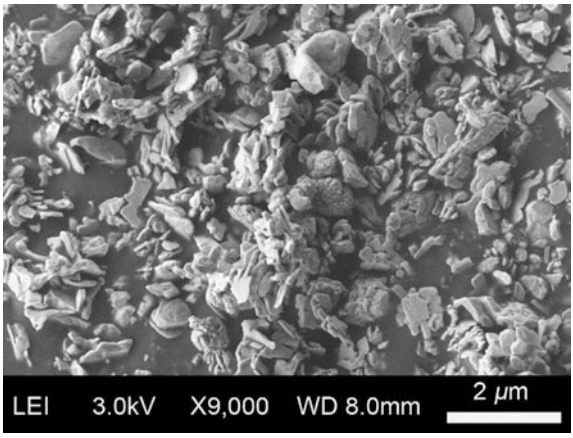

Fig. 5.2 SEM image of Mo_2C. Reprinted from Ref. [31], with kind permission from Springer Science+Business Media

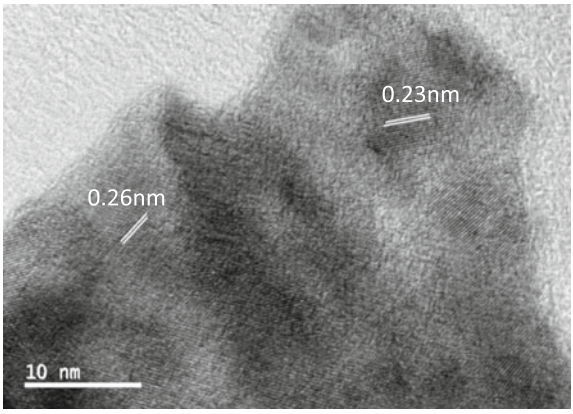

Fig. 5.3 TEM image of Mo_2C. Reprinted from Ref. [31], with kind permission from Springer Science+Business Media

The N_2-physisorption results are summarized in Fig. 5.4. The surface area was calculated as 5 m^2/g using BET method. The low surface area value is consistent with the SEM result. In the figure, the adsorption curve and the desorption curve are close to each other, indicating the pore sizes are uniform on Mo_2C. Combining the result from SEM, it could be concluded that there are scarcely any pore structure on the surface of Mo_2C.

The XRD spectra of Mo_2C are shown in Fig. 5.5. The XRD patterns confirm the formation of β-Mo_2C (JCPDS: 35-0787). The 2θ values of 34.1, 37.6, 39.5, 52.0, 61.7, 69.5, 74.6, and 75.9 correspond to the (100), (002), (101), (102), (110), (103), (112), and (201) facets of β-Mo_2C, respectively. The peak intensity at (100) and (101) is stronger than the others, indicating that the exposure rates are higher for the two facets, consistent with the TEM result.

The XRD spectra of Ni/Mo_2C with different Ni loadings are shown in Fig. 5.6. It could be seen from the figure that the Mo_2C phase is present on each of the

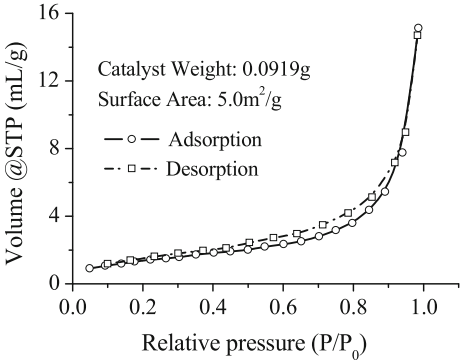

Fig. 5.4 N_2-physisorption result of Mo_2C. Reprinted from Ref. [31], with kind permission from Springer Science+Business Media

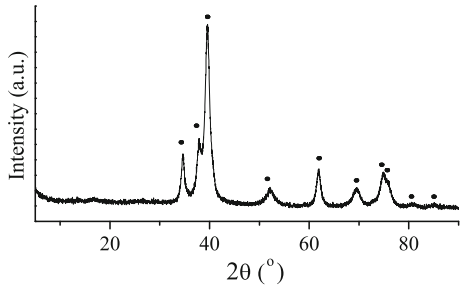

Fig. 5.5 XRD spectra of Mo_2C. Reprinted from Ref. [31], with kind permission from Springer Science+Business Media

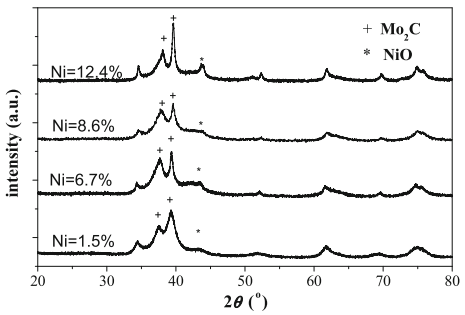

Fig. 5.6 XRD spectra of Ni/Mo_2C with different loadings

Ni/Mo_2C catalyst. With increasing loading of Ni, the amount of NiO phase increases on the catalysts. No other phases are observed from the XRD analysis.

5.3 Mo_2C for the Hydrogenation of Dienes

The hydrogenation of 1,3-butadiene, 1,3-cyclohexadiene, and 1,4-cyclohexadiene was tested in a batch reactor over Mo_2C. The performance of Pd/SiO_2 and $PdNi/SiO_2$ was also tested as references. The composition of gas phase in the batch

reactor was 7.8 Torr 1,3-BD/1,3-CHD/1,4-CHD, 17.2 Torr H_2 and 25 Torr He, with the H_2/diene ratio of 2.2:1. The catalyst loading was about 11.4 mg. The reaction was carried out at 308 K. During the diene hydrogenation reactions in a batch reactor, the gas-phase concentrations of reactants and products were monitored by FT-IR online.

5.3.1 1,3-Butadiene

The batch reactor results for the hydrogenation of 1,3-butadiene are shown in Fig. 5.7. Figure 5.7a shows the consumption rate of 1,3-butadiene. Because the exact amounts of catalyst loading, the initial reaction rates and the initial heat effects

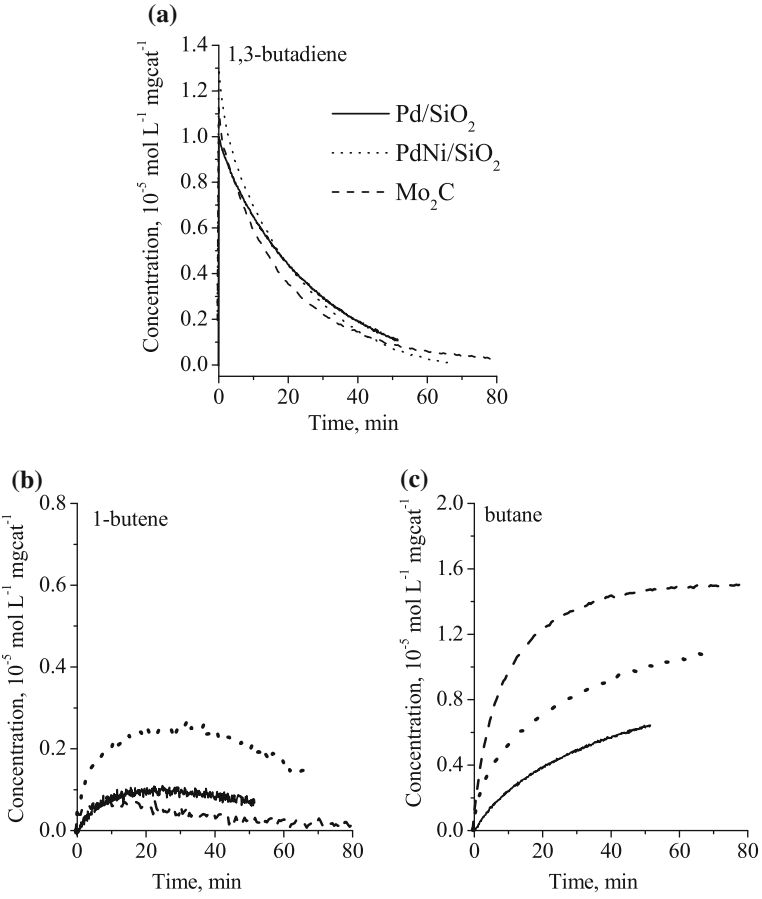

Fig. 5.7 Consumption of 1,3-butadiene (**a**) and formation of 1-butene (**b**) and butane (**c**) over Mo_2C, Pd/SiO_2, and $PdNi/SiO_2$ (T = 308 K, P_{BD} = 7.8 Torr, P_{H2} = 17.2 Torr, P_{He} = 25 Torr)

are different over the three catalysts, the initial recorded concentrations of 1,3-butadiene are different. As shown in the figure, the consumption rate of $PdNi/SiO_2$ is slightly higher than Pd/SiO_2; Mo_2C shows similar initial activity with $PdNi/SiO_2$, but after 50 min, the consumption rate decreases below the rate of Pd/SiO_2, implying the deactivation on Mo_2C.

Figure 5.7b shows the formation rates of 1-butene. The highest 1-butene formation peak is observed on $PdNi/SiO_2$, implying the possibility of producing maximum amount of 1-butene within a short contact time. The amount of 1-butene formation on Mo_2C is small, and the peak is below that of Pd/SiO_2. The low 1-butene peak indicates that once 1-butene forms on Mo_2C, it could be hydrogenated to butane easily. Therefore, the 1-butene selectivity on Mo_2C is low.

Figure 5.7c is the formation curve of butane. The butane formation rate on Mo_2C is higher than the Pd-based catalysts, consistent with the high hydrogenation activity and low 1-butene selectivity as shown in Figs 5.7a and b.

5.3.2 1,3-Cyclohexadiene

The batch reactor results for the hydrogenation of 1,3-cyclohexadiene are shown in Fig. 5.8. Figure 5.8a shows the consumption rate of 1,3-cyclohexadiene. The consumption rates for 1,3-cyclohexadiene over $PdNi/SiO_2$ and Pd/SiO_2 are similar to each other, while the apparent rate over Mo_2C is much lower than the Pd-based catalysts. Although Mo_2C shows similar initial activity as the Pd-based catalyst for the first several minutes, the activity decreases quickly and displays obvious deactivation.

Figure 5.8b shows the formation curves of cyclohexene. A broad peak is observed on $PdNi/SiO_2$, indicating the higher alkene selectivity over the bimetallic catalyst. The amount of cyclohexene continues to increase slowly on Mo_2C, possibly due to the rapidly decreased activity.

The formation curves of cyclohexane are shown in Fig. 5.8c. The concentrations of cyclohexane over Pd/SiO_2 and Mo_2C increase over time, while the formation of cyclohexane almost stopped after 10-min reaction. The results clearly show that $PdNi/SiO_2$ is better at controlling selective hydrogenation.

The benzene formation is shown in Fig. 5.8d. The benzene concentrations increase in the first 20–40 min and then do not change much. The benzene formation curves indicate the behavior of dehydrogenation reactions over the different catalysts. The steady-state benzene concentration follows the order of $Mo_2C < Pd/SiO_2 < PdNi/SiO_2$.

According to the above results, the hydrogenation and dehydrogenation both exist in the reaction. Mo_2C shows similar initial hydrogenation activity with Pd-based catalysts, but higher deactivation rate. Pd–Ni bimetallic catalyst has higher cyclohexene selectivity than the monometallic catalyst.

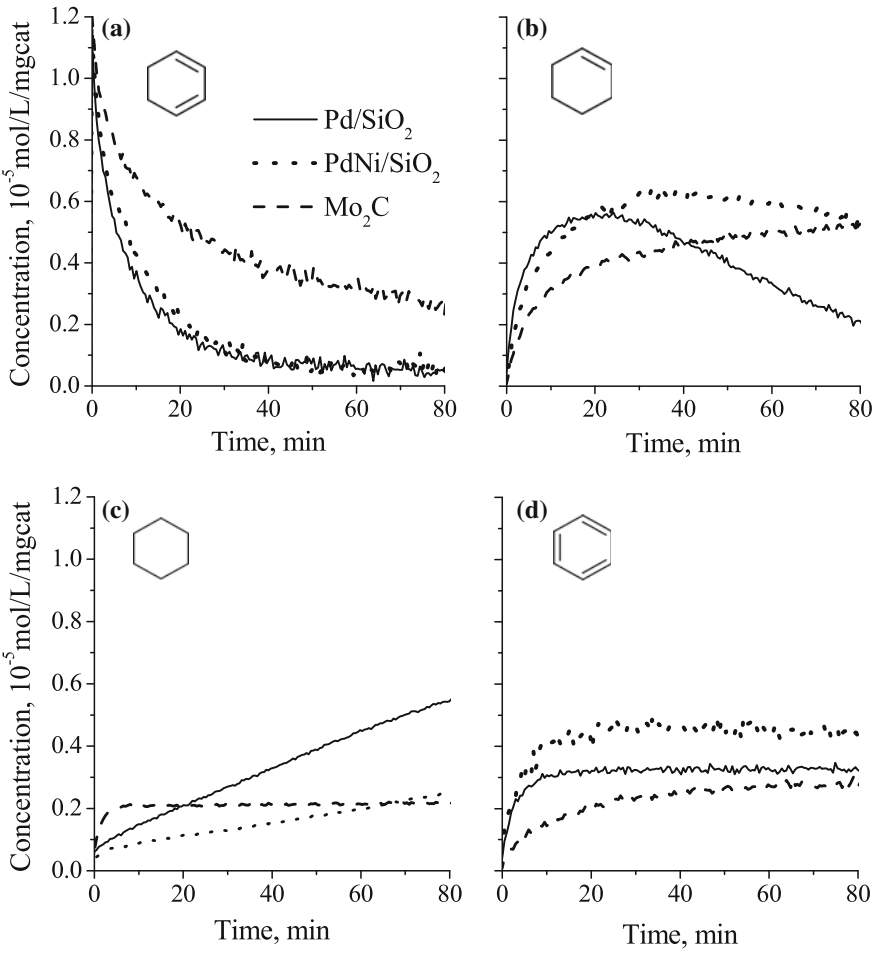

Fig. 5.8 Consumption of 1,3-cyclohexadiene (**a**) and formation of cyclohexene (**b**) cyclohexane (**c**) and benzene (**d**) over Mo_2C, Pd/SiO_2, and $PdNi/SiO_2$ (T = 308 K, $P_{1,3\text{-CHD}}$ = 7.8 Torr, P_{H2} = 17.2 Torr, P_{He} = 25 Torr)

5.3.3 *1,4-Cyclohexadiene*

The batch reactor results for the hydrogenation of 1,4-cyclohexadiene are shown in Fig. 5.9.

Figure 5.9a shows the consumption rates of 1,4-cyclohexadiene over the investigated catalysts. The consumption rate of 1,4-cyclohexadiene over $PdNi/SiO_2$ is higher than over Pd/SiO_2, while the consumption rate over Mo_2C is almost similar as $PdNi/SiO_2$. After 10-min reaction, deactivation could be observed on

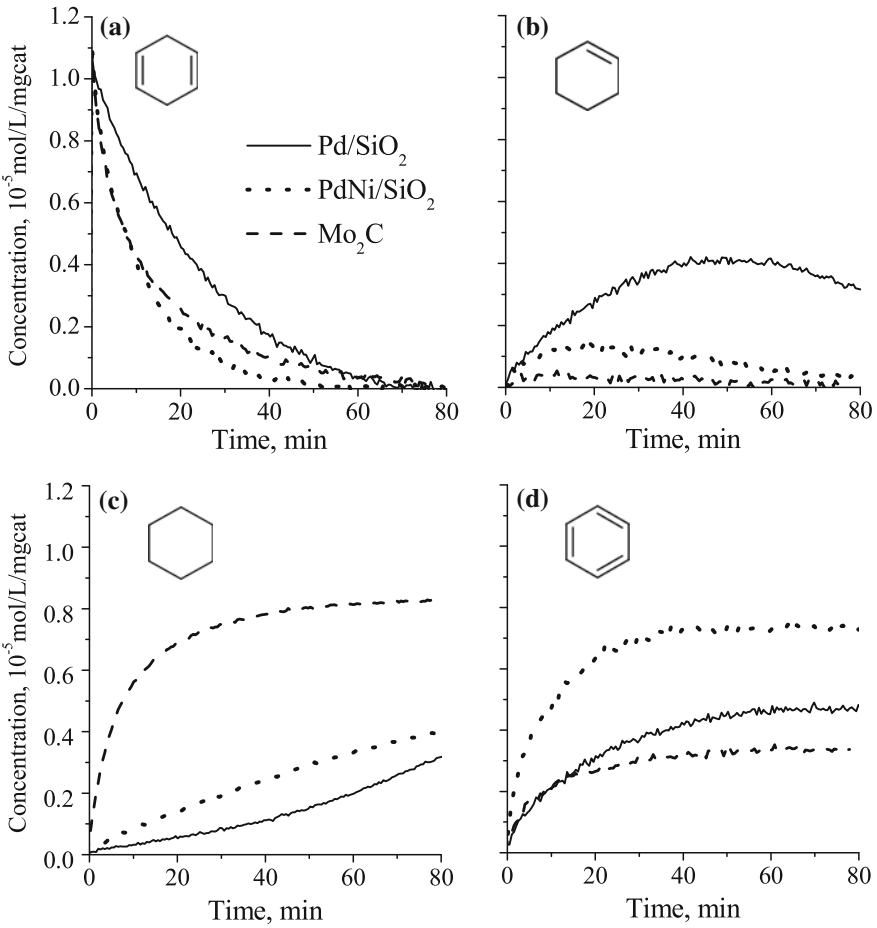

Fig. 5.9 Consumption of 1,4-cyclohexadiene (**a**) and formation of cyclohexene (**b**) cyclohexane (**c**) and benzene (**d**) over Mo_2C, Pd/SiO_2, and $PdNi/SiO_2$ (T = 308 K, $P_{1,4\text{-CHD}}$ = 7.8 Torr, P_{H2} = 17.2 Torr, P_{He} = 25 Torr)

Mo_2C that the consumption rate becomes lower than $PdNi/SiO_2$. After 60-min reaction, the consumption rate over Mo_2C decreases to the same level as Pd/SiO_2.

The formation curves of cyclohexene are shown in Fig. 5.9b. The highest formation peak of cyclohexene is observed on Pd/SiO_2, while the peak of cyclohexene over $PdNi/SiO_2$ forms at around 20 min and decreases afterward. The cyclohexene concentration over Mo_2C remains low over the whole time range.

The formation curves of cyclohexane are shown in Fig. 5.9c. The concentration of cyclohexane increases rapidly on Mo_2C, and the formation rate is much higher than the Pd-based catalysts. Figure 5.9d displays the formation of benzene. The

steady-state benzene concentration follows the order of $Mo_2C < Pd/SiO_2 < PdNi/SiO_2$.

According to the above results, the hydrogenation and dehydrogenation both exist in the reaction. Mo_2C shows similar hydrogenation activity with $PdNi/SiO_2$ and higher hydrogenation activity for the alkene hydrogenation, but with slightly higher deactivation rate.

5.4 Ni/Mo_2C for the Hydrogenation of 1,3-Butadiene

According to the results in the batch reactor, Mo_2C is as active as Pd-based catalysts for the hydrogenation reaction. However, the dienes would be easily hydrogenated to alkanes over Mo_2C. Based on the modification of Ni to Pd as studied in Chaps. 3 and 4, Mo_2C was modified by Ni to improve the selectivity to alkenes.

Mo_2C with Ni loadings of 1.5, 6.7, 8.6, and 12.4% was investigated in the batch reactor for the selective hydrogenation of 1,3-butadiene. The results were compared with Mo_2C and Pd-based catalysts, as shown in Fig. 5.10.

The 1,3-butadiene consumption curves are shown in Fig. 5.10a. The Ni-modified Mo_2C catalysts display similar activity as Mo_2C except the high loading 12.4% Ni/Mo_2C. Because the initial heat effects are different on the investigated catalysts, the initial recorded 1,3-butadiene concentrations are different. The normalized 1,3-butadiene consumption curves are shown in Fig. 5.11. With increasing Ni loading from 1.5 to 8.6%, the activities of Ni/Mo_2C only decrease slightly; when the Ni loading increases to 12.4%, the concentration of 1,3-butadiene first increases in the first 10 min and then decreases, possibly due to the desorption of 1,3-butadiene from the catalyst.

Figure 5.10b shows the 1-butene formation curves. The 1-butene formation peak on Mo_2C is the lowest; with increasing Ni loading, the 1-butene formation peak increases; when Ni loading increases to 8.6%, the 1-butene formation curve almost coincides with that over $PdNi/SiO_2$. The 1-butene concentration continues to rise within a low level over 12.4% Ni/Mo_2C because of the low hydrogenation activity.

The butane formation curves are shown in Fig. 5.10c. The results are consistent with the 1-butene formation regarding carbon balance. The butane concentration increases quickly on Mo_2C; with increasing Ni loading, the butane formation curve becomes lower. The formation curve of butane over $PdNi/SiO_2$ is lower than those over 1.5–8.6% Ni/Mo_2C.

It could be concluded that the Ni modification decreases the hydrogenation activity of 1-butene to butane and increases the 1-butene selectivity. Among the investigated catalysts, 8.6% Ni/Mo_2C shows similar 1,3-butadiene consumption rate and similar 1-butene hydrogenation activity, thus exhibiting similar 1-butene selectivity as $PdNi/SiO_2$.

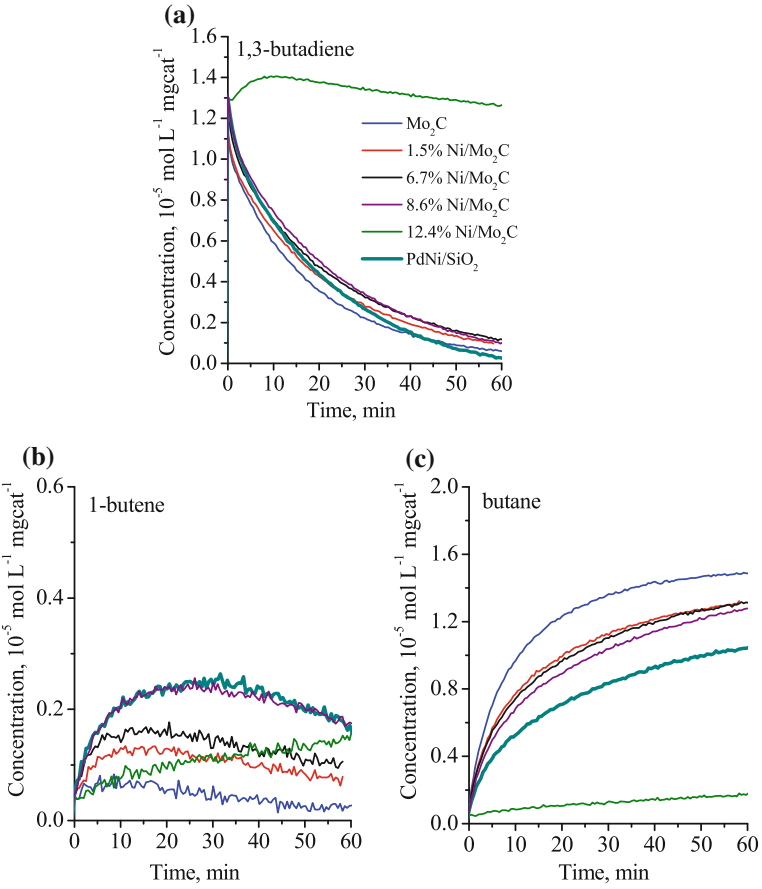

Fig. 5.10 Consumption of 1,3-butadiene (**a**) and formation of 1-butene (**b**) and butane (**c**) over Ni/Mo_2C with different loadings (T = 308 K, P_{BD} = 7.8 Torr, P_{H2} = 17.2 Torr, P_{He} = 25 Torr)

5.5 Discussion

5.5.1 Hydrogenation Activity and Stability

To make quantitative analysis of hydrogenation activity and rate of deactivation, the hydrogenation reaction rates are estimated by a first-order rate law with a second-order deactivation for the consumption of reactant dienes and are normalized by catalyst weight. A second-order deactivation model was used to fit the experimental data and to compare the deactivation between the different catalysts. It has been found that the second-order deactivation fits well for the hydrogenation reactions according to a previous study [32].

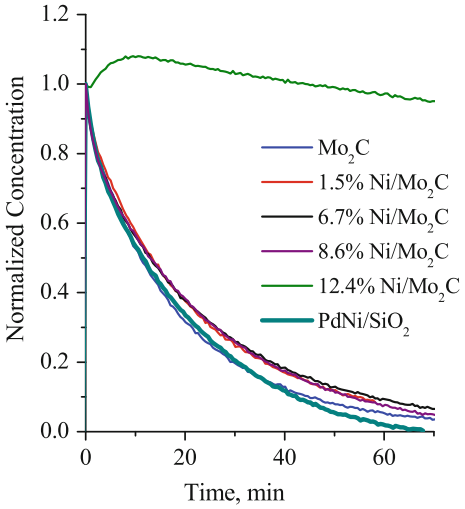

Fig. 5.11 Normalized consumption rate of 1,3-butadiene over Ni/Mo_2C with different loadings (T = 308 K, P_{BD} = 7.8 Torr, P_{H2} = 17.2 Torr, P_{He} = 25 Torr)

The derivations of the kinetic equations are shown below:

$$-r_A = -\frac{dC_A}{dt} = m_{cat}k_r a C_A \tag{5.1}$$

$$r_d = -\frac{da}{dt} = m_{cat}k_d a^2 \tag{5.2}$$

$$a = \frac{1}{m_{cat}k_d t + 1} \tag{5.3}$$

$$C_A = C_{A0}(m_{cat}k_d t + 1)^{-\frac{k_r}{k_d}} \tag{5.4}$$

C_A is the concentration of 1,3-butadiene/1,3-CHD/1,4-CHD; C_{A0} is the corresponding initial concentration; m_{cat} is the catalyst weight; r_A is the reaction rate; k_r is the reaction rate constant; r_d is the deactivation rate; k_d is the deactivation rate constant; t is time; and a is the deactivation parameter.

The fitting results using Eq. (5.4) are shown in Table 5.1.

The kinetic models for determining the hydrogenation and deactivation rate constants are the same as those described for 1,3-butadiene in a previous study [32]. The reaction rate (k_r) over $PdNi/SiO_2$ is similar to that over Pd/SiO_2 for 1,3-butadiene and 1,3-CHD hydrogenation reactions and is 2.9 times higher for 1,4-CHD hydrogenation. As shown in Figs. 5.7 and 5.8, when the activities are similar to $PdNi/SiO_2$ and Pd/SiO_2, the selectivity is better controlled over $PdNi/SiO_2$. The reaction rates over Mo_2C are similar to $PdNi/SiO_2$, and the rate for the hydrogenation of 1,4-CHD is higher than Pd/SiO_2.

Table 5.1 Summary of normalized reaction rate constants (k_r) and deactivation rates (k_d) on Mo_2C, $PdNi/SiO_2$, and Pd/SiO_2 for the hydrogenation of dienes

Normalized rate constant (min^{-1} g cat^{-1})		1,3-butadiene	1,3-CHD	1,4-CHD
Mo_2C	k_r	5.4	8.6	8.9
	k_d	1.6	18.0	4.9
$PdNi/SiO_2$	k_r	4.8	10.4	8.1
	k_d	0.6	6.9	1.9
Pd/SiO_2	k_r	4.9	12.2	3.1
	k_d	2.1	15.5	0

The deactivation rates over Mo_2C could not be ignored. The deactivation rate (k_d) over Mo_2C is generally higher than that over the Pd-based catalysts for the three diene molecules. For 1,3-butadiene and 1,4-CHD hydrogenation, the deactivation is almost absent over the Pd-based catalysts; however, for 1,3-CHD hydrogenation, the deactivation is rather significant over both Pd/SiO_2 and Mo_2C. The deactivation rates for the three diene molecules follow the order of 1,3-CHD $\gg$ 1,4-CHD > 1,3-butadiene.

The different performance in the hydrogenation reactions is most likely due to the molecular structures. 1,3-butadiene and 1,3-CHD contain conjugated structure and 1,3-CHD and 1,4-CHD contain cyclic structure. Compared with 1,3-CHD, the higher activity for 1,4-CHD over Mo_2C indicates that the conjugation in the diene molecules reduces the Mo_2C hydrogenation activity. On the other hand, the deactivation rate for the three molecules follows the trend of 1,3-butadiene < 1,4-CHD < 1,3-CHD, implying that the deactivation rate in the hydrogenation of cyclic dienes is higher than that in the hydrogenation of linear diene and that the conjugated diene is more easily to deactivate the catalysts than the corresponding unconjugated diene. Assuming that benzene is the precursor for coke formation, 1,3-CHD should have the molecular structure (both cyclic and conjugated) most facile to produce benzene and therefore leading to a faster catalyst deactivation. Other than the molecular structures, the different performance in the hydrogenation reactions might also be related to the different binding structures of the diene molecules on the different catalytic surfaces. The different surface areas of the SiO_2 supported Pd-based catalysts and the Mo_2C catalysts might also lead to differences in the hydrogenation activity and selectivity.

Although Mo_2C is more easily deactivated than Pd/SiO_2, it could be completely regenerated by H_2 treatment at 723 K. After performing H_2 treatment of the deactivated Mo_2C catalyst, the consumption curves for the three dienes were very similar to those with the fresh Mo_2C catalyst, while the Pd-based catalysts could not be completely regenerated in alkyne/diene hydrogenation reactions due to a complex metal-carbonaceous interaction. Therefore, Mo_2C is potentially a promising catalyst for diene hydrogenations in terms of both activity and catalytic regeneration.

5.5.2 Selectivity

The quantitative analysis was made for the 1,3-butadiene hydrogenation over Mo_2C, Pd/SiO_2, and $PdNi/SiO_2$, in order to compare the kinetic selectivity. Two reactions are defined as below:

$$C_4H_6 + H_2 \rightarrow C_4H_8 \quad \text{(Reaction 1)}$$

$$C_4H_8 + H_2 \rightarrow C_4H_{10} \quad \text{(Reaction 2)}$$

The rate constants were estimated by a first-order law and the derivations are shown as below:

$$\frac{dC_A}{dt} = -r_1 = -mk_1C_A \tag{5.5}$$

$$\frac{dC_B}{dt} = r_1 - r_2 = mk_1C_A - mk_2C_B \tag{5.6}$$

$$\frac{C_A}{C_{A0}} = e^{-mk_1t} \tag{5.7}$$

$$\frac{C_B}{C_{A0}} = \frac{k_1}{k_2 - k_1}\left(e^{-mk_1t} - e^{-mk_2t}\right) \tag{5.8}$$

C_A is the concentration of 1,3-butadiene; C_{A0} is the corresponding initial concentration; C_B is the concentration of 1-butene; k_1 is the reaction rate constant of Reaction 1; and k_2 is the reaction rate constant of Reaction 2. The kinetic selectivity in this study is defined as follows:

$$S_{1-\text{butene}} = \frac{k_1}{k_2} \times 100\% \tag{5.9}$$

The calculated k_1, k_2, and 1-butene selectivity are shown in Fig. 5.12 as a function of Ni loading. The corresponding rate constants and the selectivities of Mo_2C and Pd/SiO_2 are also included as references (Ni loading is 0 for Mo_2C). As shown in Fig. 5.12, with increasing Ni loading, the 1,3-butadiene hydrogenation rate remains nearly the same, but the 1-butene hydrogenation rate decreases significantly. As a result, the 1-butene selectivity increases with increasing Ni loading. When Ni loading increases to 6.7%, the selectivity reaches the same level of Pd/SiO_2. At a Ni loading of 8.6%, the selectivity is 0.43, which is higher than Pd/SiO_2. When Ni loading further increases to 12.4%, the 1,3-butadiene and 1-butene hydrogenation rates both decrease and the selectivity decreases slightly.

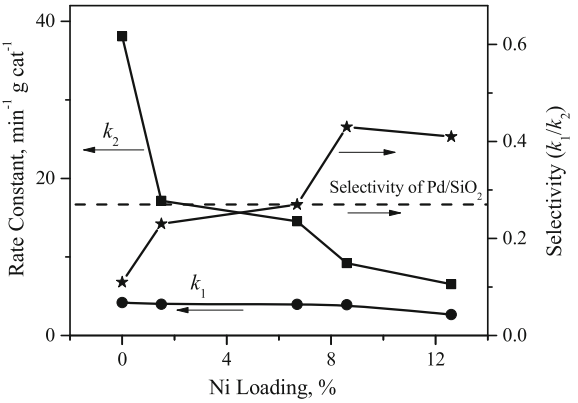

Fig. 5.12 Normalized reaction rate constants and the estimated selectivity on different loadings of Ni/Mo_2C (k_1: 1,3-butadiene → 1-butene; k_2: 1-butene → butane). Reprinted from Ref. [31], with kind permission from Springer Science+Business Media

In general, the Ni/Mo_2C catalysts retain similar 1,3-butadiene hydrogenation activity as Mo_2C at Ni loadings lower than 12.4%. However, on 12.4% Ni/Mo_2C, the 1,3-butadiene hydrogenation rate constant is only 2.7 min^{-1} g cat^{-1}, which is significantly lower than on Mo_2C (4.2 min^{-1} g cat^{-1}). The large loading of Ni likely covers some active sites on Mo_2C and inhibits the 1,3-butadiene hydrogenation. On the other hand, the increase in Ni loadings leads to a decrease in 1-butene hydrogenation activity, even at low Ni loadings. The different modification effects of Ni on the hydrogenation rate constants of 1,3-butadiene (k_1) and 1-butene (k_2) are responsible for the enhanced selectivity for 1-butene production.

Comparing the four investigated Ni/Mo_2C catalysts, the 1-butene selectivity of 8.6% Ni/Mo_2C is the highest and the 1,3-butadiene hydrogenation activity is retained close to Pd/SiO_2. The selectivities of Mo_2C and 8.6% Ni/Mo_2C are compared with Pd/SiO_2, PdNi/SiO_2, and Ni/SiO_2 as shown in Table 5.2. The 1-butene selectivity is 0.22 over Ni/SiO_2 and is 0.11 over Mo_2C, which are both lower than the selectivity of 8.6% Ni/Mo_2C, indicating that the higher selectivity over Ni/Mo_2C does not come from the separate effect of Mo_2C or Ni.

In a previous study, the 1-butene selectivity was enhanced by the modification of Ni in PdNi/Al_2O_3 bimetallic catalysts, and the higher 1-butene selectivity was

Table 5.2 Selectivity comparison of supported Pd and Ni catalysts with Mo_2C and Ni/Mo_2C catalysts

Catalyst	Selectivity (k_1/k_2)
0.9% Pd/SiO_2	0.27
1.5% Ni/SiO_2	0.22
0.9% Pd 1.5% Ni/SiO_2	0.59
Mo_2C	0.11
8.6% Ni/Mo_2C	0.43

attributed to the lower binding energy of 1-butene on the Ni–Pd bimetallic structure than on the monometallic Pd [10]. Furthermore, Ma et al. [33] reported that Ni showed strong interaction with Mo_2C on Ni/Mo_2C, and Porosoff et al. [34] reported that Co formed a $CoMoC_yO_z$ phase on Co/Mo_2C, which might also occur in the case of Ni/Mo_2C. Both studies suggest that the interaction of Ni with Mo_2C should modify the surface electronic properties, possibly leading to a decrease in 1-butene adsorption energy and thus increasing the selectivity.

5.5.3 Potential Advantage in Cost Reduction

Since the Ni/Mo_2C catalyst shows advantage in the selective hydrogenation of 1,3-butadiene, it is important to make a general comparison with Pd/SiO_2 considering both catalyst cost and activity. Cost evaluation is made for Pd/SiO_2, PdNi/SiO_2, Mo_2C, and 8.6% Ni/Mo_2C, and the results are summarized in Table 5.3. Here, a factor α is defined as follows to compare the catalysts in combining both cost and activity:

$$\alpha = \frac{\text{Price of catalyst (USD kg cat}^{-1})}{\text{Normalized Rate constant (min}^{-1}\text{ g cat}^{-1})} \tag{5.10}$$

As shown in Table 5.3, by replacing the precious metal with non-precious metal carbide, the value decreases by a factor of $\sim$4, from 0.039 to 0.009 USD min. However, the Mo_2C catalyst shows lower selectivity toward 1-butene than Pd/SiO_2 and PdNi/SiO_2, suggesting the limitation of replacing the precious metal catalysts by Mo_2C. By modifying Mo_2C with Ni, the selectivity increases to the same value of Pd/SiO_2. When the Ni loading is 8.6%, the selectivity is even higher than Pd/SiO_2. Meanwhile, the value α remains similar compared to Mo_2C. The higher 1-butene selectivity and the combined enhancement of activity and cost reduction of Ni/Mo_2C over Pd/SiO_2 suggest possible replacement of precious metal catalysts by Ni-modified non-precious metal carbide catalysts.

Table 5.3 Cost evaluation of Pd/SiO_2, Mo_2C, and 8.6% Ni/Mo_2C for 1,3-butadiene hydrogenation

Catalyst	Price (USD kg cat^{-1})	k_1 (min^{-1} g cat^{-1})	α (10^{-3} USD min)	Selectivity (k_1/k_2)
Pd/SiO_2	216.27	5.6	38.6	0.27
PdNi/SiO_2	216.28	4.8	45.1	0.59
Mo_2C	39.48	4.2	9.4	0.11
8.6% Ni/Mo_2C	38.41	3.9	9.8	0.43

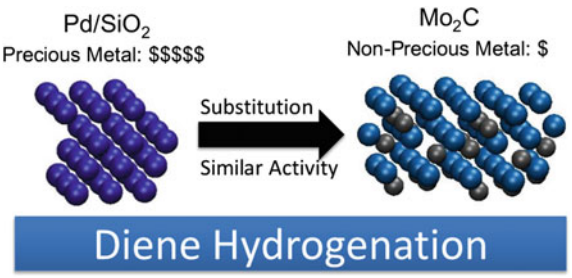

Fig. 5.13 The replacement of Mo_2C for the hydrogenation of dienes. Reprinted from Ref. [31], with kind permission from Springer Science+Business Media

5.6 Conclusion

In conclusion, the catalytic hydrogenation of 1,3-butadiene, 1,3-CHD, and 1,4-CHD has been compared over Pd/SiO_2, $PdNi/SiO_2$, and Mo_2C. The results show that Mo_2C has similar hydrogenation rate for 1,3-butadiene and 1,3-CHD, and even higher hydrogenation rate for 1,4-CHD. For 1,3-butadine hydrogenation, although Mo_2C shows similar activity with Pd/SiO_2, it gives lower selectivity to 1-butene. The Ni-modified Mo_2C catalysts significantly enhance the 1-butene selectivity, with 8.6% Ni/Mo_2C showing the highest selectivity.

Overall, both the Mo_2C and Ni/Mo_2C catalysts show enhancement in the combination of activity and catalyst cost reduction. In particular, as shown in Fig. 5.13, the combined advantages in activity, selectivity, and cost reduction of Ni/Mo_2C demonstrate the potential to use less expensive catalysts to replace precious metals for selective hydrogenation reactions. The major disadvantage of Ni/Mo_2C for industrial use is the stability, which is needed for further development.

References

1. Furlong BK, Hightower JW, Chan TYL et al (1994) 1,3-Butadiene selective hydrogenation over Pd/alumina and CuPd/alumina catalysts. Appl Catal A 117(1):41–51
2. Kripylo P, Turek F, Hempe KD et al (1975) Kinetics and hydrogenation mechanism of 1,3-dienes in presence of Pd catalysts .2. Kinetic studies of selective hydrogenation of cyclopentadiene, butadiene (1,3) and isoprene. Chem Tech (Leipzig) 27(11):675–679
3. Hightower JW, Furlong B, Sarkany A et al (1993) 1,3-Butadiene hydrogenation in 1-butene over alumina-supported Pd-Ag catalysts. Stud Surf Sci Catal 75:2305–2308
4. Sarkany A, Stefler G, Hightower JW (1995) Participation of support sites in hydrogenation of 1,3-butadiene over Pt/Al_2O_3 catalysts. Appl Catal A 127(1–2):77–92
5. Qi S, Yu W, Lonergan WW et al (2010) Low-temperature hydrogenation and dehydrogenation of 1, 3-cyclohexadiene on Pt/Ni bimetallic catalysts. Chin J Catal 31(8):955–960
6. Qi S, Yu W, Lonergan WW et al (2010) General trends in the partial and complete hydrogenation of 1,4-cyclohexadiene over Pt–Co, Pt–Ni and Pt–Cu bimetallic catalysts. ChemCatChem 2(6):625–628

7. Schrock RR, Osborn JA (1976) Catalytic hydrogenation using cationic rhodium complexes. 3. The selective hydrogenation of dienes to monoenes. J Am Chem Soc 98(15):4450–4455
8. Miura H, Terasaka M, Oki K et al (1993) Preparation of eggshell type Pd-Ag and Pd-Au catalysts by selective deposition and hydrogenation of 1,3-butadiene. Stud Surf Sci Catal 75:2379–2382
9. Hugon A, Delannoy L, Krafft J-M et al (2010) Selective hydrogenation of 1,3-butadiene in the presence of an excess of alkenes over supported bimetallic gold–palladium catalysts. J Phys Chem C 114(24):10823–10835
10. Hou R, Yu W, Porosoff MD et al (2014) Selective hydrogenation of 1,3-butadiene on PdNi bimetallic catalyst: from model surfaces to supported catalysts. J Catal 316:1–10
11. Lonergan WW, Vlachos DG, Chen JG (2010) Correlating extent of Pt–Ni bond formation with low-temperature hydrogenation of benzene and 1,3-butadiene over supported Pt/Ni bimetallic catalysts. J Catal 271(2):239–250
12. Lonergan WW, Xing XJ, Zheng RY et al (2011) Low-temperature 1,3-butadiene hydrogenation over supported Pt/3d/γ-Al_2O_3 bimetallic catalysts. Catal Today 160(1):61–69
13. Studt F, Abild-Pedersen F, Bligaard T et al (2008) Identification of non-precious metal alloy catalysts for selective hydrogenation of acetylene. Science 320(5881):1320–1322
14. Xu JH, Huang YQ, Yang XF et al (2014) Enhancement of acetylene hydrogenation activity over Ni–Zn bimetallic catalyst by doping with Au. J Nanosci Nanotechnol 14(9):6894–6899
15. Trimm DL, Cant NW, Liu IOY (2011) The selective hydrogenation of acetylene in the presence of carbon monoxide over Ni and Ni–Zn supported on $MgAl_2O_4$. Catal Today 178 (1):181–186
16. Piccolo L (2013) $Al_{13}Fe_4$ selectively catalyzes the hydrogenation of butadiene at room temperature. Chem Commun 49(80):9149–9151
17. Hwu HH, Chen JG (2005) Surface chemistry of transition metal carbides. Chem Rev 105 (1):185–212
18. Oyama S (1992) Preparation and catalytic properties of transition metal carbides and nitrides. Catal Today 15(2):179–200
19. Kitchin JR, Norskov JK, Barteau MA et al (2005) Trends in the chemical properties of early transition metal carbide surfaces: a density functional study. Catal Today 105(1):66–73
20. Ren H, Yu W, Salciccioli M et al (2013) Selective hydrodeoxygenation of biomass-derived oxygenates to unsaturated hydrocarbons using molybdenum carbide catalysts. ChemSusChem 6(5):798–801
21. Boullosa-Eiras S, Lødeng R, Bergem H et al (2014) Catalytic hydrodeoxygenation (HDO) of phenol over supported molybdenum carbide, nitride, phosphide and oxide catalysts. Catal Today 223:44–53
22. Dhandapani B, St. Clair T, Oyama S (1998) Simultaneous hydrodesulfurization, hydrodeoxygenation, and hydrogenation with molybdenum carbide. Appl Catal A 168(2):219–228
23. McCrea KR, Logan JW, Tarbuck TL et al (1997) Thiophene hydrodesulfurization over alumina-supported molybdenum carbide and nitride catalysts: effect of Mo loading and phase. J Catal 171(1):255–267
24. Szymańska-Kolasa A, Lewandowski M, Sayag C et al (2007) Comparison of molybdenum carbide and tungsten carbide for the hydrodesulfurization of dibenzothiophene. Catal Today 119(1–4):7–12
25. Lee JS, Yeom MH, Park KY et al (1991) Preparation and benzene hydrogenation activity of supported molybdenum carbide catalysts. J Catal 128(1):126–136
26. Da Costa P, Potvin C, Manoli JM et al (2001) Novel phosphorus-doped alumina-supported molybdenum and tungsten carbides: synthesis, characterization and hydrogenation properties. Catal Lett 72(1–2):91–97
27. St. Clair T, Dhandapani B, Oyama ST (1999) Cumene hydrogenation turnover rates on Mo_2C: CO and O_2 as probes of the active site. Catal Lett 58(4):169–171
28. Mamède AS, Giraudon JM, Löfberg A et al (2002) Hydrogenation of toluene over β-Mo_2C in the presence of thiophene. Appl Catal A 227(1–2):73–82

29. Alves JA, Bressa SP, Martinez OM et al (2004) Selective hydrogenation of 1,3-butadiene: improvement of selectivity by using additives. Chem Eng J 99(1):45–51
30. Schlapbach L, Züttel A (2001) Hydrogen-storage materials for mobile applications. Nature 414(6861):353–358
31. Hou R, Chang K, Chen JG et al (2015) Replacing precious metals with carbide catalysts for hydrogenation reactions. Top Catal 58(4):240–246
32. Wang T, Mpourmpakis G, Lonergan WW et al (2013) Effect of oxide supports in stabilizing desirable Pt–Ni bimetallic structures for hydrogenation and reforming reactions. Phys Chem Chem Phys 15(29):12156–12164
33. Ma YF, Guan GQ, Phanthong P et al (2014) Catalytic activity and stability of nickel-modified molybdenum carbide catalysts for steam reforming of methanol. J Phys Chem C 118 (18):9485–9496
34. Porosoff MD, Yang X, Boscoboinik JA et al (2014) Molybdenum carbide as alternative catalysts to precious metals for highly selective reduction of CO_2 to CO. Angew Chem Int Ed 126(26):6823–6827

Chapter 6
Selective Hydrogenation of Acetylene in Liquid Phase: A Novel Process

6.1 Introduction

The industrial process of the selective hydrogenation of acetylene uses a gas-phase reaction with supported Pd or Pd–Ag catalysts in a fixed-bed reactor. The front-end process requires less equipment investment and a simpler process flow than the tail-end process. However, the large amount of heat release and low ethylene selectivity could not be ignored. The released heat will lead to temperature rise or even temperature runaway in the fixed-bed reactor, which is not safe for the industrial production. In the front-end process over typical Pd-based catalysts, for example, the selectivity to ethane is $\sim$110% on Pd/Al_2O_3 and $\sim$60% on $PdAg/Al_2O_3$ at a high conversion near 100% [1]. Different methods have been investigated to suppress ethane formation, which include enhancing the dispersion of palladium [2–6], adding a second metal to form bimetallic catalysts [1, 7–14], utilizing the strong metal–support interaction [15, 16], and introducing an inhibiting gas such as CO [17] and NO_x [18–20].

Another consideration in this work was that the selective hydrogenation of pure or highly concentrated acetylene can be an alternative approach to produce ethylene. The oil crises have made the steam cracking of naphtha a less economical route to produce ethylene. A promising alternative route for the production of ethylene is to use natural gas as feedstock. As the price of natural gas is expected to dramatically decrease due to its projected production from shale gas and methane hydrate, cheap acetylene would become available from the partial oxidation process. Then, the selective hydrogenation of acetylene will be economical for the production of ethylene. However, the hydrogenation of pure or highly concentrated acetylene is very different from the removal of trace acetylene from ethylene. The gas-phase process in a fixed-bed reactor is not suitable since the reaction requires the removal of a huge amount of reaction heat. A slurry reactor for liquid-phase hydrogenation has very good heat transfer capability, and it should be used to give a uniform temperature profile.

R. Hou, *Catalytic and Process Study of the Selective Hydrogenation of Acetylene and 1,3-Butadiene*, Springer Theses, DOI 10.1007/978-981-10-0773-6_6

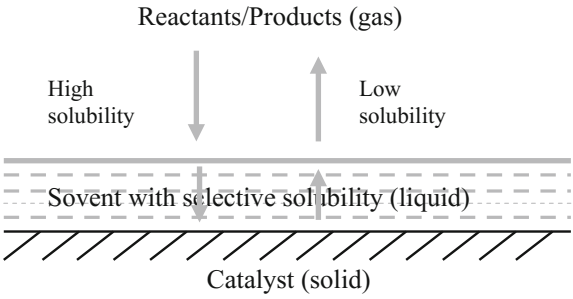

Fig. 6.1 Schematic diagram of the coupling of absorption to reaction in selective hydrogenation

In recent years, ionic liquids (ILs) have been used to improve the catalyst performance by coating the solid catalyst with an ionic liquid layer (SCILL) [21–24] or support the ionic liquid phase on the catalyst (supported ionic liquid phase, SILP) [25]. By the modification of ionic liquid, the Pd-based catalyst showed higher ethylene selectivity in a fixed-bed reactor [24, 25]. The possible reason was attributed to the selective solubility of the reported ionic liquid for acetylene over ethylene. Based on the above results, a new concept was adopted to enhance the ethylene selectivity by introducing a liquid phase to couple the selective absorption with the selective hydrogenation reaction on the catalyst surface, which is shown in Fig. 6.1. Acetylene has a high solubility in polar solvents, such as acetone, *N*,*N*-dimethylmethanamide (DMF), *N*-methyl-2-pyrrolidone (NMP), and some ionic liquids [26], while ethylene has a much lower solubility in these solvents. A selective solubility factor (α) was defined as the ratio of acetylene to ethylene solubilities [26]. Several liquids have very high selective solubility factors for acetylene and ethylene. For example, the factor α is 18.5 for NMP [27] and 45 for 1,3-dimethylimidazolium methylphosphite ([DMIM][$MeHPO_3$]) [26]. The large difference in solubility can be used to modify the acetylene and ethylene concentrations on the catalyst surface and suppress the production of ethane by introducing the solvent to the reaction system.

The introduction of liquid phase into the gas–solid reaction system could significantly enhance the heat transfer. A typical reactor type is the slurry reactor, as shown in Fig. 6.2. The liquid phase would efficiently remove the heat on the surface of the catalyst and prevent the temperature runaway.

The liquid-phase hydrogenation has been reported by several authors/institutes [28–31]. The first study on the liquid-phase hydrogenation of acetylene was reported by Edvinsson et al. [28] in 1995. In that study, they found that heptane formed a liquid film on the catalyst layer in a monolith reactor, which improved catalyst stability by removing green oil from the catalyst. In 2005, syngas filed patents and reported a liquid-phase reaction for acetylene hydrogenation [29, 30]. The technology first dissolved acetylene into a solvent, and then, the solvent contacted with the catalyst; after the reaction, ethylene was separated from the solvent and reactants. Shitova et al. [31] studied the hydrogenation of acetylene in *N*-methylpyrrolidone (NMP) in the presence of CO and observed that by

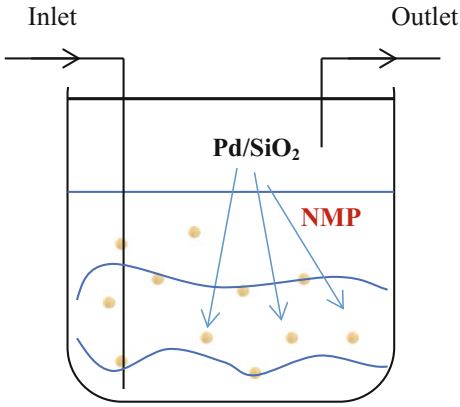

Fig. 6.2 Liquid-phase hydrogenation of acetylene in a slurry reactor

introducing NMP as the liquid phase, the selectivity to ethylene was increased to 90% at a high acetylene conversion of 96%.

Although the use of a liquid phase has been shown to give better selectivity to ethylene, there is still room for further improvement. In addition, the underlying mechanism is not yet clear. Although catalyst stability was improved by using heptane, the selectivity to ethylene was not enhanced and the highest selectivity to ethylene was 80% at a low acetylene conversion of 30% [28]. In NMP, the selectivity to ethylene was below 20% over the Pd/Sibunit catalyst without co-feeding CO [31]. For the SCILL catalysts, the presence of the ionic layer significantly decreased catalytic activity [24, 25].

In this chapter, the work aims to further improve the selectivity to ethylene while maintaining a high activity in the liquid-phase hydrogenation of acetylene. The reaction was carried out in a slurry reactor, with selective solvent as liquid phase. The presence of the liquid phase intensifies the heat transfer and enhances the selectivity to ethylene. The work in this chapter firstly optimized the reaction operating parameters and studied the solvent effects; secondly compared the liquid modifications in bulk liquid-phase reaction with the SCILL catalyst in a fixed-bed reactor; and finally optimized the reactor type and designed industrial reactor in concept according to the disadvantages of the single-stage slurry reactor.

6.2 Catalyst Characterization

The catalyst used in the liquid-phase reaction was 0.01 wt% Pd/SiO_2. The support was low surface area SiO_2 (S.A. <1.0 m^2/g). The XRD spectra, SEM image, and TEM image are shown in Fig. 6.3.

The XRD spectra shown in Fig. 6.3a present sharp SiO_2 peaks, indicating the presence of large SiO_2 particles. No Pd or PdO peak is observed because of the low Pd loading.

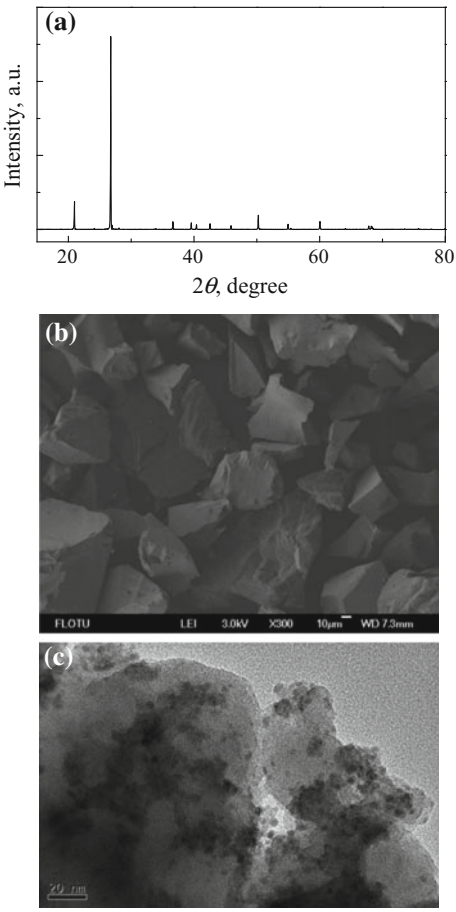

Fig. 6.3 Characterization of Pd/SiO_2: **a** XRD **b** SEM **c** TEM

Figure 6.3b shows the SEM image of Pd/SiO_2. The surface of SiO_2 is relatively flat with little pore structures. The particle sizes are between 20 and 100 μm.

Figure 6.3c shows the TEM image of Pd/SiO_2. It could be seen that the metal particles are uniformly distributed on the support and the particle sizes are between 2 and 4 nm.

The particle size distribution of Pd/SiO_2 is shown in Fig. 6.4. It could be seen that the metal particles are uniform and the average particle size is about 2.8 nm.

6.3 Optimization of Operation Parameters

The operation temperature, GHSV, and ratio of H_2/C_2H_2 were investigated and optimized for the selective hydrogenation of acetylene in the liquid phase. The results were compared with gas-phase reaction under the same reaction parameters.

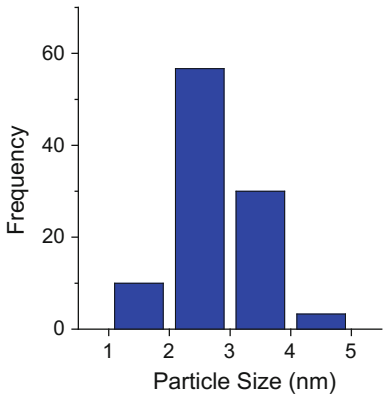

Fig. 6.4 Particle size distribution on Pd/SiO_2

The reactor for the liquid phase was a perfectly mixed slurry reactor; the liquid phase was NMP; the outlet gas phase was analyzed using an online GC. The acetylene conversion and products' selectivities were calculated as follows:

Conversion:

$$X = \frac{C_{C_2H_2,\,in} - C_{C_2H_2,\,out}}{C_{C_2H_2,\,in}} \times 100\% \tag{6.1}$$

Selectivities:

$$S_{C_2H_4} = \frac{C_{C_2H_4,\,out}}{C_{C_2H_2,\,in} - C_{C_2H_2,\,out}} \times 100\% \tag{6.2}$$

$$S_{C_2H_6} = \frac{C_{C_2H_6,\,out}}{C_{C_2H_2,\,in} - C_{C_2H_2,\,out}} \times 100\% \tag{6.3}$$

$$S_{C4} = \frac{C_{C_4H_6,\,out} + \sum C_{C_4H_8,\,out} + C_{C_4H_{10},\,out}}{C_{C_2H_2,\,in} - C_{C_2H_2,\,out}} \times 100\% \tag{6.4}$$

6.3.1 *Effect of Temperature*

The GHSV was fixed at 3600 mL $gcat^{-1}$ h^{-1}; the ratio of H_2/C_2H was fixed at 6; and the temperature range was 40–120 °C. The acetylene conversion and the products' selectivities as a function of temperature were plotted in Fig. 6.5.

The acetylene conversion trend with temperature in the liquid phase is similar to that in the gas phase: The conversion increases with increasing temperature. When the temperature rises to 80 °C, the conversions are almost 100% in both liquid phase and gas phase. However, the conversion changes differently above 80 °C in

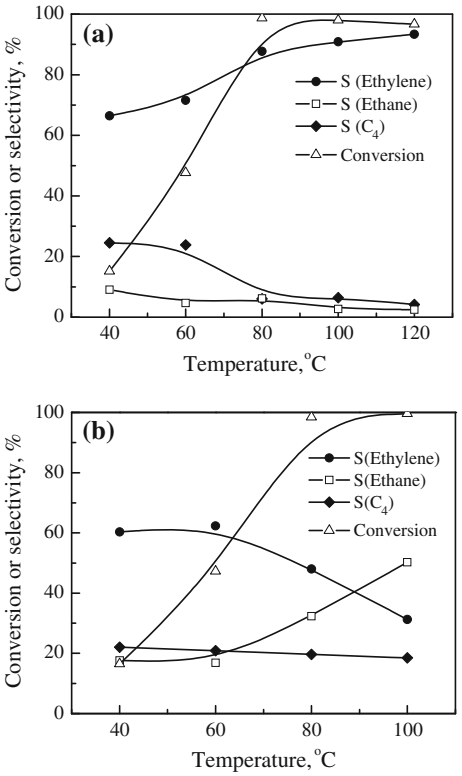

Fig. 6.5 Temperature effect in the selective hydrogenation of acetylene in **a** liquid phase and **b** gas phase (H_2/C_2H_2 = 6, GHSV = 3600 ml $gcat^{-1}$ h^{-1}). Reprinted with the permission from Ref. [32]. Copyright 2013 American Chemical Society

the two phases. In the gas phase, the conversion remains at 100% above 80 °C, while in the liquid phase, the conversion decreases slightly when the temperature rises from 80 to 120 °C. The slight decrease in conversion in the liquid phase is probably due to the decrease in acetylene solubility when the temperature rises above 80 °C. If there is not enough acetylene dissolved in the liquid and not enough transferred to the surface of the catalyst, the conversion would not reach 100%.

The selectivities to ethylene, ethane, and C4 species differ significantly in the liquid phase from those in the gas phase. In the liquid phase, the ethane selectivity decreases with increasing temperature and is generally lower than that in the gas phase. It decreases below 3% when temperature is above 80 °C in the liquid phase, while in the gas phase, it increases continuously with increasing temperature and remains above 18%. When the acetylene conversion is close to 100%, the ethane selectivity was controlled at $\sim$3% in the liquid phase, but is 32% with a lot excess hydrogenation in the gas phase.

The selectivity to C4 species decreases slightly with increasing temperature in the liquid phase. It is about 24% when temperature is below 80 °C and decreases to 4–6% when the temperature is above 80 °C. In the gas phase, the selectivity to C4 species is about ~20% and does not change much with temperature.

Due to the better control of selectivities to ethane and C4 species, the selectivity to ethylene is generally higher in the liquid phase than in the gas phase. Specially, when temperature is above 100 °C, the ethylene selectivity in the liquid phase is above 90% at the acetylene conversion of ~96%. In comparison, the ethylene selectivity is below 50% when conversion is almost 100% in the gas phase.

At higher temperature (>80 °C), the selectivity to ethylene is significantly enhanced when the liquid phase is present, which comes from the better control of the oligomerization reaction and the ethylene hydrogenation reaction. On one hand at higher conversion of acetylene at relatively high temperature, the acetylene concentration at the surface of the catalyst is low in the liquid phase, and thus, the oligomerization reaction is reduced. On the other hand at higher temperature, because of the low solubility, the ethylene could escape from the liquid phase once it forms on the surface of the catalyst, and thus, the hydrogenation reaction to ethane is better controlled.

6.3.2 *Effect of GHSV*

The ratio of H_2/C_2H_2 was fixed at 10; the temperature was fixed at 100 °C; the GHSV varied from 3600 to 24,000 ml $gcat^{-1}$ h^{-1}. The acetylene conversion as a function of GHSV is shown in Table 6.1. The products' selectivities are shown in Fig. 6.6.

As shown in Table 6.1, the acetylene conversion decreases with increasing GHSV in both liquid phase and gas phase. In the liquid phase, the acetylene conversion decreases slowly when GHSV increases from 3600 to 12,000 ml $gcat^{-1}$ h^{-1}, and decreases to 32% when GHSV increases to 24,000 ml $gcat^{-1}$ h^{-1}. In the gas phase, the acetylene conversion remains at 100% when GHSV is lower than 12,000 ml $gcat^{-1}$ h^{-1}, and decreases to 34% when GHSV increases to 24,000 ml $gcat^{-1}$ h^{-1}.

The selectivity to C4 species increases with increasing GHSV in both the liquid phase and gas phase. At low GHSV of 3600 ml $gcat^{-1}$ h^{-1}, the selectivity to C4 species in the liquid phase is lower than 5% and increases significantly with increasing GHSV, but is still generally lower than that in the gas phase. The

Table 6.1 Acetylene conversion at different GHSVs in both liquid phase and gas phase. Reprinted with the permission from Ref. [32]. Copyright 2013 American Chemical Society

GHSV (ml $gcat^{-1}$ h^{-1})	3600	8000	12,000	18,000	24,000
Liquid phase (%)	97	92	84	–	32
Gas phase (%)	100	100	100	56	34

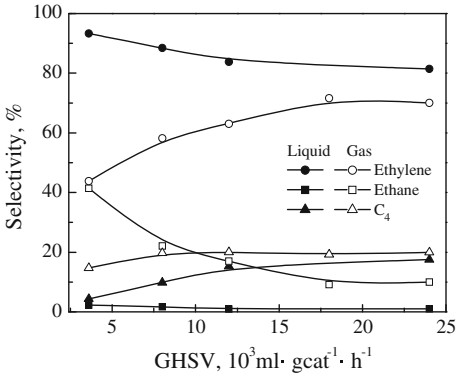

Fig. 6.6 Comparison of GHSV effect on selectivities in the liquid phase and gas phase (H_2/C_2H_2 = 10, T = 100 °C). Reprinted with the permission from Ref. [32]. Copyright 2013 American Chemical Society

selectivity to C4 species in the gas phase only increases slightly with increasing GHSV and is about 20% at the investigated GHSV range.

The selectivity to ethane does not change much with increasing GHSV in the liquid phase and remains at ~2.5%. However, the selectivity to ethane in the gas phase decreases from 41.5 to 9.1% with increasing GHSV.

The selectivity to ethylene decreases with increasing GHSV in the liquid phase and increases with increasing GHSV in the gas phase. Nevertheless, the selectivity to ethylene is still higher in the liquid phase than that in the gas phase within the investigated GHSV range. The lowest selectivity to ethylene of 81% in the liquid phase is observed at the GHSV of 24,000 ml gcat^{-1} h^{-1}, which is ~10% higher than that in the gas phase.

At high GHSVs, the acetylene concentration at the surface of the catalyst are both high in the liquid phase and gas phase, and there is little enhancement in the control of oligomerization reaction. On the contrast, the low GHSV is beneficial to control the C4 selectivity. The ethane selectivity is not much affected by GHSV, and the higher ethylene selectivity in liquid phase mainly comes from the better control of the excess hydrogenation.

6.3.3 *Effect of H_2/C_2H_2 Ratio*

The GHSV was fixed at 3600 ml gcat^{-1} h^{-1}; the temperature was fixed at 100 °C; the ratio of H_2/C_2H_2 was decreased from 40 to 4 in the experiment. The acetylene conversions were close to 100% under the investigated reaction conditions in both liquid phase and gas phase. The selectivities to different products with increasing ratio of H_2/C_2H_2 are shown in Fig. 6.7.

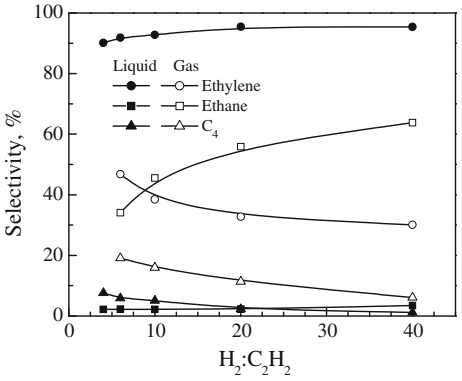

Fig. 6.7 Comparison of H_2/C_2H_2 ratio effect on selectivities in the liquid phase and gas phase (GHSV = 3600 ml $gcat^{-1}$ h^{-1}, T = 100 °C). Reprinted with the permission from Ref. [32]. Copyright 2013 American Chemical Society

The selectivity to C4 species increases with decreasing H_2/C_2H_2 ratio in both liquid phase and gas phase. When the H_2/C_2H_2 ratio decreases from 40 to 4, the selectivity to C4 species increases from 1.2 to 7.6% in the liquid phase and increases from 6.1 to 19.1% in the gas phase. Higher H_2/C_2H_2 ratio enhances the competitive adsorption of hydrogen to acetylene on the catalyst and reduces the oligomerization reaction.

The ethane selectivity is much better controlled in the liquid phase and remains below 3% at the investigated H_2/C_2H_2 ratios, while in the gas phase, the selectivity to ethane decreases from 64 to 34% when the H_2/C_2H_2 ratio decreases from 40 to 4. The ethylene concentration on the surface of the catalyst is effectively controlled in the liquid phase due to the selective absorption; thus, the ethylene hydrogenation to ethane is much depressed compared with the gas-phase hydrogenation.

The selectivity to ethylene decreases from 95 to 92% in the liquid phase when the H_2/C_2H_2 ratio decreases from 40 to 4, while that in the gas phase increases from 30 to 47%. The ethylene selectivity is much higher in the liquid phase within the investigated H_2/C_2H_2 ratio range, and the advantage is more significant at higher H_2/C_2H_2 ratio.

Additional experiments (results shown in Fig. 6.8) were carried out in the liquid phase to study the effect of H_2/C_2H_2 ratio at different reaction temperatures.

The conversion of acetylene increases with decreasing H_2/C_2H_2 ratio at 80 and 100 °C. The conversion is close to 100% at 60 °C at all H_2/C_2H_2 ratios, but the selectivity to ethylene is much lower (79–85%) than those at 80 and 100 °C. The formation of C4 species is the main side reaction at low H_2/C_2H_2 ratios, while the complete hydrogenation to ethane is the main side reaction at high H_2/C_2H_2 ratios. The selectivity to ethylene is 90% at 80–100 °C. The highest selectivity to ethylene of 96% is obtained at 80 °C, H_2/C_2H_2 = 40, and GHSV = 3600 ml $gcat^{-1}$ h^{-1}.

The conversion and selectivity in the liquid-phase hydrogenation are sensitive to the reaction temperature. At a low reaction temperature (60 °C), the acetylene

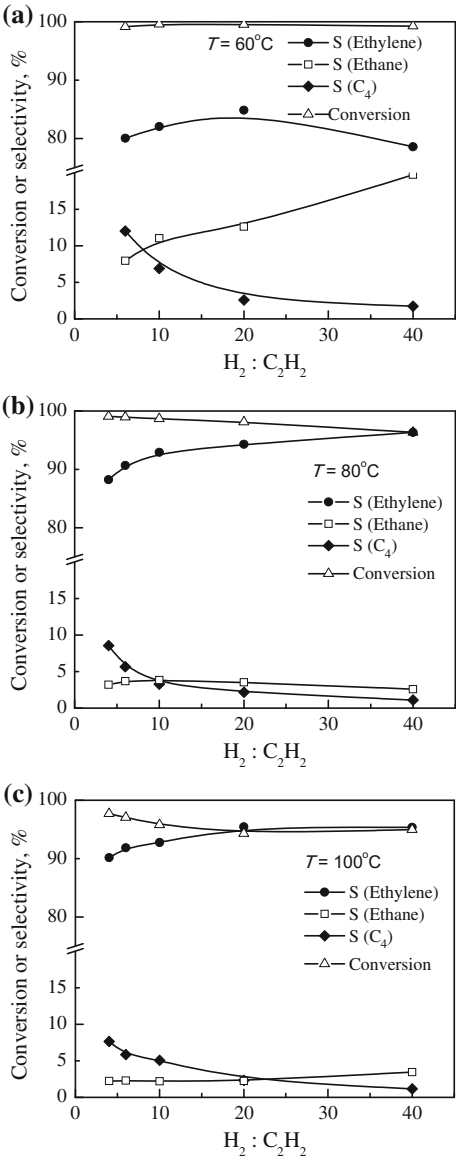

Fig. 6.8 Effect of H_2/C_2H_2 ratio in the liquid-phase hydrogenation at **a** 60 °C, **b** 80 °C, and **c** 100 °C (GHSV = 3600 ml $gcat^{-1}$ h^{-1}). Reprinted with the permission from Ref. [32]. Copyright 2013 American Chemical Society

conversion is high, but the selectivity to ethylene is much lower than those at 80 and 100 °C. The reason is that the solubility values are relatively high at a low temperature. It is believed that the high concentration of ethylene in the liquid would result in an increased selectivity to ethane; the high concentration of

acetylene in the liquid would lead to high acetylene coverage on the catalyst surface and an enhanced selectivity to C4 species.

The effect of the H_2/C_2H_2 ratio was explained by the competing adsorption of H_2, C_2H_2, and C_2H_4 on the Pd surface, together with the formation of the carbide phase and hydride phase [33]. As the acetylene concentration decreased with increasing H_2/C_2H_2 ratio, the selectivity to C4 species increased and the selectivity to ethane decreased. This was consistent with the results of García-Mota et al. [33] who reported that the selectivity to alkane increased with increasing H_2/alkyne ratio. In that study, the authors proposed that at higher H_2/alkyne ratios, the formation of Pd–H changed the reaction selectivity toward alkanes. This mechanism also explained the results of the present work about why a much lower selectivity to ethane was obtained in the liquid phase compared to that in the gas-phase hydrogenation. In the liquid phase, the formation of the hydride phase was significantly reduced due to the low solubility of hydrogen, and thus, the formation of ethane was much less.

6.3.4 Comparison with Gas-Phase Reaction

The selectivities to ethylene in the liquid phase and gas phase were summarized and replotted against acetylene conversion in Fig. 6.9. Despite the different reaction conditions, the data fell on the same trend line for both the liquid-phase and the gas-phase reactions.

The selectivity to ethylene is about 70% in the gas phase and is about 80% in the liquid phase at conversions below 80%. At conversions above 80%, the selectivity to ethylene decreases with increasing conversion in the gas phase and decreases to ~60% at the conversion close to 100%; in the liquid phase, the selectivity to ethylene increases with increasing conversion and is about 93% when conversion is close to 100%.

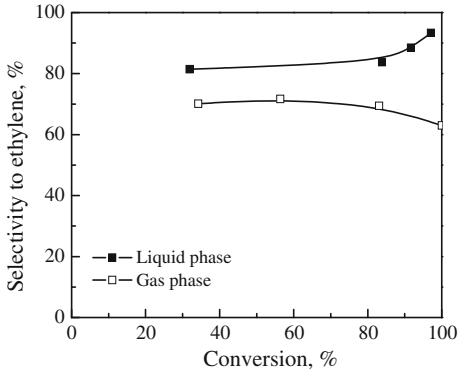

Fig. 6.9 Comparison of the ethylene selectivity as a function of acetylene conversion in the liquid phase and gas phase. Reprinted with the permission from Ref. [32]. Copyright 2013 American Chemical Society

At high acetylene conversions, the selectivity to ethylene differs significantly in the two systems. In the gas phase, as acetylene is hydrogenated, ethylene is more concentrated on the catalyst surface and is more easily hydrogenated to ethane. In the liquid phase, ethylene could escape away from the liquid phase due to its low solubility, and ethylene concentration on the catalyst surface is low, which leads to the suppression of complete hydrogenation. Moreover, as acetylene is converted, the acetylene concentration on the catalyst surface is reduced in the liquid phase and the oligomerization reaction is better controlled. As a result, the selectivity to ethylene is high at high acetylene conversion.

The high selectivity to ethylene at a high acetylene conversion in the liquid phase is an important advantage of the liquid-phase hydrogenation because a very high conversion is needed for the selective hydrogenation of acetylene for the purification of the ethylene stream [34]. For example, the acetylene conversion must be higher than 99.95% to reduce the acetylene concentration to below 5 ppm in a C2 stream with 1% acetylene.

6.4 Solvent Effect

6.4.1 Selective Solubility

To examine the effect of the selective solubility of acetylene in the liquid phase, a comparative experiment was carried out using decane as a non-selective solvent. The solubilities of acetylene and ethylene in NMP and decane are shown in Fig. 6.10. As shown in the figure, acetylene has a much higher solubility than ethylene in NMP, whereas acetylene and ethylene have low and similar solubilities

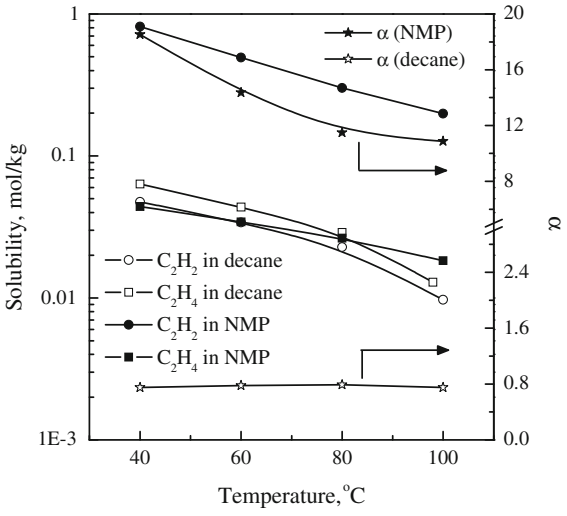

Fig. 6.10 Solubilities of acetylene and ethylene along with α at different temperatures in NMP and decane (α = dissolved acetylene/dissolved ethylene). Reprinted with the permission from Ref. [32]. Copyright 2013 American Chemical Society

in decane. For a quantitative description, a selective solubility factor was defined as follows:

$$\alpha = \frac{\text{dissolved acetylene (mol/kg)}}{\text{dissolved ethylene (mol/kg)}} \tag{6.5}$$

The selective solubility factor α of NMP is larger than 10, which indicates that NMP is a highly selective solvent for acetylene. With increasing temperature, the solubility of acetylene in NMP decreases much faster than that of ethylene. As a result, the value of α in NMP decreases from 18.5 at 40 °C to 10.9 at 100 °C. In contrast, acetylene and ethylene have very similar solubilities in decane, with that of ethylene being a little higher. The value of α for decane is less than 1, and it is almost independent of temperature, indicating that decane is a non-selective solvent for acetylene.

The liquid-phase hydrogenation using NMP and decane was studied at a H_2/C_2H_2 ratio of 10 and GHSV of 3600 ml $gcat^{-1}$ h^{-1}. The results are shown in Fig. 6.11. At all temperatures, the conversion of acetylene is near 100% in NMP and 90–94% in decane. This is due to the much lower solubility of acetylene in decane. The selectivity to ethane is much higher in decane than in NMP. Accordingly, the selectivity to ethylene in decane is about 70%. In contrast, in NMP, the selectivity to ethylene is about 90%. These results indicate that a selective solvent effectively suppresses the production of ethane and C4 species. Besides the selective solubility factor, the absolute values of the acetylene and ethylene solubilities are also important. High acetylene solubility tends to give more C4 by-product, while high ethylene solubility gives more ethane from complete hydrogenation. This explains the lower selectivity in NMP at 60 °C where the solubilities of both acetylene and ethylene are higher than those at 80–100 °C.

6.4.2 Viscosity

[DMIM][Me_2PO_4] was reported to have high selective solubility of 45 at room temperature [26], which is even higher than NMP. The high value of α might enhance the ethylene selectivity more effectively than NMP according to the results in Sect. 6.4.1. In this section, [DMIM][Me_2PO_4] was chosen as the liquid phase for the hydrogenation of acetylene. The results are shown in Fig. 6.12.

The selectivity to ethylene in [DMIM][Me_2PO_4] is generally higher than in the gas phase. It increases from ~75 to ~90% when temperature increases from 80 to 160 °C. However, within the investigated temperature range, the acetylene conversion remains at a low level. The conversion is only 34% when temperature is 160 °C. In comparison, the conversion of acetylene in the NMP liquid phase is almost 100% when temperature is 80 °C.

During the liquid-phase reaction in [DMIM][Me_2PO_4], large gas bubbles were observed moving slowly in the liquid and were not broken. It could be indicated

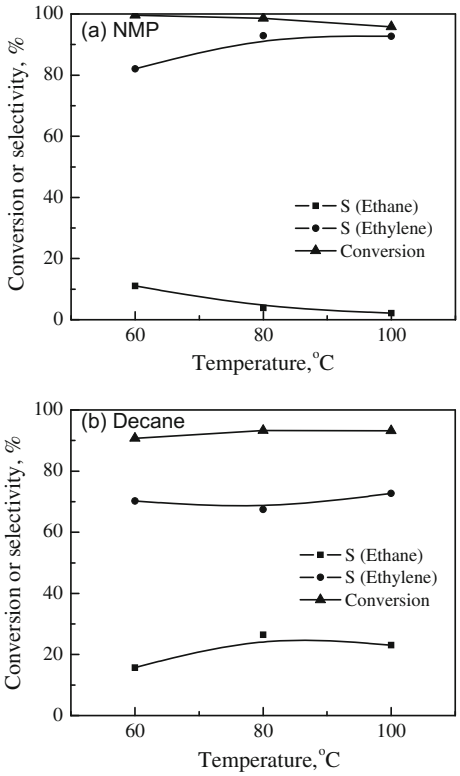

Fig. 6.11 Effect of selective solvents in the liquid-phase hydrogenation **a** NMP and **b** decane. (H_2/C_2H_2 = 10, GHSV = 3600 ml $gcat^{-1}$ h^{-1}). Reprinted with the permission from Ref. [32]. Copyright 2013 American Chemical Society

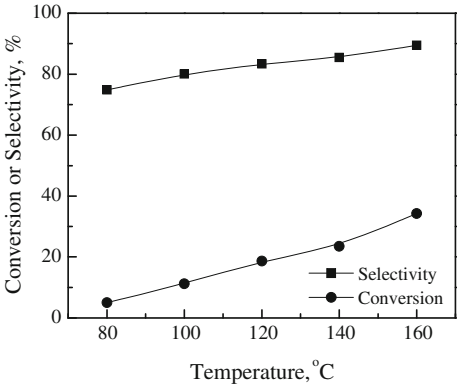

Fig. 6.12 Liquid-phase hydrogenation in [DMIM][Me_2PO_4] (GHSV = 3600 ml $gcat^{-1}$ h^{-1}, H_2/C_2H_2 = 6)

Table 6.2 Physical properties of NMP and [DMIM][Me_2PO_4]

Solvent	Viscosity (mPa s)	α
NMP	1.65	18.5
[DMIM][Me_2PO_4]	363	45

that there is a lot of mass transfer resistance in the ionic liquid. The viscosities and the selective solubilities of NMP and [DMIM][Me_2PO_4] are listed in Table 6.2. Although the α value is much higher in [DMIM][Me_2PO_4], the viscosity is two magnitudes lower than NMP, which inhibits the mass transfer from the gas phase to the liquid phase, and leads to a low acetylene conversion even at high temperature.

6.5 Induction Period

Under some reaction conditions, an induction period was observed in the liquid-phase hydrogenation in NMP. The induction period was investigated at T = 60 °C, H_2/C_2H_2 = 40, and GHSV = 3600 ml $gcat^{-1}$ h^{-1} within the first 720 min. The conversion of acetylene and selectivities to products is shown in Fig. 6.13.

Three stages could be observed in the first 720 min. The first stage is 0–75 min, during which the conversion of acetylene increases, the selectivity to ethane increases, and the selectivity to C4 species decreases rapidly. The second stage is 75–250 min, during which the conversion continues to increase, the selectivity to ethane decreases, and the selectivity to C4 species decreases slightly. The third stage is after 250 min, during which the reaction reaches the steady state, and the conversion and selectivities do not change much. According to the phenomenon, it

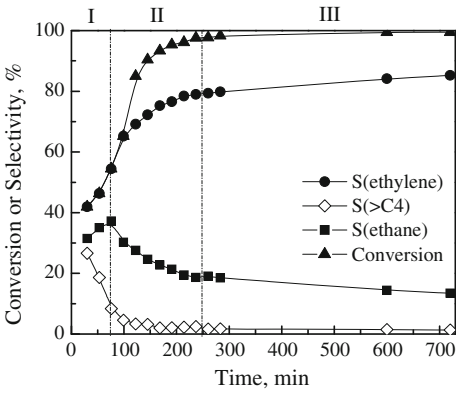

Fig. 6.13 Induction period in the liquid-phase hydrogenation in NMP (T = 60 °C, H_2/C_2H_2 = 40, GHSV = 3600 ml $gcat^{-1}$ h^{-1})

could be implied that the first stage is period of the PdH_x formation, because PdH_x enhances ethane formation and suppresses C4 formation. The second stage should be the formation of PdC_x, which suppresses the hydrogenation of ethylene to ethane.

6.6 Catalyst Stability

The catalyst in the liquid-phase hydrogenation showed good stability, but only under certain conditions, namely a relatively high temperature, high H_2/C_2H_2 ratio, and low space velocity. No green oil was observed under these conditions after 12 h of reaction. However, severe deactivation occurred at low reaction temperatures, low hydrogen ratios, and high space velocities. Under these latter conditions, some dark brown flecks were formed on and around the catalyst and in the solvent within the first two hours. The deactivation process is shown in Fig. 6.14. In the early

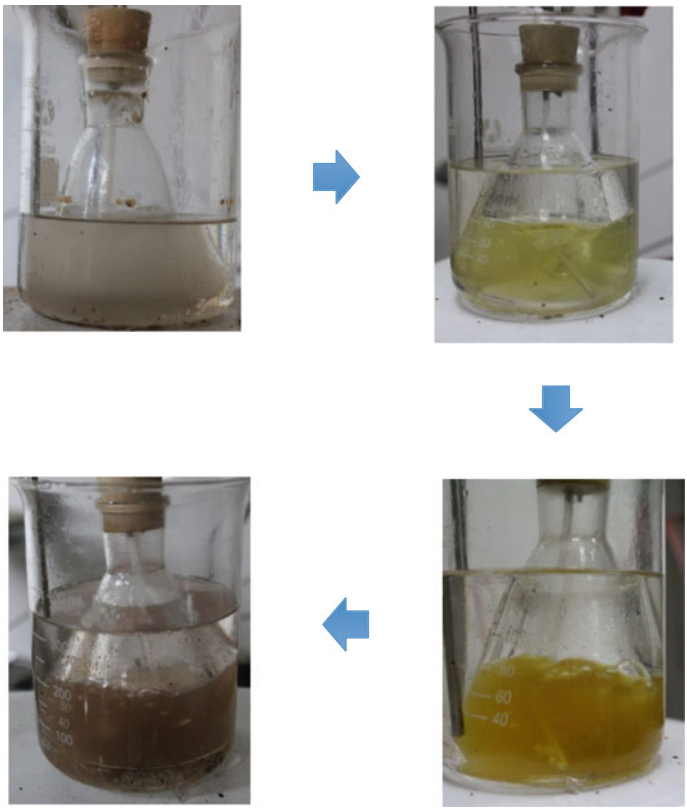

Fig. 6.14 Catalyst deactivation process in the liquid-phase hydrogenation in NMP

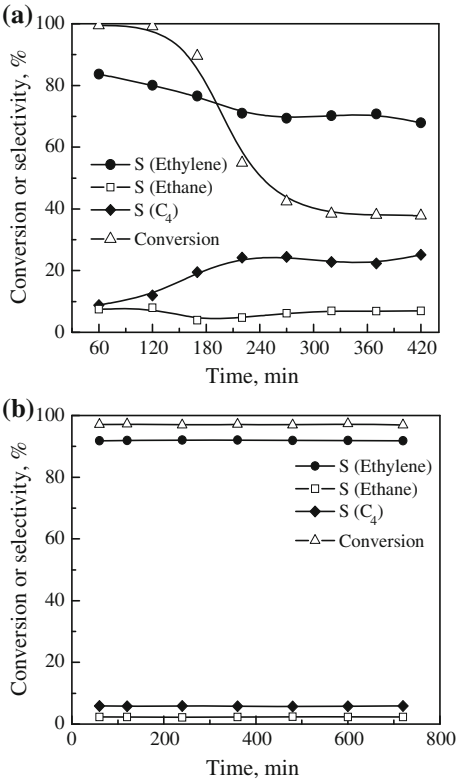

Fig. 6.15 Typical deactivation and non-deactivation processes in the liquid-phase hydrogenation in NMP **a** T = 60 °C; **b** T = 100 °C (H_2/C_2H_2 = 6, GHSV = 3600 ml $gcat^{-1}$ h^{-1}). Reprinted with the permission from Ref. [32]. Copyright 2013 American Chemical Society

stage, the catalysts in the reactor existed as gray slurry (gray is the initial color of the reduced catalyst); after some time when the green oil accumulated and dissolved in the liquid phase, the liquid color turned to transparent light yellow; when more green oil formed, the liquid color gradually turned to dark yellow and finally to opaque khaki. The catalysts were recycled and dried after reaction. Dark brown flocs were observed on the surface of the catalysts, and significant weight loss was observed in the TGA characterization.

Figure 6.15 shows the catalyst stability at 60 and 100 °C with the H_2/C_2H_2 of 6 and GHSV of 3600 ml $gcat^{-1}$ h^{-1}. At a low temperature (60 °C), the catalyst suffers severe deactivation in the first two hours, with the acetylene conversion decreasing from 100 to 40%, and the selectivity to ethylene decreasing from 83 to 70%. In contrast, the catalyst at a higher temperature (100 °C) shows much better stability, with no detectable deactivation in 12 h. The main cause of deactivation is the high coverage of acetylene and C4 species on the Pd particles. Both acetylene and C4 species have high solubilities in NMP, as shown in Table 6.3 [35]. It is

Table 6.3 Solubilities of C4 species in NMP, summarized from [35]

Temperature (°C)	20	40	60
C_2H_4	1.9	1.17	–
C_2H_2	38.7	24.0	14.75
i-C_4H_8	32	16	8.5
C_4H_6	94	43	24
C_4H_4	–	292	95

commonly accepted that the C4 species are the precursors of green oil [36]. For the conditions where catalyst stability is poor, the acetylene and C4 species concentrations in the liquid are high, which in turn lead to high coverage of these species on the catalyst surface and further lead to catalyst deactivation.

6.7 A Comparison with Solid Catalyst with Ionic Liquid Layer (SCILL)

In the selective hydrogenation of acetylene, the introduction of ionic liquid into the supported catalyst could enhance the ethylene selectivity by the coupling of selective absorption in the liquid phase to the selective hydrogenation on the solid catalyst surface. Ruta et al. [25] synthesized SILP catalyst by supporting the ionic liquid phase together with the Pd precursor onto the catalyst support and reported that over SILP Pd nanoparticles, the ethylene selectivity was only slightly enhanced at temperatures lower than 100 °C and was greatly enhanced to 85% at 150 °C, compared with the ethylene selectivity of 60% over an IL-free catalyst. However, the ethylene selectivity was measured at low acetylene conversions of $\sim$10% and it depended strongly on the temperature. Herrmann et al. [24] have reported that the ethylene selectivity increased from 79 to 83% by coating the Pd–Ag catalyst with 5 wt% [DMIM][$MeHPO_3$] or 10 wt% [BMIM][DCA].

The ionic liquid modification could enhance the ethylene selectivity to some extent, but the effect is limited according to the data reported in the literature. In order to identify the better liquid modification, a SCILL-type catalyst was synthesized using [DMIM][$MeHPO_3$] (α = 45), and the catalytic performance was compared with the unmodified catalyst in the bulk NMP liquid phase.

6.7.1 A General Comparison

The selectivities as a function of conversion were summarized and plotted in Fig. 6.16, for a general comparison of the modifications by the bulk NMP liquid phase, the ionic liquid layer over SCILL-Pd/SiO_2, and the non-modified gas-phase reaction over Pd/SiO_2.

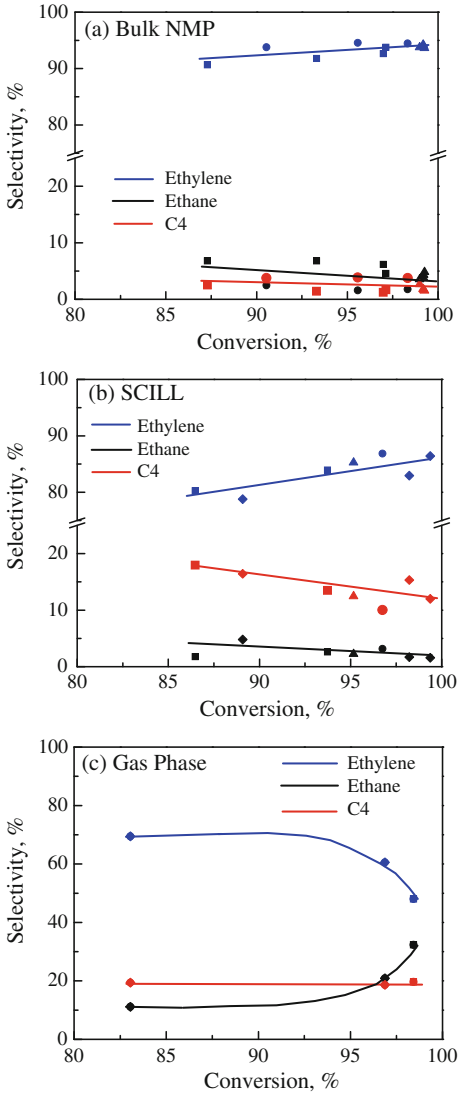

Fig. 6.16 Selectivities as a function of conversion over 0.01%Pd/SiO_2 in three systems **a** bulk NMP liquid phase, **b** SCILL, and **c** gas phase. Reprinted from Ref. [36], Copyright 2015, with permission from Elsevier

Compared with the gas-phase hydrogenation, as shown in Fig. 6.16, the ethylene selectivity is enhanced by both types of liquid modification—the liquid-phase modification by SCILL and by NMP bulk can both suppress the ethane selectivity. Over the neat Pd/SiO_2, the ethylene selectivity is ~70% at low acetylene conversions and decreases to below 50% at conversions close to 100%. Over SCILL, the ethylene selectivity is about 80% at low conversions and increases to ~85% when the acetylene conversion is close to 100%. In the bulk NMP liquid phase, the ethylene selectivity is always above 85%; when the conversion increases close to 100%, the ethylene selectivity is about 95%. As compared in Figs. 6.16a, b, the

major difference between the bulk NMP modification and the ionic liquid layer modification comes from the control of C4 species.

6.7.2 Selectivity

To better understand the different performance in selectivity in bulk NMP and on SCILL, additional experiments were carried out using the catalyst with a higher Pd loading (0.09 wt%) to obtain conversions near 100% at optimized conditions. Figure 6.17 shows the comparison of the selectivities in bulk NMP and over SCILL under the same reaction conditions. As shown in Fig. 6.17a, the ethylene selectivity is 6–10% higher in bulk NMP than over SCILL. The enhanced ethylene selectivity in bulk NMP is due to the effective suppression of both C4 species and ethane formation. The ethane selectivity is ~2% lower, and the C4 selectivity is 4–8% lower in bulk NMP than over SCILL, as shown in Fig. 6.17b, c, respectively.

The selectivities to the products show different trends with time in the three systems. In the bulk NMP liquid phase, the ethane selectivity increases with time; the selectivity to C4 species does not change much; and the selectivity to ethylene decreases with time. Over SCILL, the selectivity to ethane increases with time, and the selectivity to C4 species decrease with time, while the selectivity to ethylene does not change much. The ethylene selectivity difference between the bulk NMP and SCILL decreases with time, from ~10 to ~6%.

6.7.3 Stability

During the investigated 54 h, the two types of liquid modification behave differently in catalyst stability. The acetylene conversions and ethane selectivities are shown in Fig. 6.18.

The activity of SCILL decreases and the ethane selectivity increases with time on stream, while the conversion in bulk NMP does not decrease, indicating a possible catalyst deactivation over SCILL. The acetylene conversion decreases from 98 to 94%, and the selectivity to ethane increases from 5 to 7%. The decrease in activity is mainly caused by the formation of "green oil," because the selectivity to C4 species is relatively high over SCILL and the C4 species are considered as the precursors of green oil [37].

The appearances of fresh and used SCILL catalysts are shown in Fig. 6.19. The catalyst was a light gray color before reaction and became yellow after reaction, indicating the formation of green oil. The TGA results in Fig. 6.20 verified the green oil formation. The fresh SCILL has ~10% weight loss, which corresponds to the loss of ionic liquid, while the used SCILL has ~2% more weight loss than the fresh SCILL, which corresponds to the weight of green oil. No color changes or weight gain was observed on the catalysts in NMP after reaction.

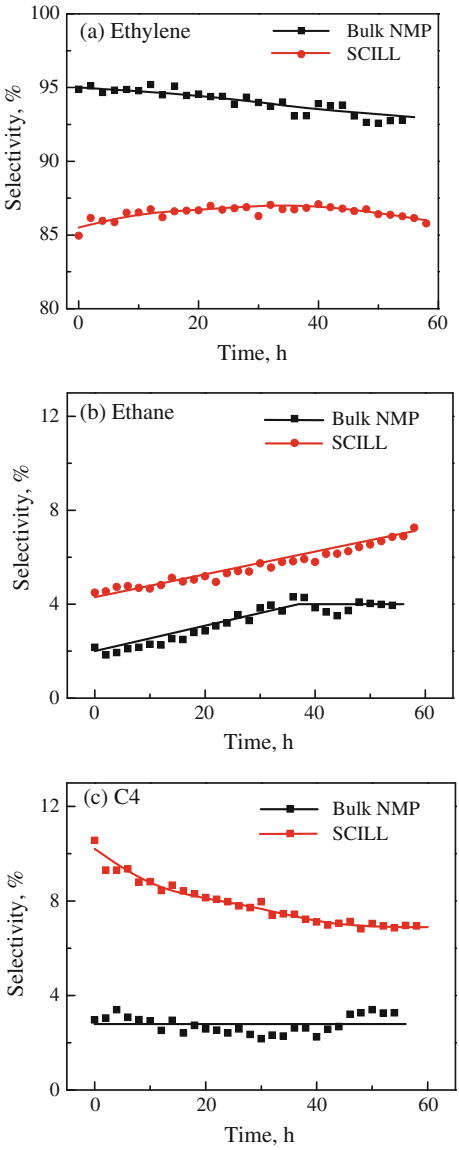

Fig. 6.17 Selectivities to **a** ethylene, **b** ethane, and **c** C4 species in bulk NMP liquid-phase and over SCILL (0.09% Pd/SiO_2, T = 90 °C, H_2/C_2H_2 = 10, GHSV = 3600 ml $gcat^{-1}$ h^{-1}). Reprinted from Ref. [36], Copyright 2015, with permission from Elsevier

As the formation of green oil was verified over SCILL, the deactivation mechanism could be speculated. Because the mass transfer resistance in the ionic liquid layer of SCILL increases the contact time of the produced C4 species with the catalyst, the C4 species are more likely to undergo polymerization reactions.

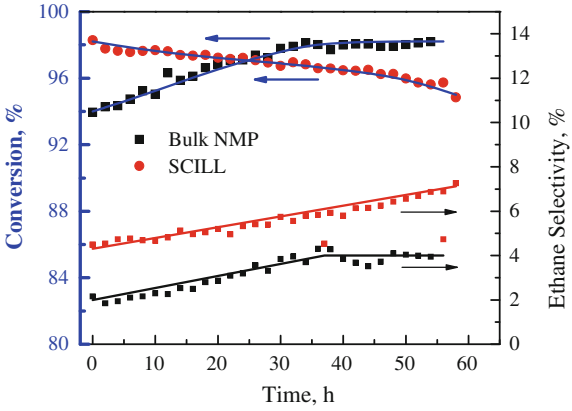

Fig. 6.18 Comparison of catalyst stability in bulk NMP liquid phase and over SCILL (0.09% Pd/SiO_2, T = 90 °C, H_2/C_2H_2 = 10, GHSV = 3600 ml $gcat^{-1}$ h^{-1}). Reprinted from Ref. [36], Copyright 2015, with permission from Elsevier

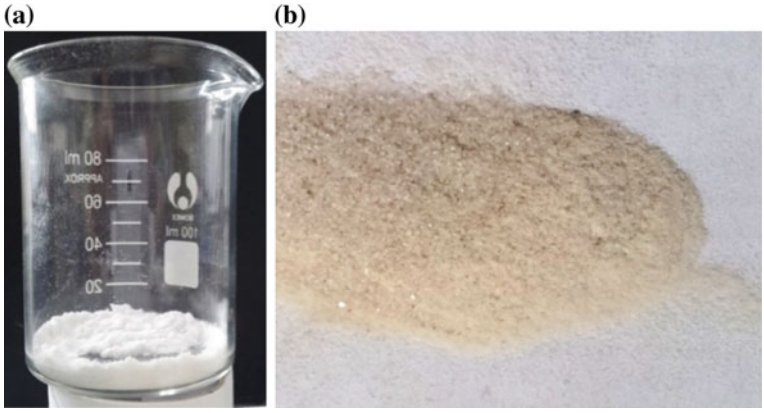

Fig. 6.19 0.09%Pd 20%IL/SiO_2 **a** before and **b** after reaction. Reprinted from Ref. [36], Copyright 2015, with permission from Elsevier

The green oil existing in the ionic liquid layer accumulates with time and blocks the active sites, and thus deactivates the catalyst. The increase in ethane selectivity can be caused by the loss of ionic liquid. An increase in activity was observed on 20% IL Pd/SiO_2 after flowing nitrogen for 12 and 24 h.

An increase in ethane selectivity is also observed in bulk NMP. This is caused by the long induction period due to the slow formation of Pd hydride, because an increase in activity is also observed in the first 33 h. In bulk NMP, the hydrogen concentration is low and the Pd hydride forms slowly. Because the Pd hydride formation enhances the hydrogenation activity [38], the activity in bulk NMP increases gradually with time on stream.

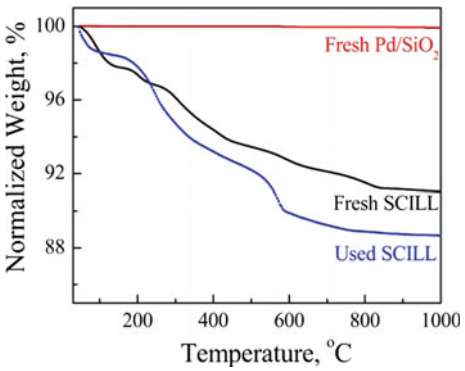

Fig. 6.20 TGA weight-loss curves of fresh and used SCILL. Reprinted from Ref. [36], Copyright 2015, with permission from Elsevier

6.7.4 Discussion

The selectivities and the stability of catalysts show obvious difference between the bulk NMP liquid phase and the SCILL-type catalyst. With careful analysis, the difference is due to the physical properties of liquids and the type of reactors.

The difference in ethylene selectivity is closely related to the mechanism of liquid modifications. In a bulk liquid phase, the vigorous stirring intensifies the mass transfer of the produced ethylene from the catalyst surface to the liquid and from the liquid to gas phase. Over SCILL, however, the mass transfer resistance is eliminated only at low GHSV; and it becomes significant with increasing GHSV due to the high viscosity of ionic liquid.

In order to compare the mass transfer effect in the two types of liquid modification, the conversions of acetylene were plotted in Fig. 6.21 under different GHSVs in both bulk NMP and over SCILL. The data on the neat Pd/SiO_2 were included as reference. The conversion in bulk NMP is only slightly lower than over neat Pd/SiO_2,

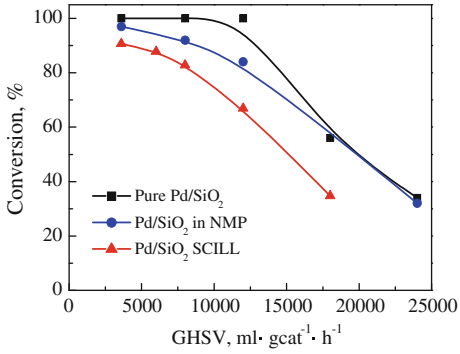

Fig. 6.21 Conversion of acetylene as a function of GHSV in the three systems (0.01%Pd/SiO_2, T = 100 °C, H_2/C_2H_2 = 10). Reprinted from Ref. [36], Copyright 2015, with permission from Elsevier

while the conversion over SCILL is much lower than in bulk NMP, indicating a more significant mass transfer resistance in the ionic liquid layer than in NMP.

Because acetylene has a higher solubility in NMP and a stronger binding energy on the active sites compared with ethylene, the concentration ratio of acetylene to ethylene is much higher on the active sites in the liquid phase than that in the gas phase. Therefore, the produced ethylene can easily escape from the catalysts and transfer to the gas phase when the mass transfer is not the limiting step. In a highly viscous ionic liquid, however, the gas–liquid mass transfer rate is slow, which tends to increase the ethylene concentrations and decrease the acetylene concentrations both in the liquid and on the active sites. This will further decrease the conversion of acetylene and selectivity to ethylene. Therefore, both the selective solubility and the mass transfer rate have effects on the reaction performance. The mass transfer resistance in the ionic liquid layer increases the contact time of the produced ethylene with the catalysts, which in turn leads to a higher selectivity to ethane. Furthermore, the shorter contact time of ethylene in bulk NMP has been verified by a control experiment using only ethylene feed in NMP bulk phase.

As shown in Table 6.4, when the feed gas is ethylene and hydrogen, very little ethylene is hydrogenated at either 60 or 80 °C in bulk NMP. On the other hand, much more (three magnitude higher than in bulk NMP) ethylene converts into ethane in the gas phase under the same reaction conditions. According to the literature [39], the SCILL exhibited similar activity with uncoated catalysts in ethylene hydrogenation. Based on these results, the higher ethylene selectivity is due to the shorter contact time in bulk NMP.

The difference in selectivity to C4 species is mainly due to the different types of reactor and the distribution of acetylene concentration in the reactors. As shown in Fig. 6.22, the acetylene concentration on the catalyst surface differs from each other for the two types of liquid modification. In the stirred reactor used for the bulk liquid-phase hydrogenation, the liquid phase is intensively mixed; therefore, the concentration of dissolved acetylene is similar as that in the outlet and is much smaller than the saturated concentration corresponding to the gas feed. In contrast, the acetylene concentration in a fixed-bed reactor is high in the inlet region and decreases gradually as the reactant gas flows through the catalyst bed. Because the dimerization reaction strongly depends on the acetylene concentration on the catalyst surface, the C4 production is effectively suppressed in the perfectly mixed reactor used for the bulk liquid-phase hydrogenation. As a result of a higher mass transfer rate and lower acetylene concentration, the production of both ethane and C4 is suppressed more effectively in bulk NMP than over SCILL. Therefore, an enhanced selectivity to ethylene is obtained in the bulk liquid-phase hydrogenation.

Table 6.4 Conversion of ethylene in NMP liquid phase and gas phase (pure ethylene feed)

Temperature (°C)	Conversion of ethylene (%)	
	Gas phase	Liquid phase
60	14	0.06
80	16	0.03

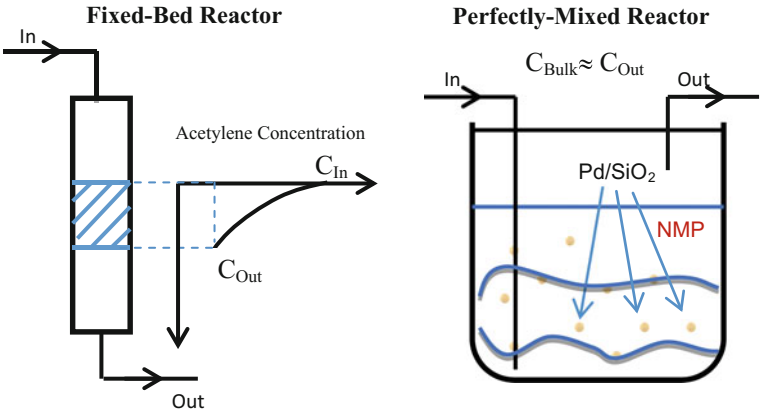

Fig. 6.22 Acetylene concentration distribution in gas phase and liquid phase. Reprinted from Ref. [36], Copyright 2015, with permission from Elsevier

Moreover, the catalyst stability on the one hand depends on the amount of C4 formation. There is more C4 species formation over SCILL; with the mass transfer resistance, the C4 species contact longer with the catalyst and undergo oligomerization reactions to form green oil. As a result, the catalyst is less stable in the SCILL-type modification.

The better mass transfer and low acetylene concentration in the bulk NMP liquid phase effectively controlled the complete hydrogenation and oligomerization reactions. The selectivity to ethylene, the mass transfer effect, and the catalyst stability are better in the bulk NMP than over SCILL. Furthermore, in the slurry reactor, the liquid phase can continuously remove the heat produced from the hydrogenation reaction and can prevent the temperature runaway in industrial operation. The liquid-phase process can not only overcome the disadvantages in the front-end process, but can also solve the difficulties in the high-concentration-feed acetylene hydrogenation.

6.8 Process Optimization and Reactor Design

Although the selective hydrogenation in liquid phase of NMP shows more advantages than in the gas phase in terms of ethylene selectivity and heat removal, the back mixing in the reactor prohibited the acetylene to undergo full conversion. The acetylene concentration in the outlet is still high (1–3%) and cannot meet the demand for the polymerization-grade ethylene. In this section, a second stage was introduced into the slurry reactor, and the pressure was increased to enhance the hydrogen dissolution and to increase the acetylene conversion. The gas-phase concentration in the inlet was 1.9% C_2H_2, 60.6% C_2H_4, and 37.5% H_2.

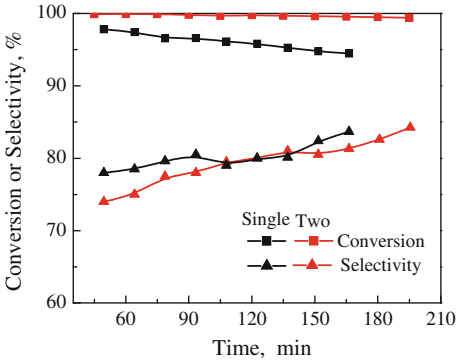

Fig. 6.23 Acetylene hydrogenation in single-stage and two-stage slurry reactors (GHSV = 6000 ml $gcat^{-1}$ h^{-1}, H_2/C_2H_2 = 20, T = 60 °C)

6.8.1 Two-Stage Slurry Reactor

A second stage was introduced in the slurry reactor in order to increase the conversion of acetylene by increasing the total contact time of acetylene on the catalyst surface.

The results in the single-stage reactor and in the two-stage slurry reactor are shown in Fig. 6.23. The conversion of acetylene is about 96% in the single-stage reactor and is above 99.9% in the two-stage slurry reactor. It could be concluded that by connecting the slurry stages in series, the acetylene conversion could be enhanced. By calculating the required contact time of acetylene to produce the polymerization grade of ethylene, the number of stages could be obtained.

The selectivity to ethylene in the two-stage slurry reactor is similar to that in the single-stage reactor. The multi-stages could retain the high selectivity while enhancing the acetylene conversion. According to the results in Table 6.4, when pure ethylene was fed into the liquid phase, only minor ethylene was converted into ethane, implying that the ethylene contact time is short in the NMP liquid-phase reactor. As a result, the multi-stage reactor only enhances the conversion of acetylene and can control the complete hydrogenation reaction.

It can also be observed in the figure that the conversion of acetylene decreases slower with time in the two-stage reactor than in the single-stage reactor. The catalysts in the first reactor of the two-stage process deactivate at the same speed as in the single bed reactor, while the catalysts in the second reactor deactivate much slower because of the low acetylene concentration.

6.8.2 Pressure Effect

Because the solubility of hydrogen in NMP is low, the hydrogen partial pressure on the catalyst surface is relatively low. By increasing the reaction pressure, the

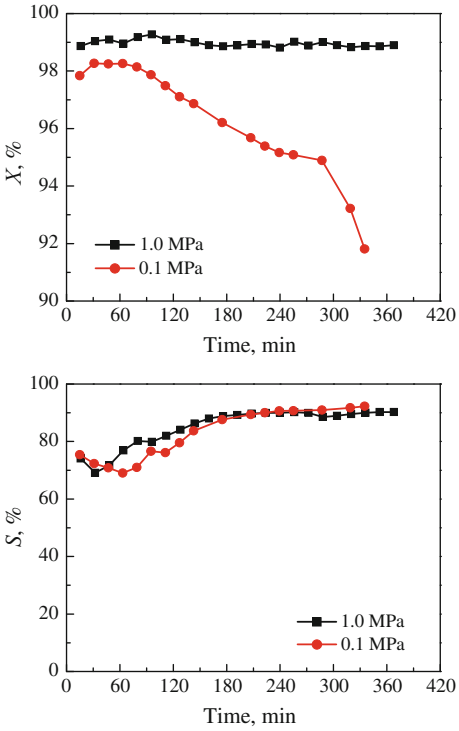

Fig. 6.24 Pressure effect in the liquid-phase hydrogenation of acetylene (GHSV = 6000 ml gcat^{-1} h^{-1}, H_2/C_2H_2 = 20, T = 60 °C)

hydrogen partial pressure could be increased and further the conversion of acetylene. In the experiment, the reaction pressure was increased from 0.1 to 1.0 MPa for a single-stage slurry reactor.

As shown in Fig. 6.24, the acetylene conversion under 1.0 MPa is about 99% in the first 6 h; under 0.1 MPa, the conversion decreases from 98% to about 92%, indicating that by increasing the reaction pressure, the catalyst stability could be enhanced. The increased pressure could increase the hydrogen concentration in the liquid phase, thus increasing the partial pressure on the catalyst surface. On the other hand, because the acetylene concentration in the liquid phase is much smaller than the saturated concentration, the increased operation pressure does not affect much on the acetylene partial pressure on the catalyst surface. The higher hydrogen partial pressure can effectively suppress the dimerization of acetylene and decrease the formation of green oil, thus increasing the catalyst stability.

The ethylene selectivity under 1.0 MPa is similar as that under 0.1 MPa. The selectivity increases from ~70 to 89% in the first 6 h. It seems that the pressure does not affect the ethylene selectivity, probably due to the pressure effect on the selectivities to ethane and C4 species. The higher pressure suppresses the oligomerization reaction and decreases the selectivity to C4 species, but enhances

the hydrogenation reaction and increases the selectivity to ethane. The decrease in C4 selectivity and the increase in the ethane selectivity are not significant and could be neutralized. As a result, the selectivity to ethylene is not affected by the pressure change.

6.8.3 *Design of Multi-Stage Reactor*

The multi-stage slurry reactor and the increased pressure can both enhance the acetylene conversion and retain high ethylene selectivity. Accordingly, a multi-stage reactor was designed and is plotted in Fig. 6.25. The operation process is as follows:

(1) The liquid solvent is loaded in the reactor, which has a high solubility to acetylene and a low solubility to ethylene; the catalyst particles are dispersed in the liquid phase.

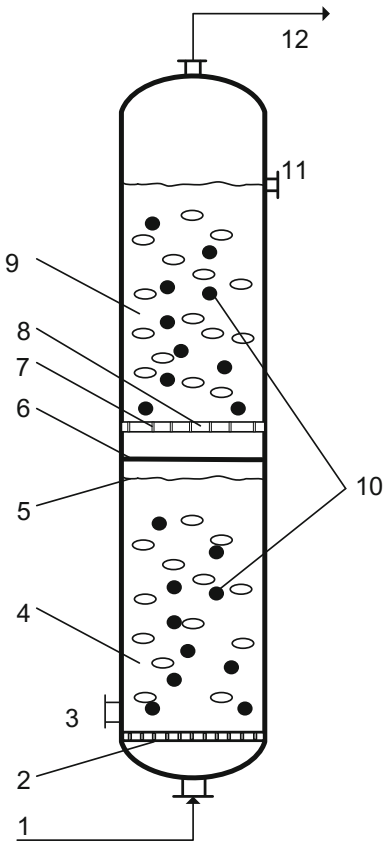

Fig. 6.25 Graphic demonstration of the proposed multi-stage slurry bed reactor *1* inlet for gas phase; *2* gas distributor; *3* inlet for liquid phase in the first stage; *4* first stage; *5* liquid level of the first stage; *6* division plate; *7* gas-phase pass between phases; *8* component plate between phases; *9* second stage; *10* supported catalyst; *11* inlet for liquid phase in the second stage; *12* outlet for gas phase

(2) Acetylene and hydrogen are mixed and introduced into the reactor; the gas phase with high concentration of ethylene is condensed and collected in the top outlet; the liquid phase is collected in the condenser and is sent back to the reactor.
(3) The gas phase from the outlet is separated, and the polymerization-grade ethylene is obtained.

US20050049445 and WO2005049533A1 [29, 30] reported a process of liquid-phase hydrogenation of acetylene. Acetylene was firstly dissolved into the liquid solvent; the solvent then contacted with the hydrogenation catalyst bed; finally, the product ethylene was separated from the liquid phase and the other gases. The process is not continuous and is of low capacity. It consumes high energy and is not economic. It is specially not suitable for large-scale production of ethylene from acetylene, because of the following: Firstly, the large amount of acetylene will demand a large amount of liquid solvent and the operational cost will be extremely high; secondly, the fixed-bed reactor cannot realize the hydrogenation of high concentration acetylene due to the large amount of released heat.

The designed multi-stage slurry reactor is continuous when in operation, and the liquid solvent remains in the reactor and does not need any energy for the circulation. Besides, the capacity for acetylene could be high and the investment for the reactor is low. It shows great advantage than the previous reactors for the hydrogenation of acetylene.

6.9 Conclusion

A novel process was designed for the selective hydrogenation of acetylene by introducing a liquid phase to couple the selective absorption with the selective hydrogenation reaction on the catalyst surface, in order to enhance the ethylene selectivity as well as to enhance the heat removal. The liquid-phase hydrogenation of acetylene in NMP outperforms the SCILL-type catalyst in terms of liquid modification, as shown in Fig. 6.26. The results lead to the following conclusions:

(1) The introduction of a selective solvent significantly enhances the selectivity to ethylene. The selectivity to ethylene is 80–96% in NMP, while it is less than 70% in the gas phase.
(2) In the liquid-phase hydrogenation, the selectivity to ethylene strongly depends on the selective solubility, while the conversion depends on the viscosity of the solvent. A selective solvent (NMP) significantly enhances the selectivity to ethylene, while a non-selective solvent (decane) does not affect the selectivity.
(3) A high reaction temperature, low space velocity, and high H_2/C_2H_2 ratio give increased selectivity to ethylene in NMP and effectively stabilizes the catalyst by the suppression of green oil formation.

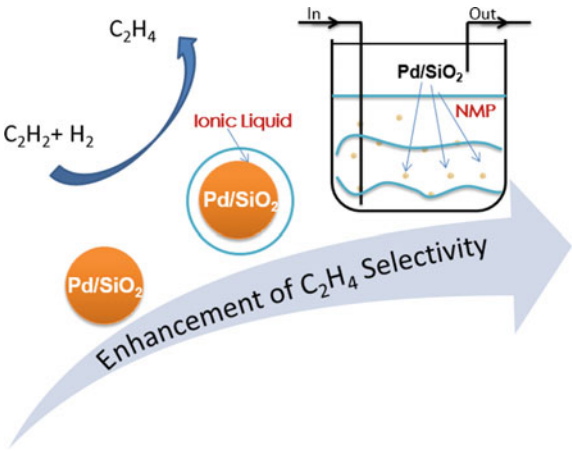

Fig. 6.26 Enhancement of ethylene selectivity by liquid phase. Reprinted from Ref. [36], Copyright 2015, with permission from Elsevier

(4) The intense mixing of gas phase and liquid phase in the slurry reactor can remove the heat from the catalyst surface effectively and prevent the runaway of temperature.
(5) The liquid-phase hydrogenation of acetylene is suitable not only for the front-end process in the purification of ethylene but also for the production of ethylene from high concentration acetylene feed, with a higher selectivity to ethylene and a more uniform temperature distribution than the gas-phase hydrogenation.
(6) Compared with the modification of ionic liquid by SCILL, the selectivity to ethylene and the catalyst stability show better performance in the bulk NMP liquid phase.
(7) The multi-stage and the increased pressure can both enhance the acetylene conversion in the slurry reactor and retain the high ethylene selectivity. By rational design of reactor, the concentration of acetylene can meet the requirement of the polymerization-grade ethylene.

References

1. Zhang QW, Li J, Liu XX et al (2000) Synergetic effect of Pd and Ag dispersed on Al_2O_3 in the selective hydrogenation of acetylene. Appl Catal A-Gen 197(2):221–228
2. Duca D, Frusteri F, Parmaliana A et al (1996) Selective hydrogenation of acetylene in ethylene feedstocks on Pd catalysts. Appl Catal A-Gen 146(2):269–284
3. Liu JY, Lu HM, Ling ZG et al (2008) Catalytic properties of supported Pd/SBA-15 catalyst for selective hydrogenation of alkadienes. Chin J Catal 29(3):206–208
4. Riyapan S, Boonyongmaneerat Y, Mekasuwandumrong O et al (2014) Improved catalytic performance of Pd/TiO_2 in the selective hydrogenation of acetylene by using H_2-treated sol-gel TiO_2. J Mol Catal A-Chem 383:182–187

5. Komhom S, Mekasuwandumrong O, Panpranot J et al (2009) Influence of preparation method on the nanocrystalline porosity of α-Al_2O_3 and the catalytic properties of Pd/α-Al_2O_3 in selective acetylene hydrogenation. Ind Eng Chem Res 48(13):6273–6279
6. Zakumbayeva GD, Toktabayeva NF, Kubasheva AZ et al (1994) Influence of the degree of dispersion of palladium on the selective hydrogenation of acetylene in an ethane-ethylene fraction. Petro Chem 34(3):249–258
7. Khan NA, Uhl A, Shaikhutdinov S et al (2006) Alumina supported model Pd–Ag catalysts: a combined STM, XPS, TPD and IRAS study. Surf Sci 600(9):1849–1853
8. Khan NA, Shaikhutdinov S, Freund HJ (2006) Acetylene and ethylene hydrogenation on alumina supported Pd–Ag model catalysts. Catal Lett 108(3–4):159–164
9. Sheth PA, Neurock M, Smith CM (2005) First-principles analysis of the effects of alloying Pd with Ag for the catalytic hydrogenation of acetylene-ethylene mixtures. J Phys Chem B 109 (25):12449–12466
10. Ma Y, Diemant T, Bansmann J et al (2011) The interaction of CO with PdAg/Pd(111) surface alloys—a case study of ensemble effects on a bimetallic surface. Phys Chem Chem Phys 13 (22):10741–10754
11. Osswald J, Giedigkeit R, Jentoft RE et al (2008) Palladium-gallium intermetallic compounds for the selective hydrogenation of acetylene—part I: preparation and structural investigation under reaction conditions. J Catal 258(1):210–218
12. Osswald J, Kovnir K, Armbruester M et al (2008) Palladium-gallium intermetallic compounds for the selective hydrogenation of acetylene—part II: surface characterization and catalytic performance. J Catal 258(1):219–227
13. Kovnir K, Osswald J, Armbruester M et al (2006) PdGa and Pd_3Ga_7: highly-selective catalysts for the acetylene partial hydrogenation. Scientific bases for the preparation of heterogeneous catalysts, In: Proceedings of the 9th international symposium, vol 162, pp 481–488
14. Armbruester M, Wowsnick G, Friedrich M et al (2011) Synthesis and catalytic properties of nanoparticulate intermetallic Ga–Pd compounds. J Am Chem Soc 133(23):9112–9118
15. Tauster S, Fung S, Garten R (1978) Strong metal-support interactions. Group 8 noble metals supported on titanium dioxide. J Am Chem Soc 100(1):170–175
16. Kang JH, Shin EW, Kim WJ et al (2002) Selective hydrogenation of acetylene on TiO_2-added Pd catalysts. J Catal 208(2):310–320
17. Borodzinski A, Bond GC (2008) Selective hydrogenation of ethyne in ethene-rich streams on palladium catalysts, part 2: steady-state kinetics and effects of palladium particle size, carbon monoxide, and promoters. Catal Rev 50(3):379–469
18. Praserthdam P, Phatanasri S, Meksikarin J (2000) Activation of acetylene selective hydrogenation catalysts using oxygen containing compounds. Catal Today 63(2–4):209–213
19. Ngamsom B, Bogdanchikova N, Borja MA et al (2004) Characterisations of Pd–Ag/Al_2O_3 catalysts for selective acetylene hydrogenation: Effect of pretreatment with NO and N_2O. Catal Commun 5(5):243–248
20. Panpranot J, Aungkapipattanachai S, Sangvanich T et al (2007) Effect of N_2O pretreatment on fresh and regenerated Pd–Ag/α-Al_2O_3 catalysts during selective hydrogenation of acetylene. React Kinet Catal Lett 91(2):195–202
21. Arras J, Paki E, Roth C et al (2010) How a supported metal is influenced by an ionic liquid: In-depth characterization of SCILL-type palladium catalysts and their hydrogen adsorption. J Phys Chem C 114(23):10520–10526
22. Jess A, Kern C, Korth W (2012) Solid catalyst with ionic liquid layer (SCILL)—a concept to improve the selectivity of selective liquid and gas phase hydrogenations. Oil Gas-Eur Mag 38 (1):38–45
23. Kernchen U, Etzold B, Korth W et al (2007) Solid catalyst with ionic liquid layer (SCILL)—a new concept to improve selectivity illustrated by hydrogenation of cyclooctadiene. Chem Eng Technol 30(8):985–994

24. Herrmann T, Roessmann L, Lucas M et al (2011) High-performance supported catalysts with an ionic liquid layer for the selective hydrogenation of acetylene. Chem Commun 47 (45):12310–12312
25. Ruta M, Laurenczy G, Dyson PJ et al (2008) Pd nanoparticles in a supported ionic liquid phase: highly stable catalysts for selective acetylene hydrogenation under continuous-flow conditions. J Phys Chem C 112(46):17814–17819
26. Lee JM, Palgunadi J, Kim JH et al (2010) Selective removal of acetylenes from olefin mixtures through specific physicochemical interactions of ionic liquids with acetylenes. Phys Chem Chem Phys 12(8):1812–1816
27. Hou R, Wang T, Lan X (2013) Enhanced selectivity in the hydrogenation of acetylene due to the addition of a liquid phase as a selective solvent. Ind Eng Chem Res 52(37):13305–13312
28. Edvinsson RK, Holmgren AM, Irandoust S (1995) Liquid-phase hydrogenation of acetylene in a monolithic catalyst reactor. Ind Eng Chem Res 34(1):94–100
29. Johnson MM, Peterson ER, Gattis SC et al (2005) US Patent 2005049445-A1
30. Cheung TP, Johnson MM (2005) US Patent 2005107649-A1
31. Shitova NB, Shlyapin DA, Afonasenko TN et al (2011) Liquid-phase hydrogenation of acetylene on the Pd/sibunit catalyst in the presence of carbon monoxide. Kinet Catal 52 (2):251–257
32. Hou R, Lan X, Wang TF (2013) Enhanced selectivity in the hydrogenation of acetylene due to the addition of a liquid phase as a selective solvent. Ind Eng Chem Res 52(37):13305–13312
33. Garcia-Mota M, Bridier B, Perez-Ramirez J et al (2010) Interplay between carbon monoxide, hydrides, and carbides in selective alkyne hydrogenation on palladium. J Catal 273(2):92–102
34. Borodzinski A, Bond GC (2006) Selective hydrogenation of ethyne in ethene-rich streams on palladium catalysts. Part 1. Effect of changes to the catalyst during reaction. Catal Rev 48 (02):91–144
35. Chen B (1988) Handbook of petroleum and chemical engineering: Basic materials. Chemical Industry Press, Beijing
36. Hou R, Lan X, Wang TF (2015) Selective hydrogenation of acetylene on Pd/SiO_2 in bulk liquid phase: A comparison with solid catalyst with ionic liquid layer (SCILL). Catal Today 251:47–52
37. Ahn IY, Lee JH, Kum SS et al (2007) Formation of C4 species in the deactivation of a Pd/SiO_2 catalyst during the selective hydrogenation of acetylene. Catal Today 123(1–4): 151–157
38. Tew MW, Janousch M, Huthwelker T et al (2011) The roles of carbide and hydride in oxide-supported palladium nanoparticles for alkyne hydrogenation. J Catal 283(1):45–54
39. Knapp R, Jentys A, Lercher JA (2009) Impact of supported ionic liquids on supported Pt catalysts. Green Chem 11(5):656–661

Chapter 7
Conclusions

This thesis covers the catalytic and process study of the selective hydrogenation reactions, in order to improve the alkene selectivity, to decrease the catalyst cost, and to stabilize the temperature control. Pd–Ni bimetallic catalysts were studied from fundamental to application. Based on the better performance of Ni modification, a non-precious metal catalyst was designed. Furthermore, a novel process of liquid-phase hydrogenation was investigated by coupling the selective absorption in the liquid phase to the selective hydrogenation on the catalyst surface. The novel process was optimized, and the concept of a multi-stage slurry reactor was proposed.

The conclusions of the thesis are as follows:

1. Hydrogenation of 1,3-butadiene has been studied on Pd–Ni bimetallic catalysts using a combination of DFT calculations and TPD experiments on model surfaces, together with reactor evaluation over supported catalysts. DFT results show that the PdNiPd(111) surface has a lower activation barrier for each step of 1,3-butadiene hydrogenation and shows a lower adsorption energy for 1-butene than the Pd(111) surface, indicating a higher activity and a higher 1-butene selectivity over PdNiPd(111). The UHV-TPD results verified the higher hydrogenation activity on PdNiPd(111). By evaluating the supported catalysts in the batch reactor and the fixed-bed reactor, the high hydrogenation activity and 1-butene selectivity make PdNi/γ-Al_2O_3 a better catalyst for 1,3-butadiene removal than the Pd monometallic catalyst. The Pd–Ni bimetallic catalyst also shows better performance in acetylene hydrogenation. The good correlation between model surfaces and supported catalysts demonstrates the feasibility of designing selective hydrogenation catalysts using well-defined single-crystal surfaces.
2. Five oxide supports (γ-Al_2O_3, SiO_2, ZrO_2, CeO_2, and TiO_2) were used for the Pd–Ni bimetallic catalysts, in order to investigate the oxide support effect in the selective hydrogenation of 1,3-butadiene. The activity is not affected by the nature of the support, whereas TOF is mainly affected by the metal dispersion.

R. Hou, *Catalytic and Process Study of the Selective Hydrogenation of Acetylene and 1,3-Butadiene*, Springer Theses, DOI 10.1007/978-981-10-0773-6_7

The metal–support interaction influences the selectivity behavior. The possible SMSI effect and oxygen defects are possible reasons for the lower 1-butene selectivity on PdNi/CeO_2, PdNi/ZrO_2, and PdNi/TiO_2.

3. By replacing Pd with Mo_2C, non-precious metal catalysts were designed to reduce the catalyst cost. The Mo_2C-based catalysts show similar activity as Pd-based catalysts. By modifying Mo_2C with Ni, the selectivity to 1-butene is greatly enhanced. Among the investigated catalysts, 8.6%Ni/Mo_2C exhibits highest 1-butene selectivity while maintaining similar activity as Pd/SiO_2.
4. The liquid-phase hydrogenation of acetylene was found to enhance the ethylene selectivity and the heat transfer by introducing a solvent with selective solubility into the gas–solid reaction system. The solvent has a high solubility for acetylene but low solubility for ethylene. By coupling the selective absorption and the selective hydrogenation, the ethylene selectivity is greatly enhanced. At a conversion close to 100%, the highest selectivity to ethylene is 96%. The liquid phase intensifies the heat removal from the catalyst surface and makes the system safer and more stable. Reaction conditions of low GHSV, high H_2/C_2H_2 ratio, and high temperature (>80 °C) are optimal to obtain a high selectivity to ethylene and higher catalyst stability. In the selection of solvent, the selective solubility as well as the viscosity should be considered. The SCILL-type catalyst modified by ionic liquid was compared with the bulk NMP liquid-phase hydrogenation. The bulk liquid-phase hydrogenation outperforms the selective hydrogenation over SCILL in terms of ethylene selectivity, catalyst stability, and heat removal. The process was further optimized by a multi-stage slurry reactor and by increasing the reaction pressure. Via rational design, the concentration of acetylene could reach the standard of polymerization grade ethylene.

The innovations of the thesis are as follows:

1. Pd-Ni bimetallic catalyst was designed from model surfaces using DFT and UHV methods. The catalytic properties were verified by the evaluation of supported catalyst, demonstrating the good correlation between model surfaces and supported catalysts.
2. The non-precious catalyst Ni/Mo_2C was designed by the analysis of the inorganic materials' properties. The similar performance of Ni/Mo_2C with Pd-based catalyst gives possibility of replacing the precious metal catalyst by non-precious metal compounds.
3. The novel process of liquid-phase hydrogenation was designed by the concept of coupling absorption to reaction. The selectivity to ethylene was greatly enhanced, and the heat removal was intensified.
4. The mechanism of liquid-phase hydrogenation was analyzed. Accordingly, a high-pressure multi-stage slurry reactor was proposed for the improvement in acetylene conversion.

Based on the thesis, it is suggested to further research into the followings:

1. Structural study of Pd–Ni bimetallic catalyst at nanoscale.
2. Systematic study of Pd–Ni bimetallic catalyst in the selective hydrogenation of acetylene.
3. The deactivation behavior and mechanism over Mo_2C-based catalysts in fixed-bed reactor.
4. Industrial design of multi-stage slurry reactor and operational optimization.